MODELING OF CLT CREEP BEHAVIOR AND REAL-TIME HYBRID SIMULATION OF A CLT-LIFS BUILDING

by

TU T. NGUYEN

THANG N. DAO, COMMITTEE CHAIR
KENNETH J. FRIDLEY, COMMITTEE CO-CHAIR
MICHAEL E. KREGER
SRIRAM AALETI
SEMIH M. OLCMEN

A DISSERTATION

Submitted in partial fulfillment of the requirements
for the degree of Doctor of Philosophy
in the Department of Civil, Construction and Environmental Engineering
in the Graduate School of
The University of Alabama

TUSCALOOSA, ALABAMA

2017

ABSTRACT

CLT-LiFS is an innovative hybrid structural system. This type of structure has emerged as a promising structural system for mid-rise to tall wood buildings in the seismic areas. CLT-LiFS is made by integrating post-tensioned Cross Laminated Timber (CLT) panels with Light Frame Wood Systems (LiFS). The post-tensioned CLT panels can provide excellent load bearing and self-centering capacity. And the LiFS can dissipate a large amount of energy through the slip of fasteners when it deforms. The behaviors of CLT-LiFS have been studied through a series of experimental tests under cyclic loading protocols and earthquake motions at different hazard levels using real-time hybrid simulations. Results from the experimental tests showed that the CLT-LiFS performed well under MCE (Maximum Considered Earthquake) hazard level with the maximum drift less than 1%. To obtain a good self-centering performance, the post-tensioned tendon force in CLT panels needs to be maintained at a desired level in long-term until the earthquake hits. Under the creep behavior, the post-tensioned force in the tendon will reduce as a function of time and moisture content in CLT panels. In this dissertation, a moisture content diffusion model was introduced by applying Fick's law to estimate the moisture content migration in CLT panels under the variation of environmental relative humidity. A numerical model combined with data from a series of moisture content experiments were used to obtain the moisture content diffusion coefficients for CLT material. The four-element creep model was also proposed. This creep model could predict the creep deformation of CLT panels versus time under variations of ambient environmental conditions. A 3D finite element model (FEM) was developed with an integration of the creep and moisture content diffusion model to predict the

tendon force of post-tensioned CLT panels versus time. This FEM model was used to predict the loss of tendon force in CLT panels. This tendon force loss did not include the instant loss at the beginning due to anchor slip or other factors.

DEDICATION

This dissertation is dedicated to my wife, Linh Bach. I could not have completed this dissertation without her love, emotional support, and encouragement. She has motivated me when necessary, provided advice on critical matters and been a comforting companion. Despite her intense MBA program, she has always been an incredible mother to our little daughters, Ngoc "Emily" Nguyen and Trang "Alice" Nguyen. They are wonderful individuals thanks to the integrity, compassion, and guidance provided by their mother. I admire and appreciate her.

This dissertation is also dedicated to my father, mother, brother, and sister for giving me unconditional love and support. My interest in academia comes from my parents, lifelong teachers who gave me strength and direction to be successful. I also dedicate this dissertation to my father-in-law, mother-in-law, and brother-in-law, who have always believed in me and supported me unconditionally. I am fortunate to have you all present in my life.

LIST OF ABBREVIATIONS AND SYMBOLS

β	Ratio between CLT stiffness and cable stiffness
τ	Time delay
Φ	Moisture concentration driving potential
σ	Constant applied stress
ω	Relative moisture content
θ	Relative temperature
μ_ω	Mechano-sorptive constant
$\varepsilon(t)$	Total strain at time *t*
μ'_{ms}	Constant with units force per unit area
Δ_c	Cable elongation
ε_c	Cable strain after post-tension
μ_k	Viscosity of delayed elasticity
ΔMC	Moisture content difference
$\Delta P(t)$	Loss of cable force
Δt	Time step
μ_v	Viscosity of unrecovered strain
$[C]$	Moisture content stiffness
$[K]$	Structural stiffness

$[N]$	Element shape function matrix
$[N']$	Derivative of element shape function matrix
$[R]$	Matrix of diffusion coefficients
A_c	Cable cross section
A_w	CLT panel cross section
b	CLT panel width
B_ω	Moisture equilibrium constant
CLT	Cross-Laminated Timber
C_p	Proportional gain
C_v	Velocity gain
D	Dead load
DAQ	Data Acquisition
DBE	Design Basis Earthquake
DEMEC	Demountable Mechanical strain gauges
E	Modulus of elasticity of CLT
E_c	Cable modulus of elasticity
$E_w(t)$	CLT modulus of elasticity history
f_c'	CLT compressive strength
G	Learning gain
h	CLT panel thickness
K_c	Cable stiffness
K_e	Modulus of Elasticity
K_k	Modulus of delayed elasticity

K_w	CLT panel stiffness
K_{wt}	CLT panel stiffness at time *t*
L	Live load
L_{co}	Rested cable length
LiFS	Light-Frame Wood Systems
LVDT	Linear Variable Differential Transformer
LVL	Laminated Veneer Lumber
M	Actual moisture content
MC	Moisture Content
MC_a	Reference moisture content
MCE	Maximum Considered Earthquake
MC_i	Specimen Moisture content time *t*
M_o	Reference moisture content
MOE	Modulus of elasticity
NPE	Normalized Peak Error
P(t)	Post-tensioned force history
P_0	Post-tensioned force
PSL	Parallel Strand Lumber
PT	Post-tensioned
RH	Relative Humidity
RMS	Root Mean Square
R_u	Diffusion coefficient
R_x	Diffusion coefficient in x direction

R_{xa}	Absorbing diffusion coefficient in x direction
R_{xd}	Desorbing diffusion coefficient in x direction
R_y	Diffusion coefficient in y direction
R_z	Diffusion coefficient in z direction
SCL	Structural Composite Lumber
SPC	Specimen
SPF	Spruce, Pine, and Fir
t	Time
T	Actual temperature
T_o	Reference temperature
u^d	Designed displacement
u^m	Measured displacement
V	Volume
W	Specimen weight
W_0	Oven-dry specimen weight
α	Ratio between CLT MOE at time t and at the beginning

ACKNOWLEDGEMENTS

I would like to express my deepest gratitude to all individuals who helped make this dissertation possible. Without my advisors', Dr. Thang Dao and Dr. Kenneth Fridley, guidance, support, and encouragement, this dissertation would never have happened.

I would like to thank my committee members, Dr. Michael Kreger, Dr. Sriram Aaleti, and Dr. Semih Olcmen, for their insights, comments, and suggestions. My thanks are also extended to Korbir Hossain, Collin Sewell, and other colleagues for their enormous help and support throughout my Ph.D.

Finally, I would like to thank the support from the National Science Foundation (NFS) under the grant N0. – 1537788, and Vietnam International Education Development (VIED) and the Department of Civil, Construction and Environmental Engineering, the University of Alabama for the financial assistance.

CONTENTS

LIST OF TABLES

LIST OF FIGURES

CHAPTER 1

INTRODUCTION

1.1. Background and necessity of the research

Traditional Light Frame Wood Systems (LiFS), have been used for the low-rise buildings for a long time in the earthquake-prone areas thanks to its good seismic resistance (low mass and large energy dissipation through the deformation of connections, van de Lindt, 2004). However, the traditional LiFS configurations may not be feasible as the major structures in the tall wood buildings in which both large lateral and vertical loads may occur and structural stability is needed to avoid a collapse in a seismic event. Cross Laminated Timber (CLT) is a relatively new structural system first introduced in Europe in the early 1990s. CLT is classified as heavy timber and can provide both bearing and lateral force resisting capabilities. CLT has a larger mass than LiFS does and would result in a larger inertia force during an earthquake event. Therefore, the combination of CLT and LiFS is a perfect hybrid wood system that has a high resistance of both vertical and lateral loads and large energy dissipation during a seismic event. This study tries to address the problems arises when combining these two types of structures into a new hybridized wood system, CLT-LiFS.

1.2. Performances of the hybrid structural system under cyclic and earthquake loads

The lateral reversed-cyclic loading protocol was used to study the interaction between LiFS frame and the post-tensioned CLT panels. In this test, the CUREE protocol was applied under a displacement control on the top of a CLT-LiFS wall. This sub-component test is to

understand the challenge arising when combining CLT and LiFS structure to form the hybridized wood structure. The challenges may include the behavior of connections between the two, the ability to reserve good properties of each type of structure in the combination such as self-centering capability and energy dissipation. A real-time hybrid simulation was used to investigate the behaviors of CLT-LiFS building structure under dynamic loadings. The tested structure was a 3-story light-frame wood building with an integration of a hybrid wall in the first story. In this study, a real-time delay updated algorithm has been developed to reduce the undesirable effects of time delay to the real-time hybrid tests. A series of real-time hybrid simulations under different earthquake motions with different hazard levels were conducted to validate the time delay updated algorithm and to observe the behaviors of CLT and LiFS panels in a seismic event. The results are documented in chapter 2 of this dissertation.

1.3. Moisture content diffusion and creep behavior of CLT material

The performance of CLT-LiFS is governed by the self-centering capacity of the post-tensioned CLT panels and the energy dissipation in LiFS wall. The self-centering capacity in post-tensioned CLT panels relies on post-tensioning force in the tendon, which may reduce over time due to creep behavior in CLT panels. Therefore, the creep behavior of axially loaded CLT panel needs to be investigated so that such loss of tendon force can be controlled. The moisture content migration in CLT panels also needs to be considered in the study since it affects the creep behavior of CLT panels. Therefore, the moisture content diffusion and creep behavior of CLT are necessary to do research. Wood structures are susceptible to variation of the ambient environmental conditions such as relative humidity. Changing environmental conditions may lead to the change of the moisture content in a CLT specimen. Moisture content in a specimen can migrate from a point of higher moisture content to another point of lower moisture content,

thus the law of diffusion can be applied to model the moisture migration process. A series of moisture content tests were performed to observe the migration of moisture content in CLT material. A numerical model was developed and used to fit the experimental data to obtain moisture content diffusion coefficients. Besides moisture content diffusion, the creep deformation behaviors of CLT were also studied. A four-element creep model was proposed. This creep model included both the effects of changing ambient RH and viscous creep behavior. Experimental data under constant environmental conditions were used to calibrate the viscous creep model. A numerical example was also performed to validate the performances of the creep model under periodic RH change. The outcomes are reported in chapter 3.

1.4. Estimating the loss of cable force

Creep deformations in a material may cause additional deformations in CLT panels which could lead to the stress loss in pre-stressed cables. Controlling the loss in cable force in the post-tensioned CLT panels can help maintain the effectiveness of the post-tensioning system. A loss cable force model was developed to estimate the loss of cable force over time under the variations of the environmental conditions. The effects of changing environmental conditions were accounted for by adjusting the modulus of elasticity of CLT through the creep model that proposed in the previous part. Creep data under the constant environmental conditions from the previous study were also used to calibrate a FEM model. In order to avoid the complexity of the numerical analysis during the design process, a simplified equation was also developed to predict the change of post-tensioned cable force over time. A series of numerical analyses were also conducted to evaluate the simplified equation. The contents are presented in chapter 4.

The conclusions, outcomes of this study and recommendations for future research work are listed in chapter 5 of this dissertation.

CHAPTER 2

SEISMIC ASSESSMENT OF A THREE-STORY WOOD BUILDING WITH AN INTEGRATED CLT-LIGHTFRAME SYSTEM USING RTHS

Abstract

This chapter presents the results of an experimental study whose objective was to investigate the behavior of a hybrid wood shear-wall system defined herein as a combination of traditional light-frame wood shear walls with post-tensioned rocking Cross-Laminated Timber (CLT) panels. The post-tensioned CLT panels in the hybrid system offer both vertical and lateral load resistance and self-centering capacities. The traditional Light-Frame Wood Systems (LiFS) provide additional lateral load resistance along with a large amount of energy dissipation through the friction of nail connections. Thus a combination of these two types of structures may provide an excellent structural solution for mid-rise to tall wood buildings, where there is a need for resisting large lateral and vertical loads as well as structural stability. In this study, a real-time hybrid testing algorithm using a combination of time-delay updating and Newmark-Beta feed forward to reduce the undesirable effects of time delay was introduced. The top two-stories of a three-story building were modeled as a numerical substructure with the first story as the experimental CLT-LiFS substructure. The experimental results of the hybrid wall are presented and discussed in this chapter.

2.1. Introduction

Two types of structural systems, one based on a post-tensioning technology and one traditional and widespread can be optimally combined to exploit their beneficial features and

yield a new building system for tall wood buildings. Traditional wood-frame (light-frame wood) is light, as its name implies, would produce less earth quake force than other established post-tensioned heavy timber under an earthquake event. Cross-laminated timber (CLT) has both bearing and lateral force resisting capabilities. This chapter presents the results of an experimental study of a hybrid construction system (referred to hereafter as CLT-LiFS) which combines post-tensioned rocking CLT panels with traditional Light-Frame Wood Systems. The idea of post-tensioned rocking CLT walls is borrowed from a similar concept which was introduced for post-tensioned precast concrete building systems and Laminated Veneer Lumber (LVL) multi-storey buildings, (Priestley et al., 1999; Palermo et al., 2005).

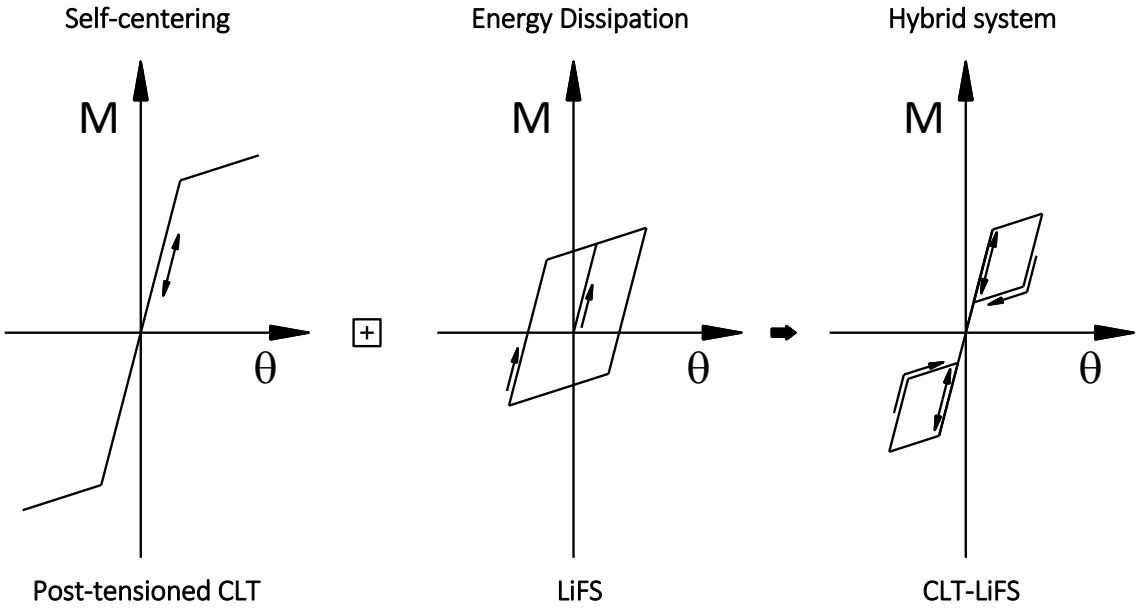

Fig. 2-1 Idealized flag-shaped hysteresis behavior

In the CLT-LiFS system, the post-tensioned rocking CLT panels provide re-centering capabilities for the structure, thus reduce the permanent residual deformations, and the energy dissipation is generated through the deformation of the light-frame wood shear-walls. A

reasonable combination of these two components produces flag-shape hysteretic behavior for hybrid system under cyclic loading, as shown in Fig. 2-1.

In a traditional light-frame wood system, wood studs are often framed to carry the gravity load. The sheathing (typically plywood or oriented strand board) is attached in one or two sides of the frame via fasteners such as nails or screws to increase the shear strength and in-plane stiffness of the walls. The nailed light-frame wood structure exhibits a good seismic-performance capacity due to its low seismic mass and large amount of energy dissipation via deformation of connections (van de Lindt, 2004). Tests have been conducted on the shear wall frames using monotonic, pseudo-dynamic, and shake tables to investigate the performance of the wood shear-walls with different types and schedules of fasteners as well as with various types of sheathing (e.g., Atherton, 1983; Nelson et al., 1985; Falk and Itani, 1987; Deam et al., 1991; Karacabeyli and Ceccotti, 1998; Pardoen et al., 2003).

While the behavior of traditional light-frame wood shear-wall structures under seismic loads is well understood (Folz and Filiatrault, 2004; van de Lindt and Dao, 2009; Shinde and Symans, 2010), only a handful of studies have implemented the use of CLT for shear walls subjected to earthquake loads (see e.g. Pei et al., 2013b; Sustersic, 2015; Rinaldin and Fragiacomo, 2016). CLT is an advanced wood-based product, initially developed in the mid-1990s in Europe. Many low-rise and mid-rise buildings using CLT as the main load resisting components have been built around the world since then (Rethinkwood, 2014). The popularity of CLT shows evidence of the practical and useful applications for this material. CLT is typically made by gluing small pieces of lumber stacked crosswise at a 90-degree angle to provide similar properties in both orthogonal directions. The dimensions of CLT panels vary from different manufactures and depend on the transportation means and the role of the CTL in a structure.

These often range from 2 ft. (0.61 m) to 16.5 ft. (5.03 m) in width and up to 60 ft. (18.29 m) in length. The number of layers is often 3, 5 or more, and the thickness can be up to 20 in. (0.51 m) (Mohammad et al., 2012), although typical thickness for a low to mid-rise building would be on the order of 4 in to 7 in (100 to 175 mm). CLT provides numerous advantageous properties such as high fire resistance, good thermal insulation (Mohammad et al., 2012). Because CLT panels are quite rigid, CLT systems themselves have low ductility, and most of the system ductility relies on connections between CLT panels. Some researchers were trying to enhance the CLT seismic-resistance by improving its ductility using different types of connectors. As part of the SOFIE project, Ceccotti et al. (2006) performed a series of tests on CLT panels with different connection configurations subjected to monotonic and cyclic loading protocols.

In the past decade, there have been many studies on hybrid systems, which combine structural panels with energy dissipating devices. Smith et al. (2007) introduced hybrid connectors for LVL structures. This type of connector combines unbonded post-tensioned cables with mild steel bars that serve as energy dissipation devices. With this connector design, the seismic energy was absorbed through inelastic damage of mild steel while the re-centering effects were provided by post-tensioned tendons. A series of tests on post-tensioned LVL walls coupled under quasi-static and pseudo-dynamic seismic loads were performed by Iqbal et al. (2012). The LVL walls were connected together using plywood sheathings and nail connectors, which acted as the energy dissipation devices in those tests. The results from the tests show that this hybrid system offered good seismic performance and only plywood sheathing was damaged after the tests. More recently, Loo et al. (2015) applied a hold-down connector that incorporated a slip-friction device. Experimental tests on an 8×8 ft. (2.44×2.44 m) rigid timber wall made of LVL panels were carried out with this type of connector. The results validated the feasibility of

using slip-friction devices as source for energy dissipation in stiff walls. Tests have been implemented for this kind of structure with quasi-static and pseudo-dynamic loading (Ceccotti et al., 2006; Iqbal et al., 2012).

In this study, the behaviors of a new hybrid wood system, post-tensioned CLT panels and light-frame wood shear walls, were investigated using real-time hybrid simulation. Real-time hybrid testing has been used in structural engineering for several decades beginning in the 1980's (e.g. Mahin et al., 1989), but for highly nonlinear structures has only been perfected after decades (Shing et al., 1996). This method can be applied not only for base excitation (e.g. earthquake) but also for other loading conditions. A real-time hybrid test can represent time-dependent non-linear dynamic effects, such as damping effects, which are difficult to model numerically in the pseudo-dynamic testing method. In addition to these many advantages, real-time hybrid testing methods also have limitations. Perhaps the largest of those is the time delay between the command sent to the actuator and the feedback signal. This time delay may cause instability of the system and/or inaccuracy of the structural response.

There are several sources that may cause the time delay such as the amount of time for the signal to travel through the controller, the time for actuator response itself, and the time to perform the computation. Nakashima et al. (1992) proved that in a linear-elastic SDOF testing system a time delay can introduce negative damping in the system, and the response will become unstable when this negative damping is larger than structural damping. Many techniques have been proposed to mitigate the effect of time delay, and the most widespread one was introduced by Horiuchi et al. (1999). In this method, the time delay can be considered as a constant, and the previous and current displacement values are used to predict the displacement of the upcoming step. The key feature of this method is the use of a polynomial for extrapolation, and the order of

the polynomial can be determined based on the desired accuracy of the calculation balanced with the increase in computation time.

Darby et al. (1999) considered the variation of the time delay and proposed a method to estimate the online delay time τ based on the measured displacement u^m. The calculated desired displacement u^d is given by

$$\tau_n = \tau_{n-1} + C_p \cdot \tanh\left(C_v \cdot \frac{u_n^d - u_{n-1}^d}{\Delta t}\right) \cdot (u_{n-1}^d - u_{n-1}^m) \tag{2.1}$$

The two constants C_p (proportional gain) and C_v (velocity gain) in this formula need to be selected by performing a scale excitation with the initial small value of C_p, and C_v set equal to 10 times the value of C_p. After running the test with the scale excitation to find the value of C_p and C_v the test can be implemented with full-scale input. This method can provide the estimation of updated value time delay τ. However, it has two limitations; the first is that the value of C_p and C_v should be selected before performing each test. Second, the procedure for finding these values is time consuming.

Ahmadizadeh et al. (2007) presents a direct method to estimate delay time τ by using the last three data points of desired and measured u^d and u^m displacement

$$\tau_n = \tau_{n-1} + 2 \cdot G \cdot \Delta t \cdot \frac{u_n^{ad} - u_n^{am}}{u_n^m - u_{n-2}^m} \tag{2.2a}$$

$$u_n^{ad} = \frac{u_n^d + u_{n-1}^d + u_{n-2}^d}{3} \quad and \quad u_n^{am} = \frac{u_n^m + u_{n-1}^m + u_{n-2}^m}{3} \tag{2.2b, 2.2c}$$

A good advantage of this method is that no experimental setup is required. However, the constant G (learning gain) still needs to be determined before the test.

Another method to compensate for the time delay was presented in an experiment done by Shao et al. (2014). The first-order and second-order feed-forward (Lamarche et al., 2010;

Dion et al., 2011) algorithms were used to compensate for the time delay for a traditional wood shear-wall. The time delay was considered as a constant and calibrated before performing the test. The two disadvantages of this method should also be considered. First, each test will have a different optimum value of time delay, and calibration steps for estimating τ should thus be performed for every test. Second, using a constant value for τ may cause larger errors.

In this chapter, a new approach for calculating the online time delay to improve real-time hybrid testing is presented. The results for a real-time hybrid simulation of a CLT-LiFS wall using light-frame wood systems and post-tensioned rocking CLT panels subjected to cyclic and seismic loading will be presented and discussed.

2.2. Algorithms for calculating real-time delay and numerical simulation

2.2.1. Real-time delay updated algorithms

The linear interpolation method was used to find the time delay at each step of the simulation history. At each time step, the current desired displacements and the measured displacements were recorded and saved. Depending on the maximum number of intended step-backs, *n*, the corresponding number of data points were saved and updated. Within the small time interval the correlation between time and displacements is considered to be able to be approximated by a linear relation. The value of time delay τ, thus can be calculated based on u_i^d, u_i^m and u_{i-n}^d as:

$$\tau_i = n \cdot \Delta t + \Delta t \cdot \frac{u_i^m - u_{i-n}^d}{u_{i-n-1}^d - u_{i-n}^d} \tag{2.3}$$

where, u_i^d and u_i^m are desired displacement and measured (feedback) displacement at the current step *i*; u_{i-n}^d and u_{i-n-1}^d are desired displacements at time steps *i-n* and *i-n-1*; Δt is the time step. In each iteration loop, based on the current measured displacement value u_i^m a value in

the recorded measured displacements that satisfies the expression $u_{i-n-1}^{d} \leq u_i^m \leq u_{i-n}^{d}$ is determined. Within a specified number of back-tracking steps, if the desired displacement value u_i^m that fulfills the expression $u_{i-n-1}^{d} \leq u_i^m \leq u_{i-n}^{d}$ cannot be found, the result of τ_i in this step is set equal to the value of τ_{i-1} in the previous step. The flowchart for this algorithm can be seen in Fig. 2-2.

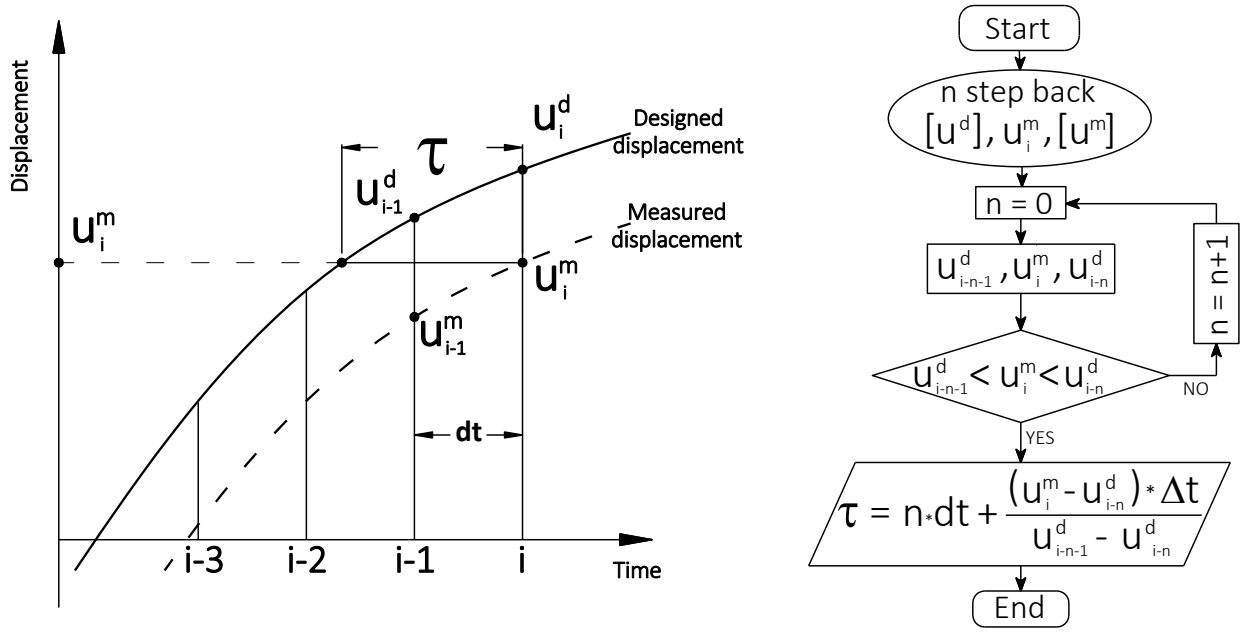

Fig. 2-2 Flowchart for finding τ

After the time delay at each integration step is calculated and updated, the Newmark-β feedforward method is used to calculate the displacement command for next time step.

2.2.2. Numerical model

A numerical model was developed for the real-time hybrid simulation conducted in this study. In this real-time hybrid simulation, the experimental substructure was assumed to be a 3-story building with an 18×36 ft. (5.48×10.97 m) rectangular footprint. The total building height was 3×8 ft. = 24 ft. (7.31 m). The physical substructure being tested was an 18×8 ft. (5.48×2.43 m) hybrid wall (CLT-LiFS) located in the middle wall line of the first floor. The floor

diaphragms were assumed to be traditional joist-sheathing structures and modeled as linear shear elements (Dao and van de Lindt 2014). The time-dependent non-linear effects in the real CLT-structures such as inertia forces, wall damping and friction forces measured by a built-in sensor in actuator load cell were updated and included in numerical calculations at each time step.

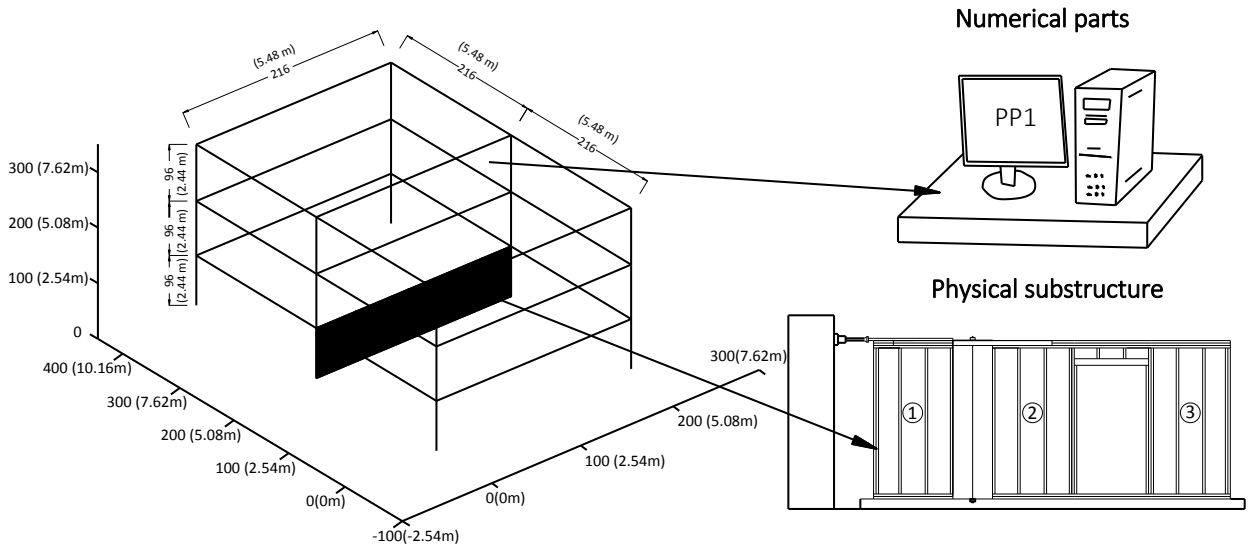

Fig. 2-3 Location of experimental panel in test structure

The other parts of the building were made of a light-frame wood system and were modeled numerically using data from a study by Shao et al. (2014) and non-linear shear element introduced by Dao and van de Lindt (2014). The configuration of the 3-story building is shown in Fig. 2-3. The total mass applied to the numerical model of the tested structure was 20 psf (0.96 kPa) of dead load plus 50 psf (2.39 kPa) of live load applied on each floor, and the wall dead load was 45 psf (2.15 kPa). The floor was considered as a linear panel with a stiffness K_0 = 5.88 kips/in (10.29 KN/cm). The nonlinear hysteretic behavior of the LiFS was modeled using the 10-parameter model introduced by Folz and Filiatrault (2001). There were two types of LiFS panels in the building, 12×8 ft. (3.66×2.44 m) and 18×8 ft. (5.48×2.44 m) panels. Table 2-1 shows the ten parameters for each panel type in which those for the 12×8ft (3.66×2.44m) panel

were obtained from a study by Shao et al. (2014). The ten parameters for the 18×8ft. (5.48×2.44m) panel were induced by scaling stiffness (or scaling K_0, F_0, F_1) over the length of the 12×8ft. (3.66×2.44m) panel. Interested readers are referred to Folz and Filiatrault (2001) for more details on the 10-parameter hysteretic model.

Table 2-1 Values of ten parameters for the LiFS hysteretic model

Parameter	K_0	r_1	r_2	r_3	r_4	F_0	F_1	δ	α	β
12×8 ft. panel	8.82	0.067	-0.132	1.164	0.012	5.0	0.58	3.81	0.75	1.10
18×8 ft. panel	13.23	0.067	-0.132	1.164	0.012	7.5	0.87	3.81	0.75	1.10

2.3. Experimental work

2.3.1. Testing objectives

This test program represents for the first time a study on a hybrid system consisting of CLT and light-frame wood, thus the experimental program aimed to enable an understanding of the structural behavior of this system under several different loading protocols. There were two phases to the experimental program in this study. In the first phase, a lateral reversed-cyclic loading protocol was used to study the interaction between traditional wood shear walls and the post-tensioned CLT panels, e.g. the damage pattern in each component and the connections between the two including potential issues of deformation compatibility. In the second phase, a series of real-time hybrid simulations were conducted under different ground motions. The purposes of these experiments were to validate the real-time delay update algorithm and to observe the behaviors of CLT and LiFS panels. In this second testing phase, a new CLT-LiFS wall (with the same configuration of the wall in phase 1) was built and integrated in the three-story numerical building as shown in Fig. 2-3.

2.3.2. Test structure

In test phase 1, the CLT-LiFS wall was 18 ft. (5.48 m) long, 8 ft. (2.44 m) high. This wall consisted of a five-layer post-tensioned CLT panel with the dimensions of 5.25 in.×2 ft.×8 ft. (0.133×0.61×2.44 m), three LiFS panels, and one door-opening panel, as shown in Fig. 2-4. The LiFS panels were made of 2×6 in. (actual dimension 1.5×5.5 in.) Spruce-Pine-Fir studs and 15/32 in. (1.19 cm) plywood sheathing. The 8d box nails (2.5×0.113 in., 6.4×0.287 cm) were used as fasteners connecting sheathing to the frame. The field nail spacing was 12 in. (30.5 cm) and the edge nails were placed 6 in. (15.2 cm) distance. The CLT panel was attached to the studs of the light-frame wood panels using six 16d common nails (3.5×0.135 in., 8.9×0.343 cm) on each side and spaced at 24 in. (0.61 m) on center. In the post-tensioned CLT panel, a tendon (7 wires with 0.5 in. (1.27 cm) diameter) was installed through a predesigned hole along the height of the panel at the cross-section center. The CLT panel was then installed in the testing position with one end of the tendon anchored in a steel beam tied-down to the strong floor and the other end anchored at the top of the load cell placed on the top of CLT panel. A steel plate was placed on the top of the CLT panel between CLT panel and load cell to prevent the CLT panel from local failure under post-tensioned load. The post-tensioned force applied in the tendon was 22 kips (97.86 KN). Table 2-2 provides the properties of CLT (CLT Handbook US Edition, 2013) and the properties of the tendon (Sumidenwire, 2014).

A set of real-time hybrid simulations on a 3D 3-story building was conducted in phase 2. The middle wall of the first story of the 3D 3-story building was a CLT-LiFS wall (as shown in Fig. 2-3) and was physically modeled during the hybrid test. The other components such as floors and other light-frame wood shear-walls were numerically modeled on computer. These

light-frame wood shear-walls had the same nail pattern and stud spacing as those used in CLT-LIFS wall, but had different lengths.

Table 2-2 CLT and tendon properties

CLT	Compressive strength parallel to grain	28	MPa	CLT Handbook US Edition
	Elastic modulus parallel to the grain	11720	MPa	CLT Handbook US Edition
Tendon	Yield strength	1530	MPa	Sumidenwire, 2014
	Ultimate strength	1860	MPa	Sumidenwire, 2014
	Elastic Modulus	200	GPa	Sumidenwire, 2014

2.3.3. Experimental Set-up

The hydraulic equipment and controller components in The Large Scale Structural Engineering Laboratory at The University of Alabama were used to perform the test. Table 2-3 presents the detailed technical specifications for the hydraulic and controller systems. The tested structures were connected to the steel beam at the bottom through the post-tensioned tendon in the CLT panel and via the 5/8 in. (1.58 cm) anchor bolts in the LiFS panels. The details of the location of the bolts are shown in Fig. 2-4.

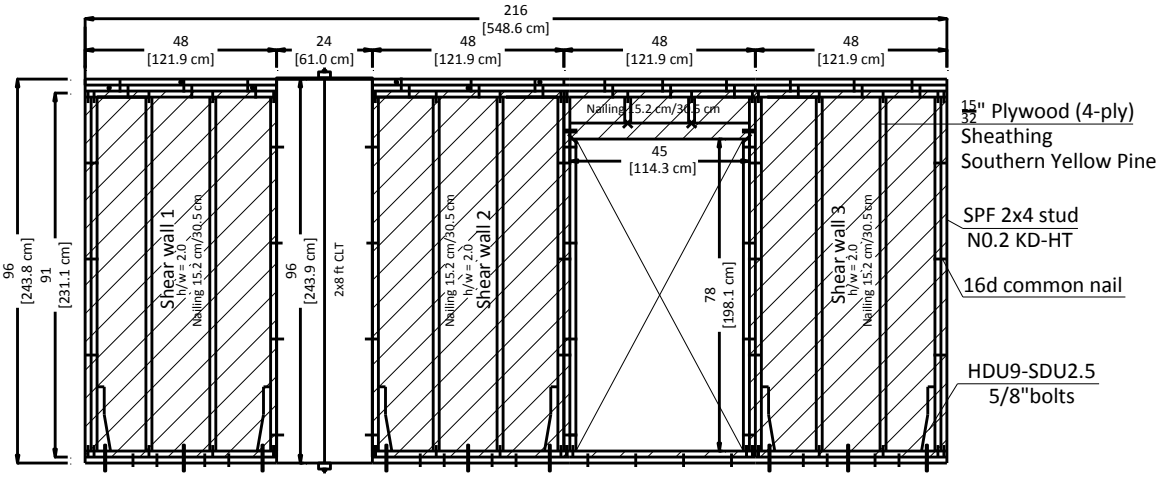

Fig. 2-4 The configuration of CLT-LiFS wall

At the double studs and single studs on both sides of the CLT panel, Simpson Strong Tie HUD9-SDU2.5 hold-downs were used to restrain the overturning effect. The cable force in CLT panel was the only the vertical load that was considered in the CLT specimen. Other types of vertical loads such as dead loads and live loads of the walls and the floors were included in the numerical model and carried by light-frame wood structures.

Table 2-3 Hydraulic equipment and Controller components

Hydraulic equipment			Controller components	
Linear hydraulic actuator	Model	MTS 244.31	Hydraulic controller	MTS series 793 w/DAQ
	Force	± 55 kips	Hybrid testing controller simulation software	Matlab/Simulink
	Stroke	± 22 inches	Hybrid testing controller interface to real-time controller	Matlab/xPC Target
	Max vel.	50 in/s	External I/O interface	SCRAMNet GT150
Load transducer		55 kips	Real-time controller	3.0 GHz Xeon Dual-Core Real-time Target PC
Servo vale		250 gpm at 2800psi		

In both CLT-LiFS walls, the load protocol was applied using displacement control for the hydraulic actuator attached to the top of the tested structure. The out-of-plane movement of the wall was resisted by six rolling bearers, as shown in Fig. 2-5.

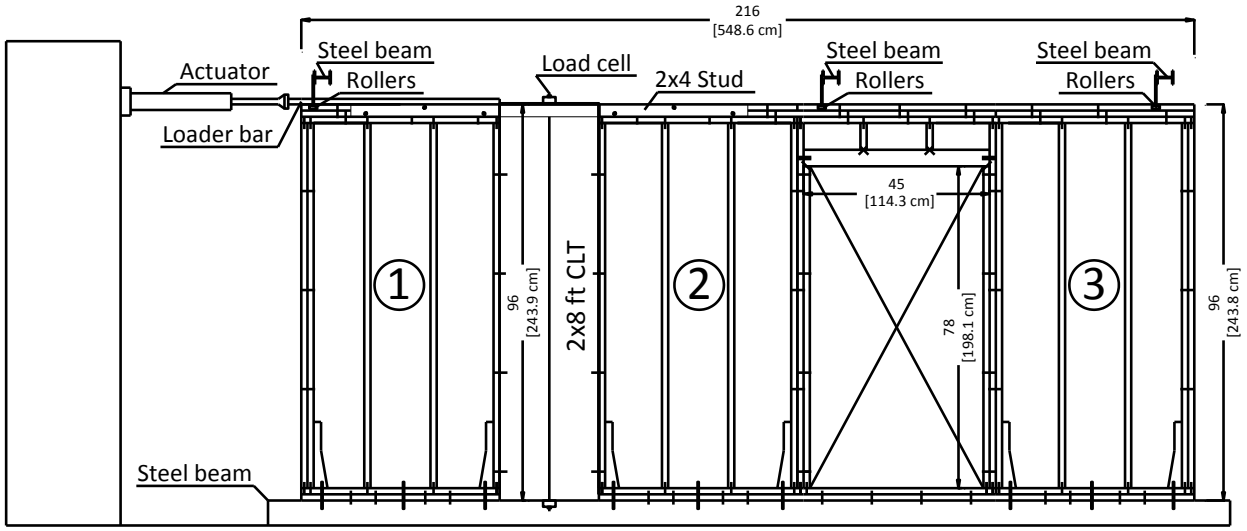

a) Schematic of the CLT-LiFS wall

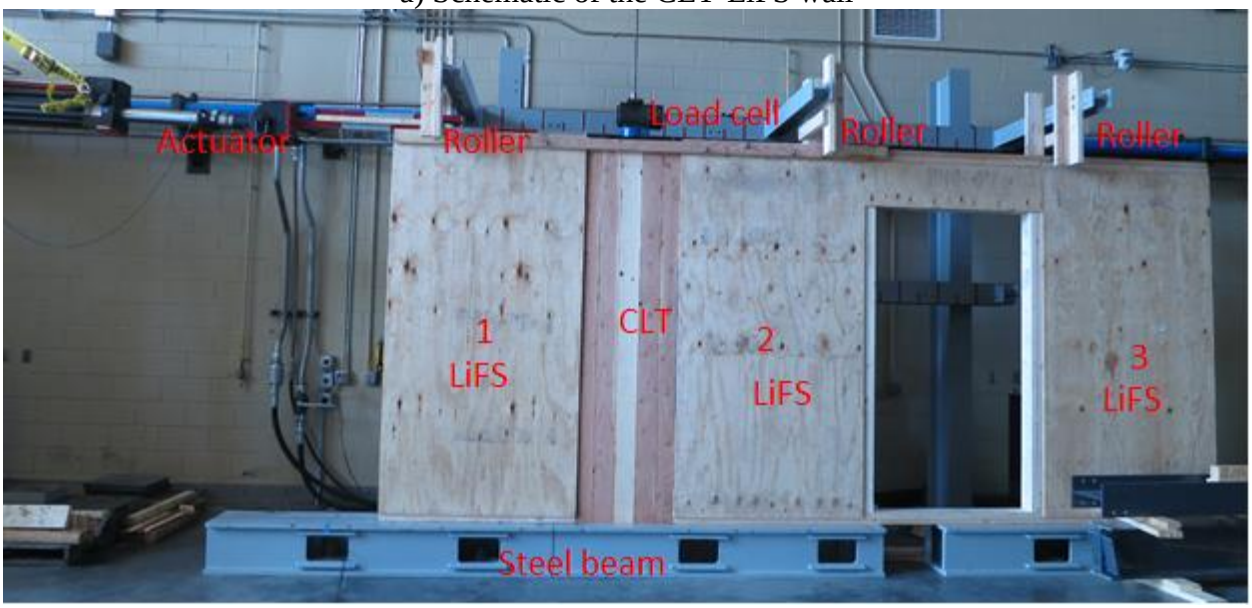

b) The CLT-LiFS wall setup ready for testing

Fig. 2-5 CLT-LiFS wall

The instrumentation included a load-cell installed on top of the CLT panel to monitor the changes of post-tensioned forces in tendon and two linear variable differential transformers (LVDTs) placed on the CLT panel edges to measure the displacements between the CLT panel and LiFS walls. The data collected from these sensors was recorded by the DAQ system.

2.3.4. Cyclic test for hybrid wall

The CUREE cyclic loading protocol (Krawinkler, 2009) was used for the cyclic test. In this cyclic test, the maximum displacement of each cycle was increased for every three cycles. An increment of 0.1 in. was exerted to peak displacement less than 1 in. After the peak displacement reached to 1 in., this increment was changed to 0.2 in., as shown in Fig. 2-6a. A hydraulic actuator was attached to the top of the CLT-LiFS wall and the test protocol was applied through this actuator under displacement control.

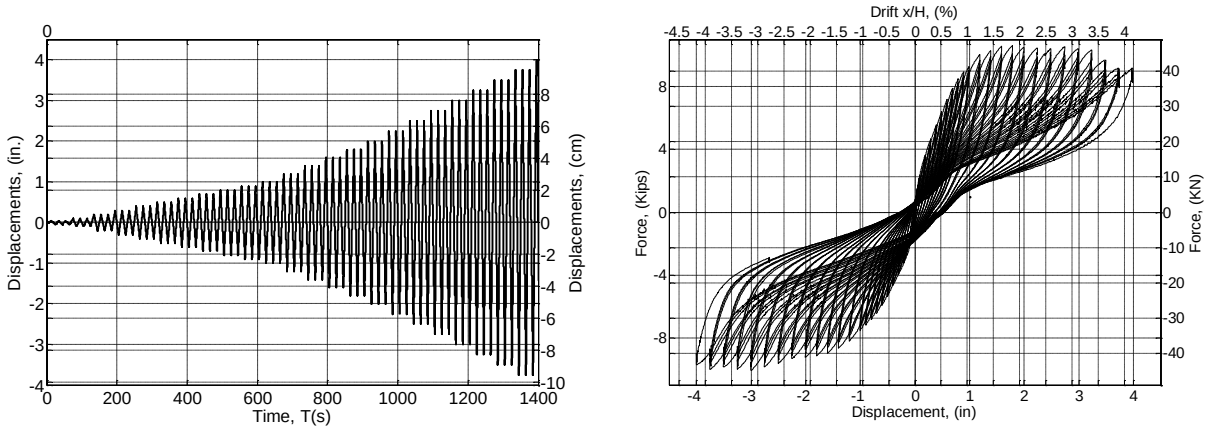

a) Test protocol b) Force-displacement hysteresis

Fig. 2-6 Cyclic loading protocol and CLT-LiFS hysteretic

The force and displacement at the top of the CLT-LiFS wall were recorded during the test using the sensors installed inside the actuator. The relationship between force and displacement is plotted in Fig. 2-6b.

2.3.4.1. Hybrid shear wall damages under cyclic loading

As can be seen in the hysteresis plot in Fig. 2-6, the CLT-LiFS wall reached the peak force of 10.5 kips (46.7 KN) with the top wall drift at 1.75 in. (4.45 cm). Due to the large displacement on the top of the CLT-LiFS wall during the cyclic test, the wall exhibited some damage. The nails that connected the post-tensioned CLT panel with LiFS wall were fractured

and large gaps between these two components were observed by the end of the tests. Some edge nails at the bottom perimeter of the LiFS wall were completely pulled out. In the other parts, the nails were partially pulled out around 1 in. (2.54 cm), but no sheared off nails were observed. From the hysteresis shown in Fig. 2-6b, a residual displacement is calculated at which the lateral force measured by sensor in actuator is zero. It can be observed that the residual displacement of the CLT-LiFS wall was very small, about 0.45 in. (1.143 cm) compared with 6 in. for light-frame wood structure alone (Shao et al. 2014). This indicates the excellent self-centering capability of the post-tensioned CLT panel in this new hybrid structural system. Fig. 2-7 shows the damages on CLT-LiFS wall after the cyclic test. Even though the self-centering effect was improved, the residual displacement of the CLT-LiFS cannot be eliminated due to the residual force (the force at zero displacement) in LiFS causes elastic displacement on the top of CLT panel, which does not depend on the post-tensioned force in tendon. This effect can be seen clearly by adding the hysteresis of top displacements of CLT panel and light-frame wood structures. For more information, the readers can refer to a study by Ho et al. (2016).

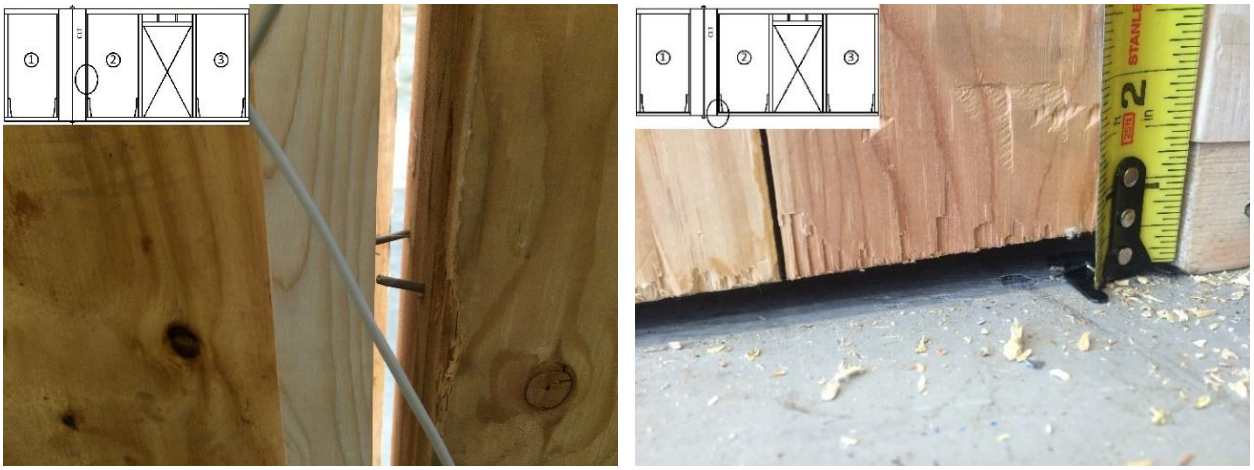

Fig. 2-7 Damages on CLT-LiFS wall after the cyclic test

2.3.5. Real-time hybrid simulations of 3D-three story Building

The 6.7 Magnitude Northridge earthquake (Beverly Hills recording) in 1994 was utilized to conduct the real-time hybrid test. Three different hazard levels, namely 44% Design Basis Earthquake (DBE) and Maximum Considered Earthquake (MCE) were considered. The DBE is defined as 2/3 of the MCE, where the MCE has a 2% probability of exceedance in 50 years.

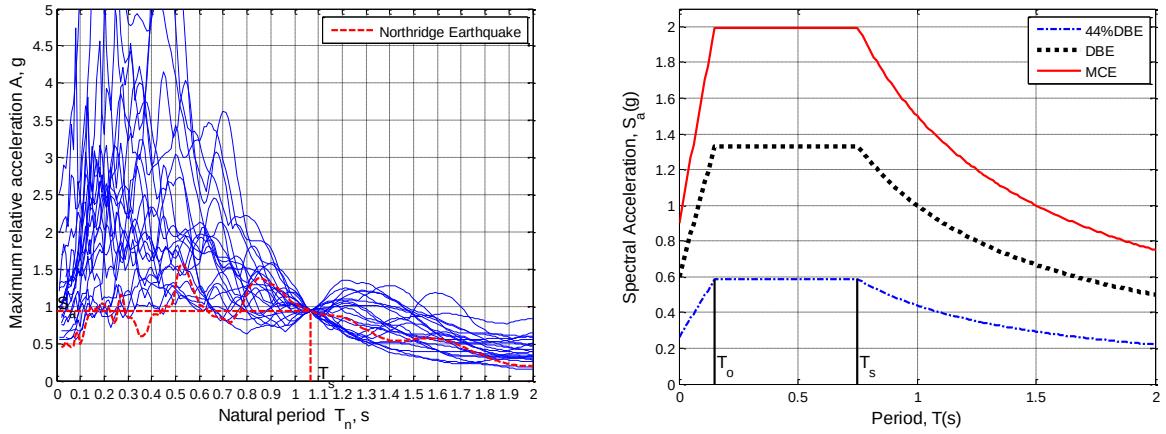

a) Scaling spectrum of earthquakes b) Design acceleration response spectra

Fig. 2-8 ATC-63 scaling spectrum and Design acceleration response spectra for 5% damping

This is an initial study to investigate the interaction between two types of structure under hybrid simulation. No specific evaluation for this hybrid type of structure has been made before.

Therefore, the three-story building with a 5% of damping has been chosen for the tests. Based on information provided in the previous sections, the natural period of the 3D 3-story building was numerically calculated as a 1.066 s. The period appears to be long due to the stiffness of the tested structure is too small. In the 3D 3-story building, the lateral structural stiffness was provided by three light-frame wood shear-walls which seems not to be stiff enough for the building under an earthquake event. The structure was assumed to be built on the stiff soil class D in California. The mapped MCE spectral response acceleration parameter at short periods S_s = 2g, and at a period 1s, S_1 = 1g were determined using the seismic maps specified by ASCE7/SEI, (2010). The site coefficient for the short period was F_a = 1 and at a period of 1 s was F_v = 1.5. The provided information was used to construct the design acceleration response spectra, as shown in Fig. 2-8. After performing the real-time hybrid simulations using the Northridge earthquake motions at 44% DBE, DBE and MCE level, the physical CLT-LIFS wall was observed to have no significant damage.

To check the statistical properties of building response, the ground motions from the ATC-63 project list (ATC, 2009) were used to perform 22 hybrid tests at 44% DBE level and 22 tests at DBE level, respectively. At the end of each test, the structural response and peak drift were recorded. In addition, numerical simulations for CLT-LiFS structure subjected to 22 earthquakes were also analyzed at the MCE level. These data then were used to fit the cumulative distribution function of the peak story drift as shown in Fig. 2-9. The experimental and numerical data were plotted in Fig. 2-9. Information of 22 ground motions, design hazard levels and peak ground acceleration are listed in Table 2-4.

Table 2-4 Earthquake, hazard level and amplitude scaling factor

Test ID	Earthquake	Record station	Hazard level	PGA (g)
1	Northridge	Beverly Hills	DBE	0.183
2	Northridge	Canyon Country	DBE	0.275
3	Duzce, Turkey	Bolu	DBE	0.354
4	Hector Mine	Hector	DBE	0.249
5	Imperial Valley	Delta	DBE	0.312
6	Imperial Valley	El Centro Array #11	DBE	0.262
7	Kobe, Japan	Nishi-Akashi	DBE	0.357
8	Kobe, Japan	Shin-Osaka	DBE	0.182
9	Kocaeli, Turkey	Duzce	DBE	0.168
10	Kocaeli, Turkey	Arcelik	DBE	0.201
11	Landers	Yermo Fire Station	DBE	0.164
12	Landers	Coolwater	DBE	0.325
13	Loma Prieta	Capitola	DBE	0.391
14	Loma Prieta	Gilroy Array #3	DBE	0.333
15	Manjil, Iran	Abbar	DBE	0.268
16	Superstition Hills	El Centro Imp. Co. Cent	DBE	0.211
17	Superstition Hills	Poe Road (temp)	DBE	0.240
18	Cape Mendocino	Rio Dell Overpass - FF	DBE	0.307
19	Chi-Chi, Taiwan	CHY101	DBE	0.123
20	Chi-Chi, Taiwan	TCU045	DBE	0.333
21	San Fernando	LA - Hollywood Stor FF	DBE	0.300
22	Friuli, Italy	Tolmezzo	DBE	0.309

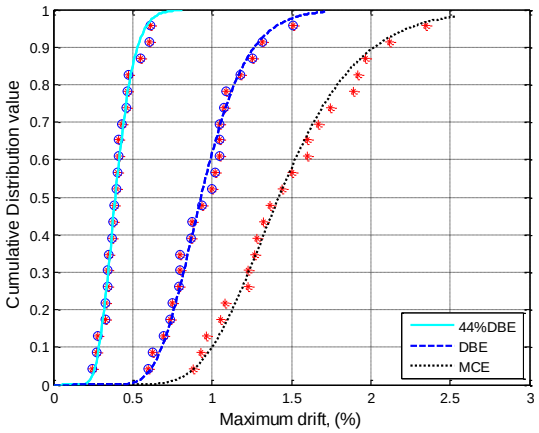

Fig. 2-9 Peak story drift distribution for 44%DBE, DBE and MCE level

2.3.5.1. Hybrid shear wall damages under earthquake motions

The CLT-LiFS wall was integrated in a 3-story numerical building and tested under the Northridge earthquake ground motion scaled at 44%DBE, DBE and MCE level. A visual check was performed at the end of each test. No major damage was observed on the CLT-LiFS wall components and connections at these hazard levels. Since the goal of this study for the new hybridized structural system was to examine the behavior of this new system, the analysis is focused more on how the post-tensioned CLT panels and light-frame wood structures work in the new system. Test result for a single post-tensioned CLT under the cyclic loading from the previous study (Ho et al., 2016) was used for reference. Fig. 2-10 shows the force-displacement hysteresis of the CLT panel. It should be noticed that at the maximum displacement of 0.8 in, there was no significant damage observed and most of the energy dissipation in the hysteretic loop was due to the friction in connections and structural components.

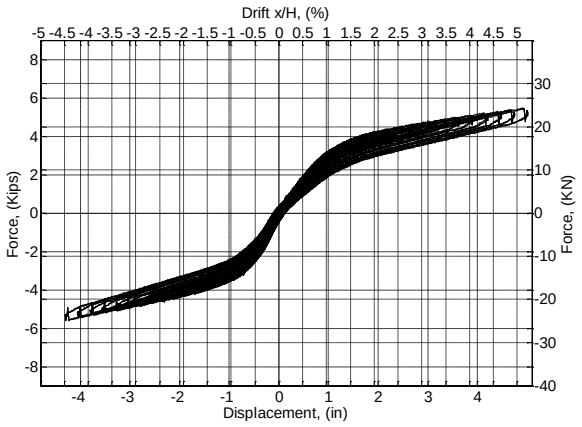

Fig. 2-10 CLT hysteretic (Ho et al., 2016)

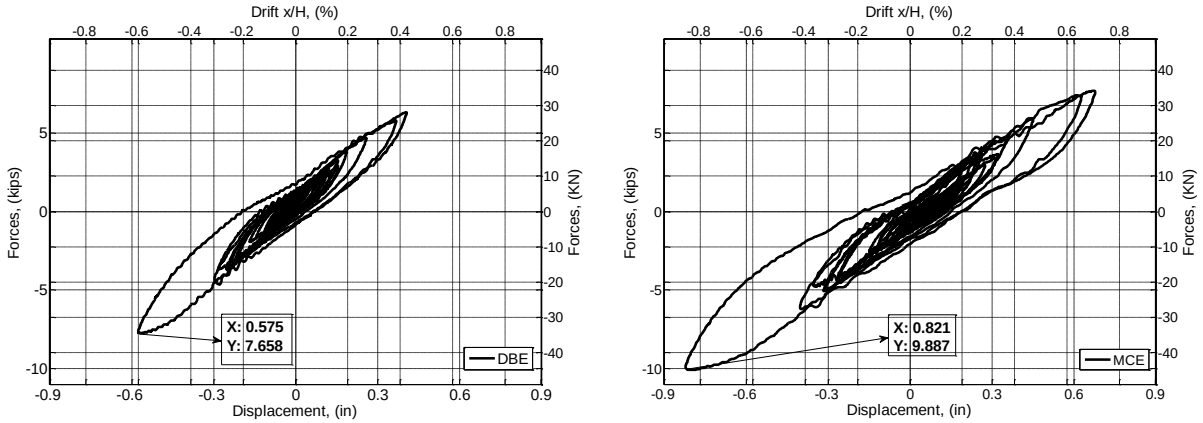

a) At DBE level b) At MCE level

Fig. 2-11 Hysteretic of Hybrid wall under Northridge Earthquake

The trend of force-displacement curve of hybrid wall in dynamic test is similar to that of cyclic test (Fig. 2-6) except the force is higher due to the inertia and damping force were included in Fig. 2-11a and Fig. 2-11b. Comparing the test results from the post-tensioned CLT under cyclic load, the energy dissipation of CLT-LiFS specimen under both cyclic and dynamic load (Fig. 2-6 and Fig. 2-11) was also larger than that of the post-tensioned CLT alone (Fig. 2-10).

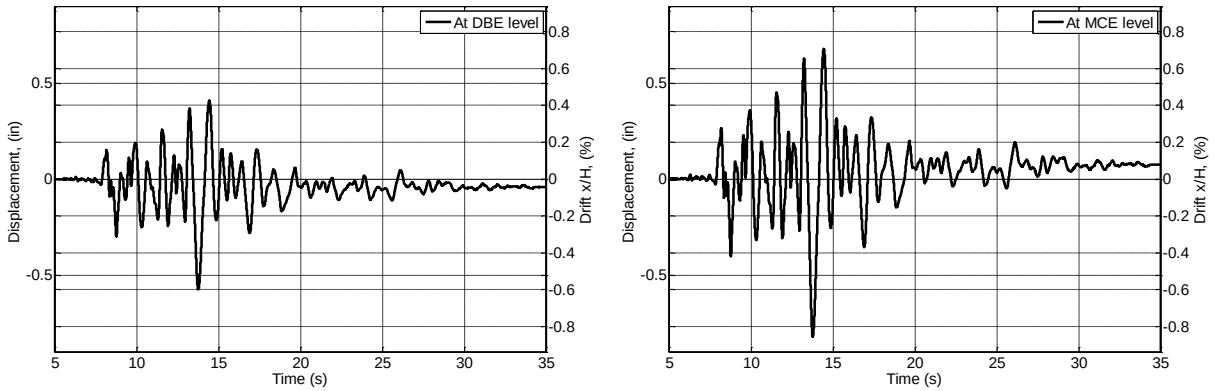

a) At DBE level b) At MCE level

Fig. 2-12 Residual deformation of Hybrid wall under Northridge Earthquake

At the DBE level, the maximum displacement on the top of the CLT-LiFS wall was 0.575 in. (1.46 cm) at which the resisting force of 7.66 kips (34.07 KN) was recorded (Fig. 2-11a). The displacement here includes the dynamic effects. The peak residual deformation in this case was at around 0.05 in. (0.127 cm), as shown in Fig. 2-12a. The maximum residual deformation in this case was smaller in comparison with that of the previous study on a light-frame wood wall (Shao et al. 2014) which was around 0.75 in. The maximum residual deformation of the CLT-LiFS under the MCE level was 0.03 in. (0.076 cm), as in Fig. 2-12b.

2.3.5.2. Time history response of RTHS with updated delay algorithm

In order to evaluate the performance of real-time hybrid tests over time, the Normalized Peak Error (NPE) and Root Mean Square (RMS) were used to calculate the difference between the desired displacements and measured displacements. Different values of NPEs and RMSs at different hazard levels were presented in Table 2-5 for the test with ground motion input recorded from the Northridge earthquake. For comparison purpose, Table 2-5 also includes results from a study by Shao et al. (2014) in which the same earthquake record but constant time delay were used.

Table 2-5 Value NPE and RMS at different hazard levels

Test	ID	Level	NPE (%)	RMS (%)
This study	1	44%DBE	2.02	1.65
	2	DBE	1.9	0.98
	3	MCE	2.25	1.11
Shao Damper wall	a	30%DBE	1.53	3.03
	b	DBE	2.13	2.64

As can be seen from Table 2-5, the experimental results showed that the new algorithm using real-time delay updated for compensating the time delay worked very well. The maximum NPE was 2.25% in the test at MCE level and the maximum value for RMS was 1.65% at 44%DBE hazard level. These values indicate that the proposed algorithm was reliable and acceptable for simulating the seismic response. Fig. 2-13b showed the differences between the measured displacements to the desired displacements of the CLT-LiFS wall under the Northridge Earthquake at DBE level.

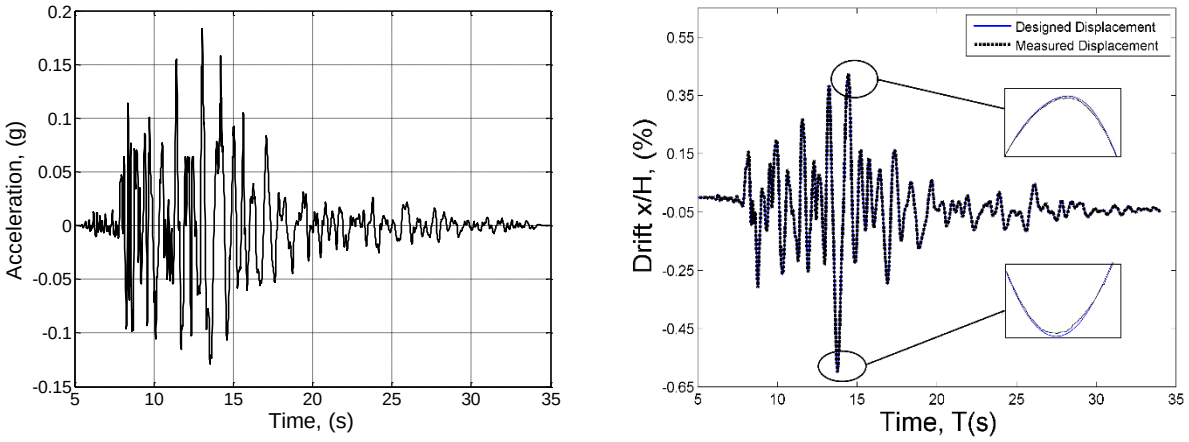

a) Northridge Earthquake b) CLTT-LiFS response

Fig. 2-13 Displacement response of CLTT-LiFS under Northridge Earthquake at DBE level

2.4. Conclusions

In this chapter, the real-time delay updated algorithm was applied to improve the real-time hybrid simulation on CLT-LiFS system. A series of experimental tests were implemented on CLT-LiFS component subjected to cyclic and earthquake loading. Results from hybrid simulation of the 3D-three story building under different ground motions were also included.

The new algorithm for calculating online updated and compensating time delay was found to be accurate enough to be used in hybrid simulation. The NPE and RMS values from the experimental test were 1.90% and 0.98%, respectively, at the DBE level. The CLT-LiFS wall performed very well under MCE level due to the high stiffness, efficient self-centering capability provided by the post-tensioned CLT panel and the large amount of energy dissipation provided by the LiFS wall. The maximum drift recorded at MCE intensity level was smaller than 1%. A minor amount of residual deformation, approximately 0.2 in. (0.508 cm), was present after the test. The stiffness of CLT panel dominated the rigidity of the CLT-LiFS wall as was expected. Finally, it can be concluded that the CLT-LiFS system shows promise and should be investigated in an array of systems including under bi-axial loading.

2.5. References

Ahmadizadeh M, Mosqueda G, Reinhorn AM. (2011). “Compensation of actuator delay and dynamics for real-time hybrid structural simulation”. Earthquake Engineering & Structural Dynamics, 37(1):21–42.

ASCE/SEI (2010). “Minimum Design Loads for Buildings and Other Structures”. Reston, VA: American Society of Civil Engineers (ASCE).

ATC (2009). “Quantification of Building Seismic Performance Factors”, ATC-63, Project Report, Applied Technology Council, Redwood City, CA.

Atherton, G. H. (1983). ‘‘Ultimate strength of structural particleboard diaphragms.’’ Forest Products. J., 33(5), 22–26.

B. Yeh, D. Kretchmann, B. J. Wang. (2013). “Cross-laminated timber Manufactoring.” Chapter 2, CLT Hanbook: Crosslaminated timber - US edition. FPInnovations, Pointe-Claire, QC, Canada.

Ceccotti A., Follesa M., Lauriola M.P., Sandhaas C. (2006b). Sofie Project – Test Results on the Lateral Resistance of Cross-Laminated Wooden Panels. First European Conference on Earthquake Engineering and Seismicity, Geneva, Switzerland.

Dao, T. N., and van de Lindt, J. W. (2014). “Numerical Seismic Performance of an Innovative CFS Mid-Rise Building Designed using DDD”. ASCE Journal of Performance of Constructed Facilities, Vol 28 (5), 04014018.

Darby, A. P., Williams, M. S., & Blakeborough, A. (1999). “Stability and delay compensation for real-time substructure testing.” Journal of Engineering Mechanics, ASCE, 128(12): 1276-1284.

Deam, B. L., Dean, J. A., and Buchanan, A. H. (1991). ‘‘Full scale testing of 3-story plywood shearwalls.’’ Proc., Pacific Conf. on Earthquake Engineering.

Dion, C., Bouaanani, N., Tremblay, R., Lamarche, C.P., and Leclerc, M. (2011). "Real-time dynamic substructuring testing of viscous seismic protective devices for bridge structures", Eng. Struct., 33(12), 3351-3363.

Falk, R. H., and Itani, R. Y. (1987). ‘‘Dynamic characteristics of wood and gypsum diaphragms.’’ J. Struct. Eng., 113(6), 1357–1370.

Folz, B. and Filiatrault, A. (2004). “Seismic Analysis of Woodframe Structures. I: Model Formulation,” Journal of Structural Engineering, 130(9), 1353-1360.

Ho, T.X., Dao, T.N., Aaleti, S., van de Lindt, J.W., Rammer, D.R. (2016). “Hybrid System of Unbonded Post-tensioned CLT Panels and Light-Frame Wood Shear Walls”, ASCE Journal of Structural Engineering; ISSN 0733-9445, 04016171.

Iqbal, A., Pampanin, S., Fragiacomo, M., Palermo, A. and Buchanan, A. (2012). “Seismic Response of post-tensioned LVL walls coupled with plywood sheets”. Auckland, New Zealand: World Conference in Timber Engineering, Jul 2012.

Iztok Sustersic, Massimo Fragiacomo, and Bruno Dujic. (2015). “Seismic Analysis of Cross-Laminated Multistory Timber Buildings Using Code-Prescribed Methods: Influence of Panel Size, Connection Ductility, and Schematization”. 10.1061/ (ASCE) ST.1943-541X.0001344. American Society of Civil Engineers.

Jayesh K. Shinde and Michael D. Symans. (2010). “Seismic Performance of Light-Framed Wood Structures with Toggle-Braced Fluid Dampers”, 2010 Structures Congress © 2010 ASCE.

Karacabeyli, E., and Ceccotti, A. (1998). ‘‘Nailed wood-frame shear walls for seismic loads: Test results and design considerations.’’ Proc., Structural Engineering Worldwide, Paper No. T207-6, Elsevier Science, New York.

Krawinkler, H., Parisi, F., Ibarra, L., Ayoub, A., Medina, R., (2001). “Development of a testing protocol for woodframe structures,” CUREE Publication, No. W-02, Richmond, Calif.

Lamarche, C.P., Tremblay, R., Léger, P., Leclerc, M. and Bursi, O.S. (2010). “Comparison between real-time dynamic substructuring and shake table testing techniques for nonlinear seismic applications”, Earth. Eng. & Struct. Dyn. 39(12): 1299–1320.

Loo, W., Quenneville, P., and Chouw, N. (2015). "Rocking Timber Structure with Slip-Friction Connectors Conceptualized As a Plastically Deformable Hinge within a Multistory Shear Wall." J. Struct. Eng., 10.1061 / (ASCE) ST.1943-541X.0001387 , E4015010.

M. Mohammad, Sylvain Gagnon, Eng., Bradford K. Douglas, P.E., Lisa Podesto P.E., (2012). “Introduction to Cross Laminated Timber.” Wood Design Focus, 22(2).

Mahin, S. A., Shing, P. B., Thewalt, C. R., & Hanson, R. D. (1989) “Pseudodynamic test method. Current status and future directions.” Journal of Structural Engineering, ASCE, 115(8): 2113-2128.

NAHB Research Center Inc. (2000). “Residential Structural Design Guide”. Chapter 3: Design Loads for Residential Buildings.

Nakashima, Kato, M., H. & Takaoka, E., (1992). “Development of real-time pseudo dynamic testing”. Earthquake Engineering and Structural Dynamics, 21(1), 79-92.

Nelson, E. L., Wheat, D. L., and Fowler, D. W. (1985). ‘‘Structural behavior of wood shear wall assemblies.’’ J. Struct. Eng., 111(3), 654– 666.

Palermo, A., Pampanin, S., Buchanan, A., and Newcombe, M. (2005). “Seismic design of multi-storey buildings using laminated veneer lumber (LVL).” 2005 NZSEE Conf., New Zealand Society for Earthquake Engineering, Wellington, New Zealand, 8.

Pardoen, G., Waltman, A., Kazanjy, R., Freund, E., and Hamilton, C., (2003). “Testing and Analysis of One-Story and Two-Story Shear Walls under Cyclic Loading CUREE,” CUREE Publication, No. W-25, Richmond, Calif.

Pei, S., van de Lindt, J. W., and Popovski, M. (2013b). “Approximate R-factor for cross-laminated timber walls in multistory buildings.” J. Archit. Eng., 10.1061/ (ASCE) AE.1943-5568.0000117, 245–255.

Priestley M J N, Sritharan S, Conley J R, Pampanin S. (1999). “Preliminary Results and Conclusions from the PRESSS Five-story Precast Concrete Test-building”, PCI Journal, 44(6): 42-67.

Rethinkwood (2014). “Summary Report: Survey of international tall wood buildings”. Retrieved from http://www.rethinkwood.com/webform/get-summary-report.

Rinaldin, G., Fragiacomo, M., (2016), “Non-linear simulation of shaking-table tests on 3- and 7-storey X-Lam timber buildings”. Engineering Structures 113, 133-148.

Shao, X., van de Lindt, J.W., Bahmani, P., Pang, W., Ziaei, E., Symans, M., Tian, J. and Dao, T. (2014). “Real-Time Hybrid Simulation of a Multi-story Wood Shear Wall with First-Story Experimental Substructure Incorporating a Rate-Dependent Seismic Energy Dissipation Device.” Smart Structures and Systems 14(6):1031-1054.

Shing, P. B., Nakashima, M., & Bursi, O. S. (1996). “Application of pseudodynamic test method to structural research.” Earthquake Spectra, EERI, 12(1):29-54.

Smith, T., Ludwig, F., Pampanin, S., Fragiacomo, M., Buchanan, A.H., Deam, B.L. and Palermo, A. (2007). “Seismic Response of Hybrid-LVL Coupled Walls under Quasi-static and Pseudo-dynamic Testing”. Palmerston North, New Zealand: New Zealand Society of Earthquake Engineering 2007 Conference (NZSEE 2007).

Sumidenwire (2014). “ASTM A416 – Low Relaxation 7 - Wire Strand”. Retrieved from http://www.sumidenwire.com.

T. Horiuchi, M. Inoue, T. Kondo and Y. Namita (1999). “Real-time hybrid experimental system with actuator delay compensation and its application to a piping system with energy absorber”. Earthquake Engng. Struct. Dyn. 28, 1121-1141.

van de Lindt and T. N. Dao, (2009). "Performance-Based Wind Engineering for Wood-Frame Buildings," Journal of Structural Engineering-Asce, vol. 135, pp. 169-177.

van de Lindt, J. (2004). “Evolution of wood shear wall testing, modeling, and reliability analysis: Bibliography.” Pract. Period. Struct. Des. Constr., 10.1061/ (ASCE) 1084-0680(2004)9:1(44), 44–53.

CHAPTER 3

NUMERICAL MODEL FOR CREEP BEHAVIOR OF AXIALLY LOADED CLT PANELS

Abstract

The performance of post-tensioned rocking Cross Laminated Timber (CLT) panels depends on the ability to maintain the post-tensioned (PT) force in the tendon. This PT force may change over time due to the creep behavior of wood; which in turn, is a function of time and moisture content in the CLT panels. In this study, a numerical moisture content diffusion model was developed to predict the moisture content migration through CLT panels when the ambient relative humidity changes. Fick's second law and the moisture content diffusion coefficients were applied to derive the differential diffusion equation for use in a numerical model. Included was a four-element creep model to estimate the creep deformation over time under the axial load on the CLT panel with changing environmental conditions. Data from a series of moisture content and creep tests under different configurations and environmental conditions were used to calibrate the proposed moisture content diffusion and creep model in CLT panels. The moisture content diffusion model was calibrated for two relative humidity (RH) steps, 50% to 70% and 70% to 90%, respectively. Then, a new creep model at material level that considers the change of moisture content in CLT panels was introduced. The viscoelastic parameters and mechano-sorptive constants have been recommended for the creep model based on creep test data. Axial strain in CLT panels varied under 2% when ambient RH switched between 50% and 70%. The axial strains in CLT panels with three layers are more sensitive to the variation of surrounding RH than that of CLT panels with five layers.

3.1. Introduction

Cross Laminated Timber is a relatively new structural system first introduced in Europe in the early 1990s and categorized as a massive timber system in the International Building Code (ICC, 2009). This new construction was developed in Europe in early 2000s; and has recently spread to North America, Japan and New Zealand. It has been utilized in over one hundred CLT construction projects around the world (CLT handbook, 2013 – Chapter 1). CLT allows constructing mid-rise and high-rise wood buildings, which is more difficult with light-frame. Increasing interest in CLT in North America has led to the publication of CLT Handbook: Cross-Laminated Timber (FPInnovations program in Canada, 2011), the American National Standard - Standard for Performance Rated Cross-Laminated Timber (ANSI/APA PRG 320) developed by the ANSI/APA CLT Standard Committee (December 2012) and the U.S. CLT Handbook (2013). In 2015, the National Design Specification for Wood Construction adopted CLT design provisions, the first design specification worldwide to do so. All these publications summarized the state of the art understanding of CLT behavior and identified the need to better understand the behavior of CLT structures.

Recently, many researchers tried to apply CLT materials in tall wood buildings either using traditional wood connections (Asiz et al. 2011; Bolvardi et al. 2016), post-tension rocking panels (Ho et al. 2016; Tugce et al. 2017), or both. In those applications, CLT panels often experience large axial loads that may cause long-term creep deformation that affects the building performance during extreme events like earthquake or high wind. Creep is the time-dependent deformation under a certain application of stress and is often characterized by creep rate or the change of creep deformation over time. The creep strain curve, as shown in Fig. 3-1, is used to express three different stages of creep (Wikipedia, 2016).

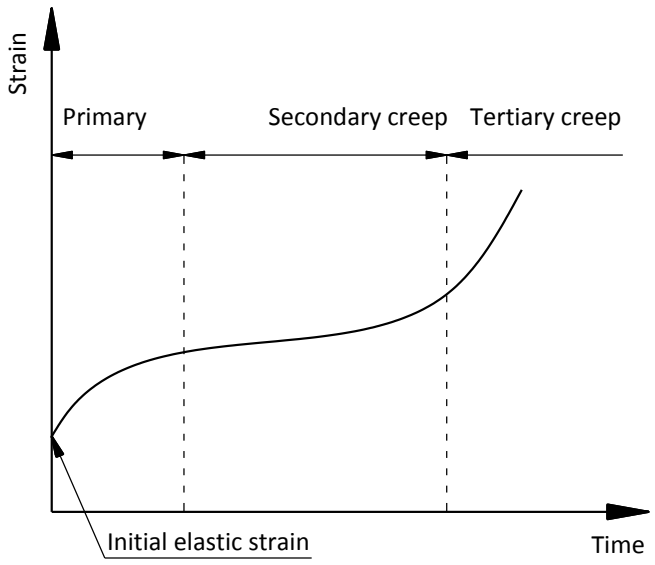

Fig. 3-1 Creep strain curve

In the primary stage, the creep rate often increases rapidly, followed by a relatively uniform secondary stage. In the tertiary stage, the creep rate accelerates significantly and ends at the point when the material fails. The creep rate can be influenced by many factors such as applied load, exposure temperature, relative humidity and time. These factors change the material properties in different levels; therefore, the creep of a certain material might be more susceptible to certain factors than another material. Wood is a hygroscopic material, thus changes in moisture content and temperature of the ambient environment can yield great effects on the change of wood's modulus of elasticity (Wood Handbook, 2010 – Chapter 4). The creep behaviors of wood under varied temperature and moisture content (MC) are extremely complex and can be split into two categories: visco-elastic creep and mechano-sorptive creep. While visco-elastic creep depends on duration of loads, types of loads and temperature, the mechano-sorptive creep in wood mainly occurs due to the change in the environmental conditions (Nordstrom et al., 1994). The influences of applied load on wood properties were studied by numerous investigators. Some research tried to determine the conditions that wood can be

considered as a linear visco-elastic material. In one of these studies, Schaffer (1982) concluded that wood demonstrated nearly linear behavior at a stress level up to 40% of its short-term strength under constant environmental conditions. Later, Nakai and Grossman (1983) compared the deflection data collected from the tests of a series of beams subjected to constant and repeatedly changing loads under constant ambient environment conditions. This study showed that non-linear behavior at high stress occurs when the loads exceed about 50% of the short-time ultimate strength.

Besides load influences, the effects of the environmental factors on wood creep were also investigated by many researchers. For example, Gerhards (1980) stated that "Moisture has the least effect on parallel-to-grain properties of modulus of elasticity (E) and tensile strength and the greatest effect on compressive strength parallel-to-the-grain". The author also pointed out that the effects of temperature on the wood properties increased at higher moisture content. Gerhards' conclusions were also confirmed by other studies such as a study by Fridley et al. (1992a). In that study, Fridley et al. (1992a) investigated the hygrothermal effects on the modulus of elasticity and modulus of rupture by performing bending tests on the selected structure Douglas-fir 2×4 lumber. They concluded that the sample's modulus of elasticity and modulus of rupture were affected by the ambient temperature and moisture. They also proposed the quadratic functions of relative temperature and relative moisture content to account for the effects of changing the surrounding environmental conditions to lumber properties.

In recent decades, there has been growing interest in using composite wood-based materials for structures. Researchers have been studied the time-dependent deformations for these types of material under the variant of environment conditions. Gowda et al. (1996) reported results of the long-term bending creep tests on glulam beams at low load levels under natural

conditions. The creep data collected from the tests of eight separate glulam beams in a heated room environment were utilized to compare with the creep data from glulam beams under natural conditions. The conclusion was that there was no difference in creep of glulam beam between heated and non-heated environment, and the creep deformation alone after 4 years was about 60% of elastic deformation. In other work, Yazdani et al. (2004) tested long-term creep behavior of the structural composite lumber (SCL) T beams under exposed weather conditions with frequent wetting and drying. They concluded that the creep deformations of the T beam made with laminated veneer lumber (LVL) were marginally smaller in comparison with that of parallel strand lumber (PSL) beams. More recently, Pirvu and Karacabeyli (2014) performed creep tests on the nine CLT billets. The data from their experiments showed that the material satisfied the three criteria specified in ASTM D6815-09, namely (i) decreasing creep rates after 90/120 days of loading, (ii) fractional deflections less than 2.0 after 90-day loading, and (iii) higher creep recovery than 20% after 30 days of unloading.

The data for the creep study in wood and composite wood-based materials including laminated members were primarily collected from the bending tests. Very few researchers have addressed the creep of laminated members subjected to compression stress under the influence of environmental factors. Through creep studies, researchers also focused on developing the models that have ability to catch the creep behavior of wood and wood-based material. Many creep models have been proposed, for example, the power law model was studied by various researchers such as Clouser (1959), Hoyle (1985) and Gerhards (1985). This model did not include the thermal effects on creep. Later, the three-element model and Burger model were used by Senft and Suddarth (1971) to account for the thermal effects on wood creep. These models produced the good results in Senft and Suddarth's (1971) experiments which were also affirmed

by Nur Yazdani et al. (2004). Later, the five-element model was employed by Fridley (1992b) to account for the mechano-sorptive effects on wood creep behavior.

Although the creep on wood structures under different environmental conditions and loading patterns has been widely investigated (Gerhards, 1980, Schaffer, 1982, Nakai and Grossman 1983, Fridley, 1992, Nordstrom, 1994), very little work has been focused on investigating the effects of surrounding environmental condition on creep of the CLT structures. Previous work only focused on the stressed laminated timber structures in bridges (Sarisley 1990, Wacker, 2009). No work has been reported on the creep behavior of the axially loaded CLT panels. Due to the effects of the orthogonal arrangement of layers and structural adhesive, CLT is more susceptible to creep than other wood-based products (Mohammad et al., 2012). Special attention is needed for the creep behavior of the axially loaded CLT panels in tall wood buildings. The goal of this study is to develop a numerical creep model to quantify the creep behavior of the axially loaded CLT panels over time. The effects of changing the surrounding environment conditions to the creep behavior of the CLT material were also included. This was enabled by creating a numerical moisture diffusion model to predict the change of moisture content within CLT panels over time. Experimental data from a series of creep and moisture content tests under different ambient environment conditions were used to calibrate the numerical models.

3.2. Moisture content diffusion model

Wood structures are susceptible to serviceability issues under varying surrounding temperatures and relative humidity. These factors are directly related to the changing of moisture content in the structural components which yield a great effect on the serviceability of this type of structure. Moisture content in a specimen can migrate from a point of higher moisture content

to another point of lower moisture content, referred to as sorption process. The absorption process is applied if the specimen gains moisture from the ambient environment. The term desorption is used to describe the process of specimen losing its moisture to surrounding environment. In general, both absorption and desorption processes can be considered as the diffusion process. Depending on the ambient environment and the saturation point, the moisture movement can happen in liquid water or water vapor. This study only focused on the diffusion of water vapor and its effects on creep behavior of CLT panels. A numerical model was developed to predict the moisture content diffusion in CLT material when subjected to the change of surrounding environment.

For steady state one-dimensional diffusion problem, Fick's second law (Fick, 1855) is applied as

$$\frac{\partial \Phi}{\partial t} = \frac{\partial}{\partial u}\left[R_u \frac{\partial \Phi}{\partial u}\right] \tag{3.1}$$

where: R_u is diffusion coefficient; Φ is moisture concentration driving potential; t is time; u is space coordinate.

In mass timber, moisture content can travel in different directions and the diffusion equation for three-dimensional problems can be written as

$$\frac{\partial}{\partial x}\left[R_x \frac{\partial \Phi}{\partial x}\right] + \frac{\partial}{\partial y}\left[R_y \frac{\partial \Phi}{\partial y}\right] + \frac{\partial}{\partial z}\left[R_z \frac{\partial \Phi}{\partial z}\right] = \frac{\partial \Phi}{\partial t} \tag{3.2}$$

in which, R_x, R_y, R_z are diffusion coefficients (or moisture content capacities) in x, y, z directions, respectively.

Using Finite Element Method (FEM) formulation, Eqs. (3.2) can be converted into the weak form for finite element approximation as (Thompson, 2005)

$$[K]\{\Phi\} + [C]\{\dot{\Phi}\} = 0 \tag{3.3}$$

where: $\dot{\Phi}$ represents the nodal point values for the derivative of Φ with respect to time

$$\dot{\Phi} = \frac{\partial \Phi}{dt} \tag{3.4}$$

and [*K*] and [*C*] are calculated by integrals:

$$[K] = \int_V [N']^T [R][N']dV \quad and \quad [C] = \int_V \{\mathrm{N}\}[\mathrm{N}]dV \tag{3.5, 3.6}$$

In these equations, [*N*] is the element shape functions matrix; [*N'*] is the derivative of the element shape function matrix versus space coordinates (see Thompson, 2005, chapter 10 for more details); [*R*] is the material properties matrix (or matrix of diffusion coefficients) and *V* is the volume. The central difference approximation was used to solve moisture content at each time step using Eqs. (3.3). At each time step, the moisture content was calculated as:

$$[CPK]\{\Phi\}_{t+\Delta t} = [CMK]\{\dot{\Phi}\}_t \tag{3.7}$$

where

$$[CPK] = [C] + \frac{\Delta t}{2}[K] \qquad and \qquad [CMK] = [C] - \frac{\Delta t}{2}[K] \tag{3.8, 3.9}$$

and Δt is the time step.

Outcomes of the moisture content diffusion model are shown in Fig. 3-2. The dimensions of the specimen were 6.75×24×24 in. The original MC in the specimen was 10.67% and the MC in the new environment was 16.16%.

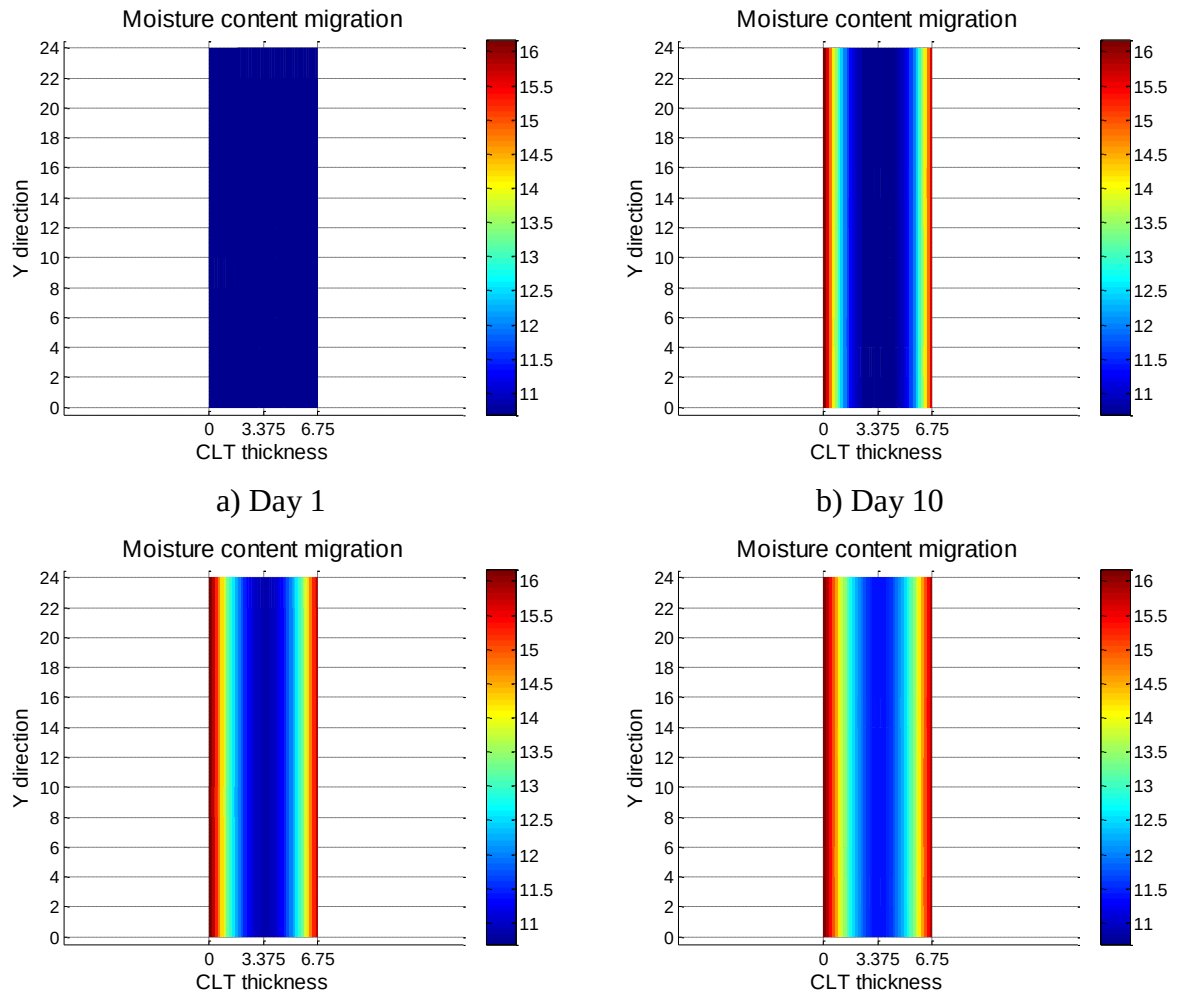

a) Day 1 b) Day 10

c) Day 19 d) Day 28

Fig. 3-2 Moisture content migration in CLT panel

3.2.1. Equilibrium moisture content tests

When a CLT specimen is exposed to a new RH condition, it takes time for that specimen to adjust to new equilibrium MC. Three sets of small CLT specimens (No.2 SPF lumber) (2017, APA - The Engineered Wood Association, Product Report) with dimension of 6×5×3.75 in. (15.24×12.7×9.525 cm) were put into environmental chamber at three different RH conditions until equilibrium was reached (the weight change in 10 days was less than 0.1%). These specimens were then dried to determine the dry weight and MCs were calculated by Eqs. (3-10).

The purpose of these tests is to estimate the equilibrium MC of CLT under different RH conditions. The results from these tests are listed in Table 3-1.

Table 3-1 Equilibrium MC of CLT at different RH

RH (%)	N0. specimens	Weight (gm)		MC (%)	Mean (%)	Variance (%)
		Equilibrium	Oven dry			
50	5	829.80	750.30	10.60	10.67	0.0064
		909.60	821.00	10.79		
		911.00	823.70	10.60		
		932.40	842.20	10.71		
		831.40	751.30	10.66		
70	5	912.30	807.20	13.02	13.16	0.0289
		956.70	846.70	12.99		
		948.00	837.70	13.17		
		951.70	840.90	13.18		
		911.20	803.40	13.42		
90	6	912.00	756.80	20.51	20.51	0.1039
		905.60	749.80	20.78		
		884.80	733.30	20.66		
		937.30	778.80	20.35		
		942.20	785.50	19.95		
		921.60	763.00	20.79		

3.2.2. Moisture content diffusion tests

In the numerical model described in the previous section, the diffusion coefficients R_x, R_y, and R_z of CLT panels need to be experimentally evaluated. A series of tests on moisture content diffusion were conducted to estimate these coefficients. In order to understand the effects of panel size on the diffusion coefficients, the CLT specimens used in the tests are divided into

three groups: 2ft×2ft three-layer panels, 1ft×2ft three-layer panels, and 1ft×1ft five-layer panels. Dimensions and number of specimens of each group are shown in Table 3-2.

Table 3-2 Specimens for moisture content and moisture diffusion tests

Group	CLT Grade by Structurlam	Sample dimensions (in.)	N0. of specimen
1	V2M1 3 layers (SLT3)	3.9×24×24	6
2	V2M1 3 layers (SLT3)	3.9×12×24	6
3	V2M1 5 layers (SLT5)	6.6×12×12	11

In buildings, CLT panels mainly absorb/desorb moisture through the surfaces exposed to the environment because the panel edges have small area and are often coved by adjacent panels or walls. For this reason, the experiments in this study focused on estimation of moisture diffusion coefficient in the direction perpendicular to the surface. To do this, in each specimen, the panel edges were coved by aluminum tape while the surfaces were exposed to controlled environmental conditions during the tests, as shown in Fig. 3-3.

a) Group 2 b) Group 3

Fig. 3-3 Specimens in group 2 and group 3 for diffusion coefficient tests

The CLT specimens were then placed in environmental chambers in which the temperature and relative humidity were controlled in a reasonable range. The environmental chambers at the University of Alabama were built to control temperature ranging from 41ºF (5ºC) to 140ºF (60ºC) and relative humidity ranging from 20% to 98%. In this study, the chamber was set at a constant temperature of 73ºF (22.8ºC) and three levels of relative humidity 50%, 70%, and 90%, respectively. At the beginning, the environmental chamber was set at temperature 73ºF (22.8ºC) and relative humidity 50%. The CLT specimens were placed in the chamber until the equilibrium of moisture contents were achieved (there was not significant change of weight in each specimen). The relative humidity of the chamber was then switched to 70% while the temperature was kept at 73ºF (22.8ºC). Change of weight in each specimen was measured to observe the moisture absorbing process in CLT. After switching the relative humidity, the CLT specimens absorbed moisture quite fast in the first two days due to the large difference of moisture contents between the surface and the inside of the CLT specimens. Over time, the absorption process slowed down as moisture contents inside the specimens increased. To have a smooth curve of moisture content change in CLT specimens, in the first two days, the weights of CLT specimens were measured for every 6 hours and the interval was changed to 12 hours after that until the specimens were believed to be close to the new equilibrium conditions. The relative humidity was then switched into a new levels and the same collecting data procedures were used for the rest of the moisture content tests. The tests were conducted for both increasing relative humidity from 50% to 70% then 90% and decreasing humidity from 90% back to 70%. During the tests, the weight of each specimen was measured using a scale that has resolution of 0.002 kg (0.005 lbs.). This high resolution scale allowed accurately capturing the change of moisture content in each specimen.

To estimate the moisture contents in each specimen, the method A (Oven-Drying) of ASTM D4442-15 (2015) was applied. All CLT specimens were dried in oven after the test, and the dry weight was measured following the specification of ASTM D4442-15. Dimensions and dry weight of each specimen are shown in Table 3-3.

The moisture content of the sample can then be calculated by equation:

$$\mathrm{MC} = \frac{\mathrm{W_1} - \mathrm{W_0}}{\mathrm{W_0}} \times 100 \text{ percent} \tag{3.10}$$

where: MC is the specimen's moisture content; W_1 is the weight of the specimen measured during the tests; W_0 is the oven-dry weight of the specimen.

3.2.3. Fitting moisture content diffusion coefficients

In this study, a FEM subroutine was developed to estimate the moisture content diffusion coefficients. By adjusting the diffusion coefficients and the boundary conditions in the numerical model, the numerical weight of a CLT specimen was fitted to the experimental data from the tests. Because the nature of CLT material, moisture absorbing and desorbing rate may vary, this phenomenon was taken into consideration by using two separate coefficients for the two processes.

Fig. 3-4 shows the fitting data for one of the tested specimens for both absorbing and desorbing moisture. (Other specimens can be seen in the Appendix). In Fig. 3-4, R_{xai} is the diffusion coefficient of absorbing process and R_{xd} is the diffusion coefficient of desorbing process. *MCi* is the boundary condition of moisture contents at the surfaces of different RHs.

Table 3-3 Specimens dry weight

Group	Name	Dimensions (in.)	Dry weight (lbs.)
Group 1 (3 layers)	L-1	3.9 × 24.00 × 23.98	35.522
	L-2	3.9 × 23.94 × 24.00	32.996
	L-3	3.9 × 23.94 × 24.00	35.926
	L-4	3.9 × 24.00 × 23.97	35.752
	L-5	3.9 × 23.98 × 23.94	36.076
	L-6	3.9 × 24.00 × 24.00	33.034
Group 2 (3 layers)	L-7	3.9 × 11.95 × 24.00	17.122
	L-8	3.9 × 11.95 × 23.98	16.602
	L-9	3.9 × 12.00 × 24.00	17.420
	L-10	3.9 × 11.92 × 24.00	17.116
	L-11	3.9 × 11.97 × 24.00	17.226
	L-12	3.9 × 11.91 × 24.00	16.606
Group 3 (5 layers)	S-1	6.67 × 12.000 ×12.000	14.690
	S-2	6.67 × 11.969 ×11.875	14.662
	S-3	6.67 × 11.906 ×11.875	15.316
	S-4	6.67 × 11.922 × 11.969	15.002
	S-5	6.67 × 11.750 × 11.953	14.992
	S-6	6.67 × 11.938 × 11.828	14.566
	S-7	6.67 × 11.969 × 11.891	14.456
	S-8	6.67 × 11.969 × 11.906	15.300
	S-9	6.67 × 11.875 × 11.922	14.906
	S-10	6.67 × 11.813 × 11.813	14.238
	S-11	6.67 × 12.031 × 11.953	15.332

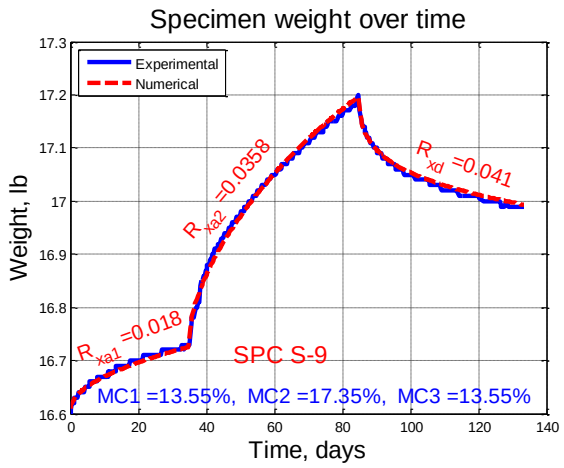

Fig. 3-4 Fit data for diffusion moisture coefficient

Since wood is a natural material, the moisture diffusion coefficient may vary from specimen to specimen. The final coefficient for a group was estimated by performing the statistical analysis to obtain the mean and variance value of coefficients in specimens. Table 3-4 shows the results of the moisture content diffusion coefficients for the three specimen groups for different RH intervals. In this table, the moisture contents at the surfaces of specimens predicted by numerical models at 70% RH and 90% RH were also included.

Statistical distributions were fitted to each of population of three moisture content diffusion coefficients, the lognormal distributions were found to be adequate representation of distribution of all coefficients. Fig. 3-5 and Fig. 3-6 illustrate the lognormal distribution plots for moisture content diffusion coefficient in different sample groups at different RH step change. The means and variances of the moisture content diffusion coefficients are shown in Table 3-5. Fig. 3-6 shows the lognormal distribution plots for moisture content diffusion coefficient of all specimens in 3 groups at different RH step change.

Table 3-4 Moisture diffusion coefficients and moisture contents at the bounds for different RH intervals

Dimensions (in.)	Specimen	R_x ($in^2.day^{-1}$)			Moisture content (%)	
		50 - 70%	70 - 90%	90 - 70%	70% RH	90% RH
Group 1 3.9×24×24 (3 layers)	L-1	0.0115	0.0265	0.0350	14.50	18.50
	L-2	0.0120	0.0360	0.0440	14.80	18.80
	L-3	0.0090	0.0245	0.0360	14.45	18.40
	L-4	0.0090	0.0245	0.0372	13.80	17.50
	L-5	0.0106	0.0230	0.0322	13.65	17.70
	L-6	0.0093	0.0355	0.0455	14.44	18.00
Group 2 3.9×12×24 (3 layers)	L-7	0.0085	0.0305	0.0485	13.55	16.95
	L-8	0.0095	0.0355	0.0447	13.90	17.35
	L-9	0.0088	0.0315	0.0430	13.95	17.50
	L-10	0.0095	0.0325	0.0440	13.65	17.25
	L-11	0.0093	0.0335	0.0395	13.70	17.35
	L-12	0.0097	0.0375	0.0475	13.80	17.51
Group 3 6.67×12×12 (5 layers)	S-1	0.0165	0.0300	0.0380	13.45	17.40
	S-2	0.0160	0.0290	0.0347	13.55	17.45
	S-3	0.0175	0.0320	0.0380	13.50	17.50
	S-4	0.0155	0.0345	0.0420	13.85	17.61
	S-5	0.0150	0.0370	0.0463	13.75	17.21
	S-6	0.0170	0.0345	0.0452	13.60	17.50
	S-7	0.0180	0.0312	0.0400	13.35	17.30
	S-8	0.0185	0.0343	0.0370	13.65	17.40
	S-9	0.0180	0.0358	0.0410	13.55	17.35
	S-10	0.0205	0.0390	0.0430	13.70	17.85
	S-11	0.0165	0.0329	0.0350	13.35	17.30

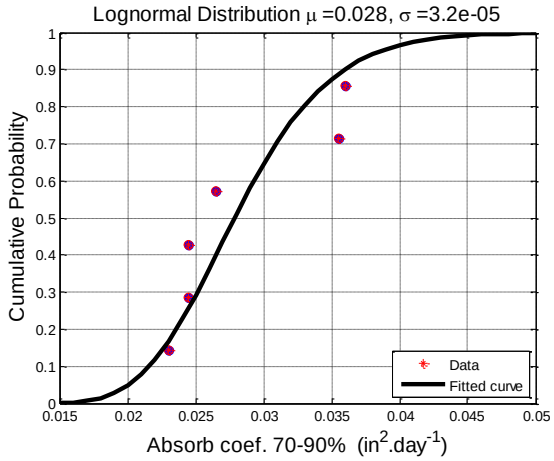

a) R_{xa2} for specimens L1-L6 at 70-90% RH

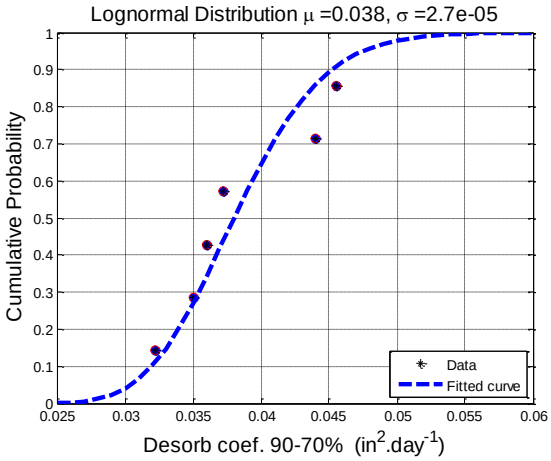

b) R_{xd} for specimens L1-L6 at 90-70% RH

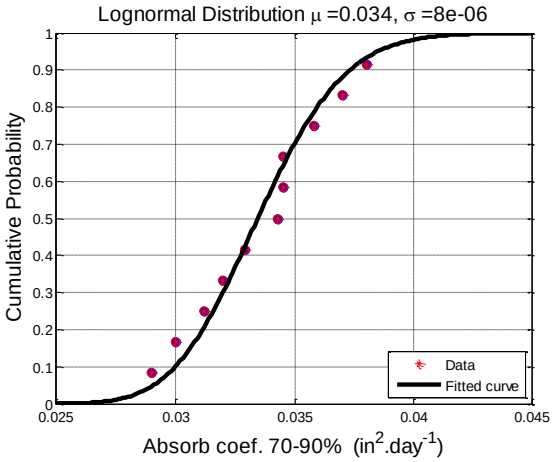

c) R_{xa2} for specimens S11-S23 at 70-90% RH

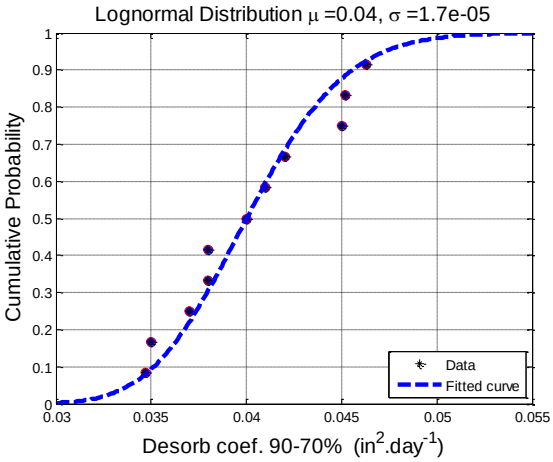

d) R_{xd} for specimens S11-S23 at 90-70% RH

Fig. 3-5 Cumulative distribution plot of R_x for different groups

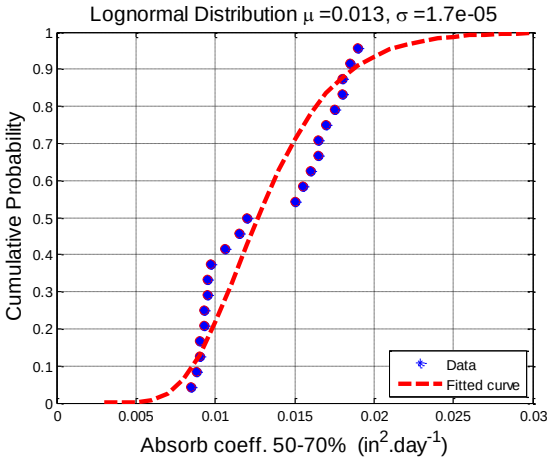

a) R_{xa1} for all groups at 50-70% RH

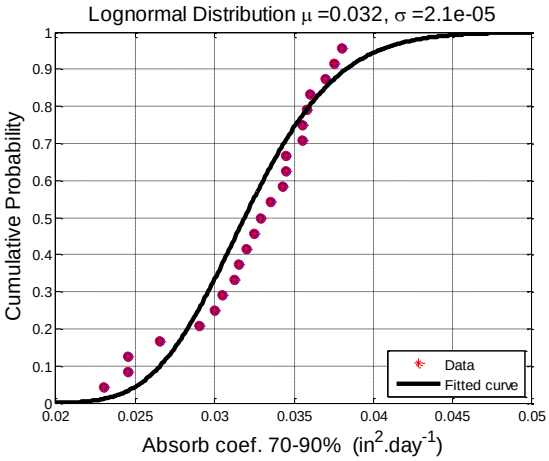

b) R_{xa2} for all groups at 70-90% RH

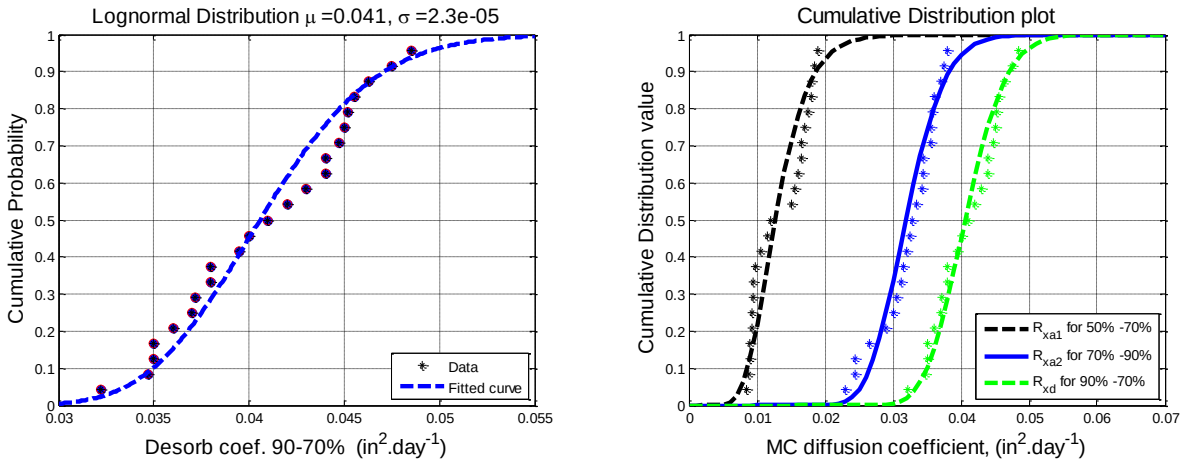

c) R_{xd} for all groups at 90-70% RH d) R_x for all groups at different RH change

Fig. 3-6 Distribution of R_x for all groups at different RH

The cumulative distribution in all groups for the numerical equilibrium moisture content at 70% RH and 90% RH, respectively, were plotted in Fig. 3-7.

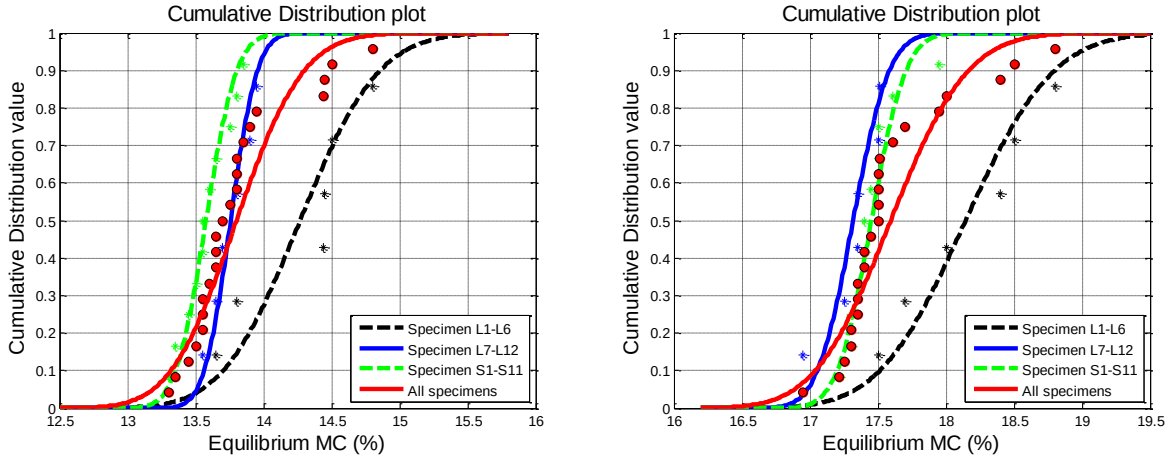

a) At 70% RH b) At 90% RH

Fig. 3-7 Distribution of equilibrium moisture content for all groups

3.2.4. Comments on experimental and numerical results for moisture content diffusion

The numerical model for moisture content diffusion proposed in this study implies that the material is homogeneous, which is not true for wood, a natural material. Not only do the effects of wood properties change in different directions (tangential, radial, and grain directions), but the properties of CLT material also depends on type of applied glue, gaps among lumbers in

the same layer, and the quality of lumber itself. In order to account for all such variation, the statistical properties of CLT material need to be investigated. Such variations were not included in the numerical model in this study. Instead, the variations were considered in the statistics of model parameters.

Table 3-5 MC diffusion coefficients and equilibrium MC in different RH and specimen

Groups	SPC	Parameters	Environment	Mean	Variance	Distribution
(1) 3 layers 3.9×24×24	6	R_x ($in^2.day^{-1}$)	50 - 70 %	0.0102	0.0000017	Lognormal
			70 - 90%	0.0284	0.0000324	
			90 - 70%	0.0384	0.0000272	
		MC (%)	70%	14.275	0.2029476	
			90%	18.151	0.2517192	
(2) 3 layers 3.9×12×24	6	R_x ($in^2.day^{-1}$)	50 - 70 %	0.0092	0.0000002	
			70 - 90%	0.0335	0.0000067	
			90 - 70%	0.0446	0.0000108	
		MC (%)	70%	13.758	0.0234299	
			90%	17.319	0.0428622	
(3) 5 layers 6.67×12×12	11	R_x ($in^2.day^{-1}$)	50 - 70 %	0.017	0.0000016	
			70 - 90%	0.0336	0.0000082	
			90 - 70%	0.0402	0.0000167	
		MC (%)	70%	13.577	0.0311834	
			90%	17.452	0.0392344	
All specimens	23	R_x ($in^2.day^{-1}$)	50 - 70 %	0.0133	0.0000168	
			70 - 90%	0.0322	0.0000213	
			90 - 70%	0.0409	0.0000228	
		MC (%)	70%	13.806	0.1468479	
			90%	17.599	0.1936946	

It can be seen in Table 3-5 that the absorption coefficients of CLT specimens vary between 0.0284 and 0.0336 $in^2.day^{-1}$ (212-251×10^{-12} $m^2.s^{-1}$) for RH range between 70% and 90%. These values are about 4-5 times greater than the values reported in a study by Liu Tong (1987) on spruce, which was 52×10^{-12} $m^2.s^{-1}$ in the transverse direction (a step change in RH

from 65% to 80%). It should be noticed that CLT panels are made of several layers of small lumbers and the gaps between two adjacent lumbers in the same layer are not glued, which allows moisture easily migrate into deeper layers. Therefore, the larger absorption coefficients of CLT in this study compared to solid timbers in Liu Tong study can be considered reasonable. Also, from Fig. 3-7d, the average absorption coefficient measured in the surrounding environment RH 70% to 90% is about 2-3 times larger than that measured in the RH 50% to 70%. This means that the absorption coefficient is not constant as moisture content changes in CLT. Therefore, to apply Fick's law in the prediction of moisture content migration, different absorption coefficients should be use for different range of moisture contents.

3.3. Creep model for axially loaded CLT panel

The Burger model has been widely used by many researchers (Senft and Suddarth, 1971; Nur Yazdani et al., 2004) to predict creep behavior for wood. Although this four-element model has an ability to capture the hygrothermal effects on creep of timber, it does not include the mechano-sorptive effects. In order to account for mechano-sorptive effects, Fridley et al. (1992b) proposed a five-element model that included a mechano-sorptive element, Fig. 3-8. The mathematical form of this model as follows:

$$\varepsilon(t) = \frac{\sigma}{K_e} + \left(\frac{\sigma}{K_k}\right)\left[1 - e^{-\frac{K_k.t}{\mu_k}}\right] + \frac{\sigma.t}{\mu_v} + \frac{\sigma}{\mu'_{ms}}|\Delta\omega|[1 - e^{-B_\omega.t_\omega}] \qquad (3.11)$$

where: $\varepsilon(t)$ is the total strain at time t; σ is the constant applied stress; K_e, K_k, μ_k, μ_v, μ'_{ms} are model constants. B_ω is a constant associated with the time required to achieve moisture equilibrium; B_ω is dependent on the size of the sample. $|\Delta w| = \omega_e - \omega_i$, where ω_e is the eventual equilibrium MC in the new environment and ω_i is the initial MC in the original environment. In that study, the two hygrothermal variables, ω and θ have been introduced as:

$$\omega = \frac{M - M_0}{M_0} \quad and \quad \theta = \frac{T - T_0}{T_0} \qquad (3.12, 3.13)$$

where: ω is a relative moisture content; M is the actual moisture content; M_o is a reference moisture content; θ is a relative temperature; T is the actual temperature; T_o is reference temperature. The quadratic functions of ω and θ have been assumed for predicting the hygrothermal effects on wood properties K_e, K_k, μ_k, μ_v.

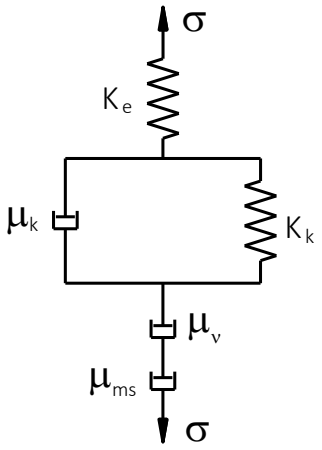

Fig. 3-8 Five-element creep model

In the past, most of the creep models were developed to predict the creep behavior at structural component level. Fridley's creep model includes size-dependent constant B_ω associated with the time required to achieve moisture equilibrium. For this reason, new test data is required to calibrate the model every time the size of the member changes. Since the sizes of lumbers are usually manufactured in fixed dimensions, this model worked well for lumbers. In CLT buildings, CLT panels vary in size depending on the number of stories and the design of each component. Therefore a new creep model at material level is favorable in predicting the creep behavior of CLT panels, and a modification of the five-element model was introduced. Also, not like bending creep behavior, in axially loaded CLT panels, the compression stress is often

designed to be in the range of 5% to 15% of the peak failure stress and the tertiary creep behavior can be neglected. And in this modification model, the tertiary creep phase was not included, thus the viscous term ($\sigma.t/\mu_v$) to describe secondary effects was removed. The mathematical form was expressed by equation

$$\varepsilon(t) = \frac{\sigma}{K_e} + \left(\frac{\sigma}{K_k}\right)\left[1 - e^{-\frac{K_k.t}{\mu_k}}\right] + \frac{\sigma}{\mu_\omega}.\Delta MC \qquad (3.14)$$

where: μ_ω is mechano-sorptive constant, ΔMC is the moisture content difference between original environment to new environment, $\Delta MC = MC_a - MC_i$; MC_i is the initial reference moisture content; MC_a is the moisture content of specimen at time t. The advantage of this modified five-element model was that it could be used to predict the creep behavior of specimens at different specimen sizes.

3.3.1. Visco-elastic creep tests for CLT

Creeps of a CLT material under changing ambient environmental conditions can be divided into a visco-elastic creep and mechano-sorptive creep. Because variation of MC in a specimen has limited effect on the visco-elastic creep behavior, creep test data under a constant environmental condition can be used to evaluate the visco-elastic creep model constants (K_e, K_k and μ_k). A series of creep tests were performed in the environmental chambers at the University of Alabama with constant ambient RH of 50% and temperature of 73ºF (22.8ºC). The influence of the CLT thickness to creep behavior was examined by using the 3-layer and 5-layer CLT test samples. Besides the effects of CLT thickness, three stress levels, at 0.05 f_c' (f_c' = 24.13 MPa is the CLT compressive strength), 0.10 f_c' and 0.15 f_c' were applied on specimens to investigate the effects of stress levels on creep behavior of CLT. Table 3-6 shows details of specimens and the actual forces that applied on each group.

Table 3-6 Details of specimens and stress levels

Group	Stress level	Force (kip)	Actual force (kips)		CLT dimensions (in.)	N0. SPC
			Left	Right		
1	3 layers 0.05 f_c' L	16.38	16.277		3.90×24×96	1
2	3 layers 0.10 f_c'	32.76	16.976	18.032	3.90×24×24	4
			17.252	16.315		
3	5 layers 0.05 f_c' L	28.35	28.041		6.75×24×96	1
4	5 layers 0.10 f_c'	56.70	28.828	28.753	6.75×24×24	4
			28.568	28.65		
5	5 layers 0.15 f_c'	85.05	27.265	29.574	6.75×24×24	4
			25.497	29.811		

The compression stresses applied on CLT specimens must stay constant during creep tests. To compensate for losses of the applied stresses due to specimens deformation during the creep tests, the entire testing system was placed on the spring supports as illustrated in Fig. 3-9b. Forces released from the spring system remained the compression stresses in CLT specimens.

Two strain gauges were used for each specimen to measure strain on the front and the back side of the specimen (Fig. 3-9a). Tensioned forces were monitored by load-cells placed on top of specimens. These devices were connected to a data acquisition system placed outside the environmental chamber. In order to obtain more strain data in different locations on CLT panels, Demountable Mechanical strain gauges (DEMEC) were also used to manually collect strain data. Detailed locations for DEMEC strain gauges are shown in Fig. 3-9. Experimental strain data were collected and then fitted with numerical model to obtain the creep model constants. Fig. 3-10 shows fitted viscoelastic model parameters using data from strain gauges and DEMECs for one of the specimens.

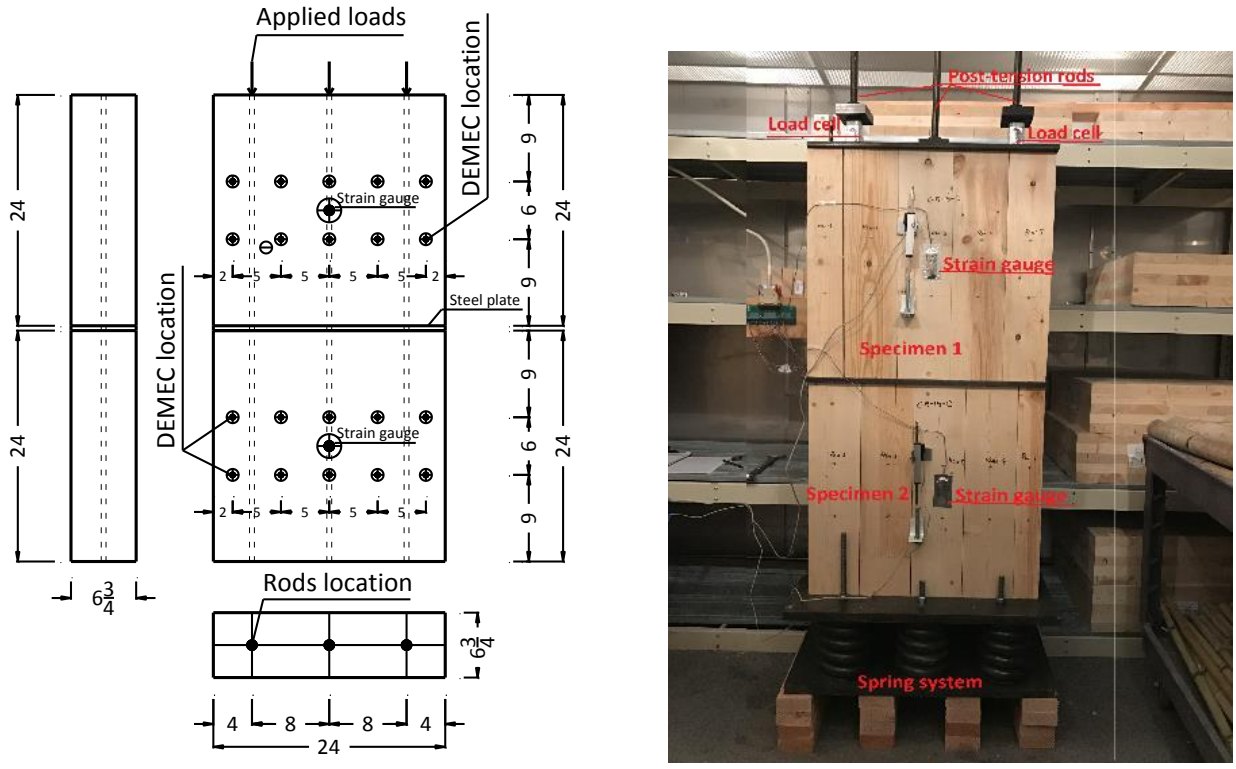

a) Schematic location b) Ready specimen

Fig. 3-9 Creep test setup of 5 layer 15% f_c' specimen

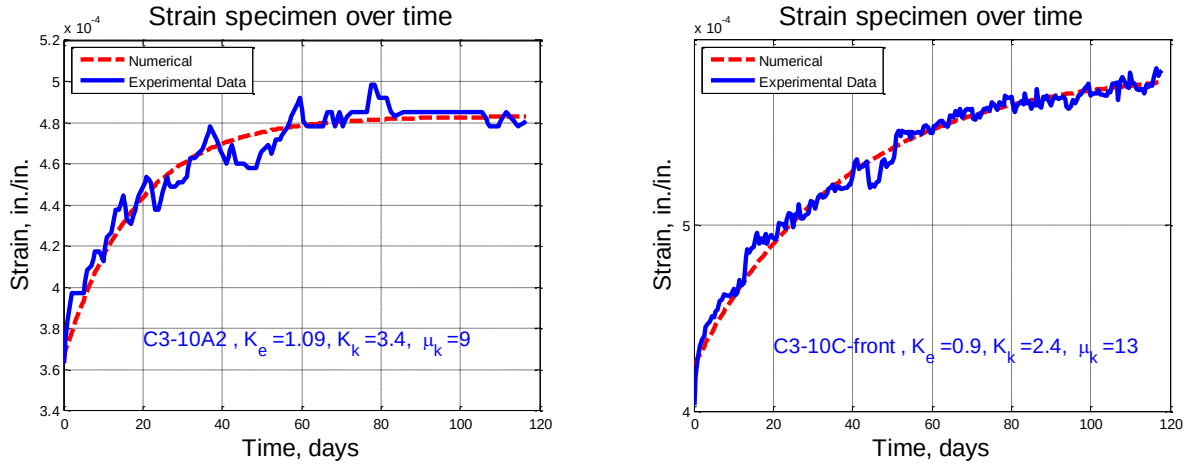

a) Data from DEMEC b) Data from strain gauges

Fig. 3-10 Fitted model constants of 3-layer 10% f_c' specimen

The results of the creep model constants for three different groups and stress levels are listed in the appendix. Statistical distributions were fitted to each group of the three model parameters. The lognormal distributions were found to be adequate representation of distribution

of all model parameters. Fig. 3-11 and Fig. 3-12 illustrate the lognormal distribution plots for parameters in multiple sample groups. The mean and deviation of each of the four parameters are shown in Table 3-7.

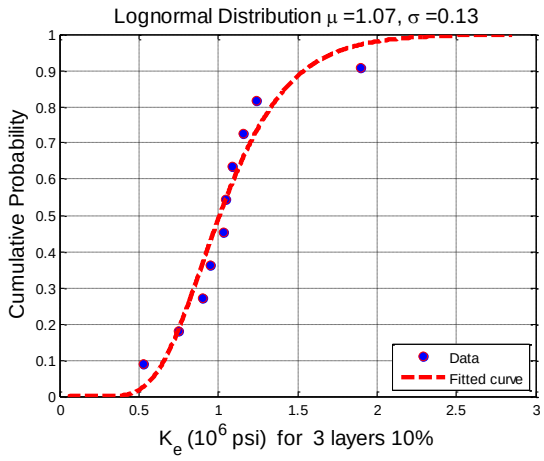

a) Elastic constant for group 2

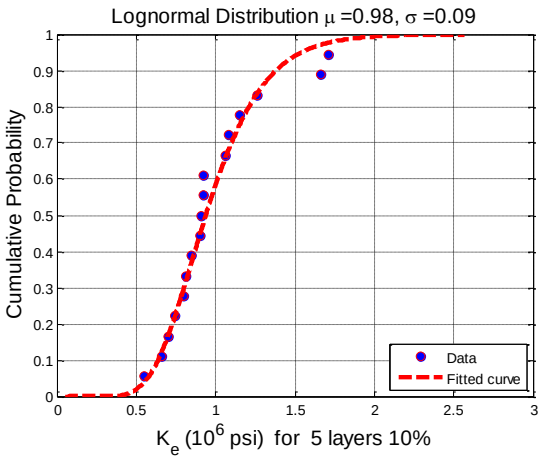

b) Elastic constant for group 4

Fig. 3-11 Lognormal distribution of elastic constant K_e for different groups

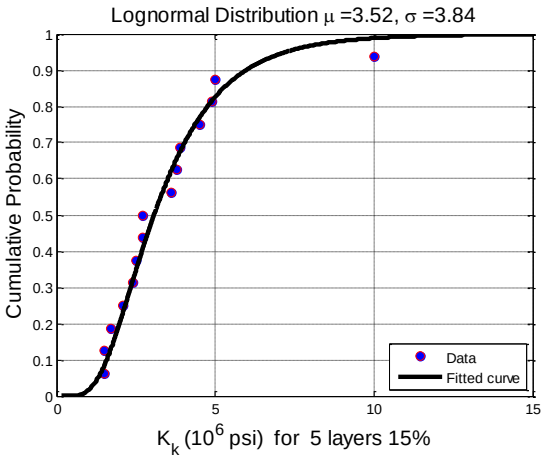

a) Elastic constant for K_k

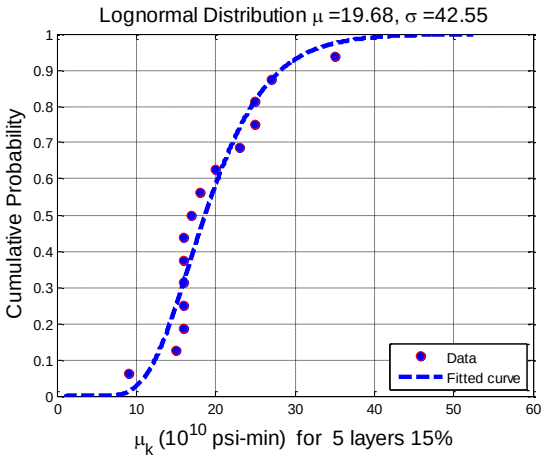

b) Viscous constant for μ_k

Fig. 3-12 Lognormal distribution of constant in group 5

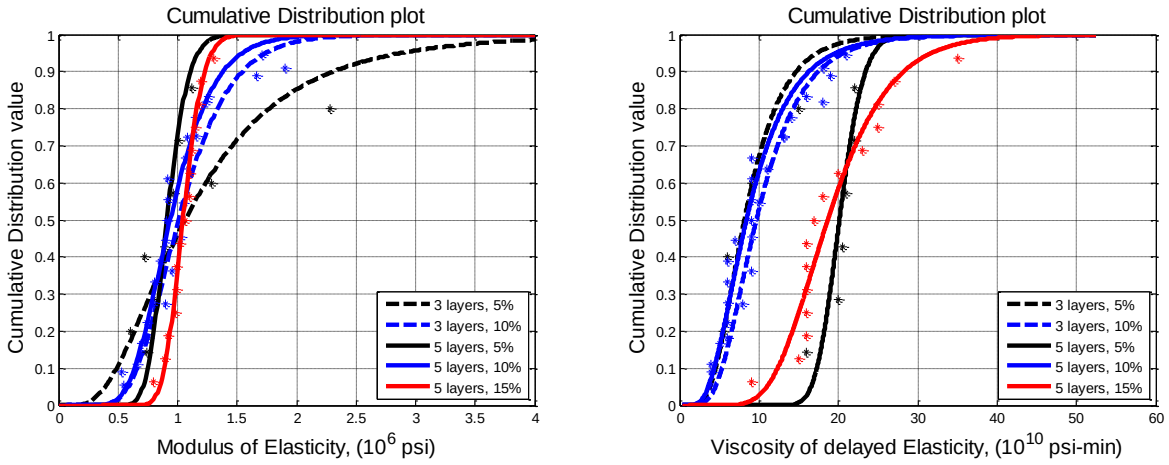

a) Elastic constant for K_k b) Viscous constant for μ_k

Fig. 3-13 Lognormal distribution for entire specimen

Table 3-7 Mean and variance values for viscoelastic model parameters

Groups	Parameter	Mean	Variance	Samples	Distribution
(1) 3 layers 0.05 f_c' L	K_e	1.28 (10^6) psi	0.72 (10^6) psi	4	Lognormal
	K_k	2.10 (10^6) psi	4.67 (10^6) psi		
	μ_k	9.07 (10^{10}) psi-min	19.26 (10^{10}) psi-min		
(2) 3 layers 0.10 f_c'	K_e	1.07 (10^6) psi	0.13 (10^6) psi	10	
	K_k	3.36 (10^6) psi	1.55 (10^6) psi		
	μ_k	10.77 (10^{10}) psi-min	27.77 (10^{10}) psi-min		
(3) 5 layers 0.05 f_c' L	K_e	0.92 (10^6) psi	0.02(10^6) psi	6	
	K_k	1.31 (10^6) psi	0.59 (10^6) psi		
	μ_k	20.28 (10^{10}) psi-min	5.85 (10^{10}) psi-min		
(4) 5 layers 0.10 f_c'	K_e	0.98 (10^6) psi	0.09 (10^6) psi	17	
	K_k	1.82 (10^6) psi	0.87 (10^6) psi		
	μ_k	9.63 (10^{10}) psi-min	28.21 (10^{10}) psi-min		
(5) 5 layers 0.15 f_c'	K_e	1.05 (10^6) psi	0.02 (10^6) psi	15	
	K_k	3.52 (10^6) psi	3.84 (10^6) psi		
	μ_k	19.68 (10^{10}) psi-min	42.55 (10^{10}) psi-min		

3.3.2. Comments on creep test results and fitted data

Observation from test data showed that at stress level of 5% f_c', three-layer CLT panels showed a clearer creep trends but larger parameter variance than five-layer CLT panels over three months. Also, at this stress level, the creep behavior takes longer time to reach to the creep deformation limit, especially for five-layer CLT layer. For this reason, fitted parameters seem not to be reliable for long term prediction of creep deformation, especially in five-layer CLT panels. To have a better fitted parameter, longer duration creep tests are recommended for future studies. Some creep tests at this stress level are ongoing in the UA labs to achieve a better data set. Creep deformations at stress level 10% f_c' and 15% f_c' showed clearer patterns, as can be seen in Fig. 3-12 and appendix. Even though the modulus of elasticity has consistent mean values between three-layer and five-layer of CLT panels at different stress levels, the creep modulus K_k and viscous damping creep parameter μ_k have large variance within each test group as well as between different CLT thickness. This showed that even though CLT is a good quality-controlled engineering material, prediction of creep behavior has high uncertainty. Therefore, the reliability analysis is needed for proposed design equations relating to creep behaviors.

3.3.3. Mechano-sorptive creep

Variations of ambient environmental RH would result in changing MC in specimens. By using the moisture content diffusion model mentioned above, the change of MC in a CLT specimen due to the change of ambient environmental RH can be predicted. The relationship between MC variations and creep behaviors is expressed in Eqs. (3.14). By adjusting the values of μ_ω, the effects of changing ambient environmental RH to creep behavior would be included. To experimentally determine constant μ_ω, an environment with a temperature of 73ºF (22.8ºC)

and ambient RH of 70% was selected as an original condition. At this environmental condition $\Delta MC = 0$ ($MC_1 - MC_1$), at time t = 0, Eqs. (3.14) becomes:

$$\varepsilon_1 = \frac{\sigma_1}{E_1} = \frac{\sigma_1}{K_e} \tag{3.15}$$

Since the outside environment changed to the second environmental condition, with moisture content MC_2 in CLT specimen. At time t = 0, Eqs. (3.14) becomes:

$$\varepsilon_2 = \frac{\sigma_2}{E_2} = \frac{\sigma_2}{K_e} + \frac{\sigma_2}{\mu_\omega}(MC_2 - MC_1) \tag{3.16}$$

From Eqs. (3.15) and Eqs. (3.16), if the stress in two conditions is identical ($\sigma_2 = \sigma_1$), the mechano-sorptive constant can be determined

$$\mu_\omega = \frac{E_1 . E_2 . (MC_2 - MC_1)}{E_1 - E_2} \tag{3.17}$$

where: E_1 modulus of elasticity of CLT specimens at original environment; E_2 is the CLT modulus of elasticity at new environment.

Experiments were conducted for three sets of CLT specimens at 50%, 70% and 90% RH at a constant temperature of 73ºF (22.8ºC), respectively, to determine the total modulus of elasticity (MOE). Test data were then used to calculate the mean of the mechano-sorptive constant μ_ω using Eqs. (3.17). Detailed information is presented in Table 3-8.

Table 3-8 Modulus of elasticity and mechano-sorptive constant value for CLT

RH (%)	Moisture content		MOE		Mean μ_ω (10^6) psi
	N0. sample	Mean (%)	N0. sample	Mean (ksi)	
50	5	10.67	6	832.97	0.122
70	5	13.16	13	711.58	
90	6	20.51	11	504.19	0.127

A subroutine was developed to numerically predict the change of axial strain in CLT specimens under the variation of the ambient RH. In this model, Eqs. (3.14) and values of mechano-sorptive constants in Table 3-8 were used. The mean values of the viscoelastic model parameters were used for different CLT configurations in both constant RH (50%) and ambient RH varied between 50% and 70%; as shown in Table 3-9.

Table 3-9 Specifications of numerical CLT specimens

Groups	Dimension (in.)	K_e (10^6) psi	K_k (10^6) psi	μ_κ (10^{10}) psi-min	Stress levels	RH
3 layers	3.90×24×24	1.03	2.57	14.06	0.10 f_c'	50% -70%
3 layers L	3.90×24×96					
5 layers	6.75×24×24					
5 layers L	6.75×24×96					

3.4. Examples, Results and Discussion

To investigate the effects of different surrounding RH on the axial strain in CLT panels, the ambient RH was kept constant at 50% for the first 60 days and then RH was suddenly switched between 50% and 70% with a four-day period. During this period the temperature was maintained at 73ºF (22.8ºC). The axial stress level of 0.10 *fc'* was applied for all tested specimens, which means the axial applied forces were equal to 32.76 kips (145.71 kN) and 56.70 kips (252.20 kN) on 3 layer and 5 layer CLT panels, respectively. Fig. 3-14 shows the moisture content profile and changes in the axial strain at different locations in a CLT specimen.

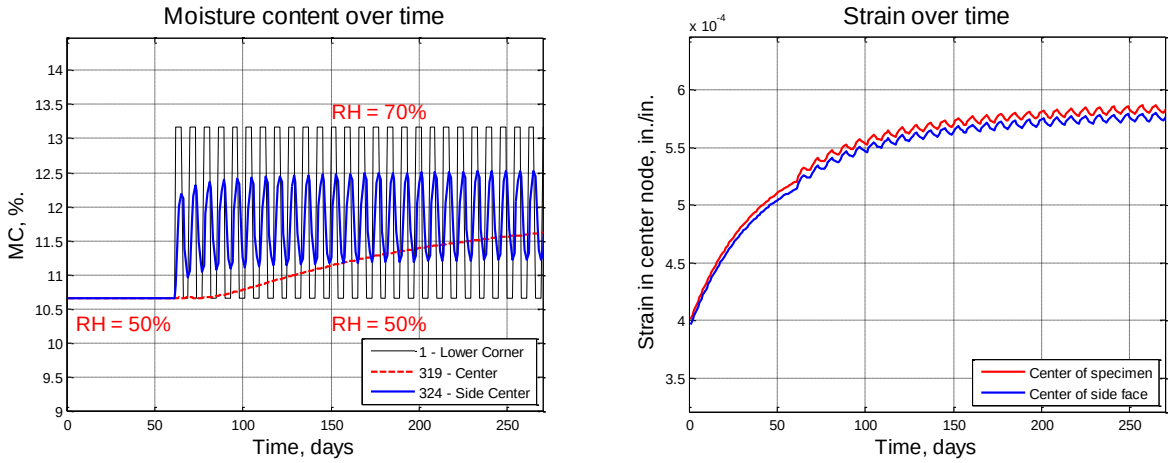

a) Moisture content profile b) Axial strain in specimen

Fig. 3-14 Moisture content and axial strain history in a 3 layer specimen

The effects of panel sizes to axial strain in CLT panels were also studied by numerically examining four different CLT panel configurations. The results are presented in Fig. 3-15.

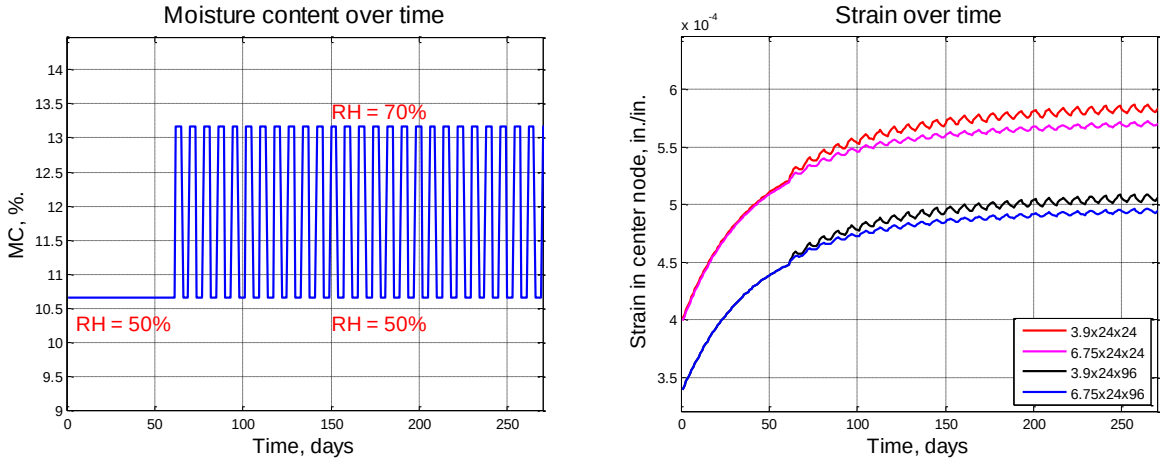

a) Moisture content profile b) Axial strain in specimen

Fig. 3-15 Axial strain history in different CLT configurations

As can be seen in Fig. 3-15, under the identical ambient RH profile (Fig. 3-15a), the axial strain in various types of CLT specimens with different configurations showed similar strain patterns (Fig. 3-15b). The variation in axial strain due to changing ambient RH between 50% and 70% is approximately 1.8% (7.2×10^{-6} in/in.) (18.29×10^{-6} cm/cm.). With the same size CLT specimens (24×24 in.) (60.96×60.96 cm) but different thickness (3.9 in. and 6.75 in.) (9.91 cm

and 17.15 cm), the axial strain variance is negligible under the constant surrounding RH of 50%. When the ambient RH changes between 50% and 70%, the differences in axial strains are significant, at around 4% (16×10^{-6} in/in.) (40.64×10^{-6} cm/cm.) The effect of changing surrounding RH on axial strain in 3 layer CLT panels is larger than that of 5 layer CLT panels (as shown in Fig. 3-15b). This can be explained that the 5 layer CLT panels are thicker than 3 layer ones, thus 5 layer CLT panels required more time to absorb moisture from the ambient environment.

3.5. Conclusions

In this chapter, a numerical model for prediction of moisture content migration in CLT panels was introduced. A series of tests on moisture content migration in CLT panels were conducted, and collected data were used to calibrate the numerical model parameters. The moisture content diffusion model was used to evaluate the absorption and desorption coefficients under different RH. A new viscoelastic mechano-sorptive creep model with four parameters was proposed to predict long-term creep deformation in CLT panels.

From the experimental data and model parameter calibration, an absorption coefficient of 0.013 $in^2.day^{-1}$ (96×10^{-12} $m^2.s^{-1}$) and 0.032 $in^2.day^{-1}$ (237×10^{-12} $m^2.s^{-1}$) were recommended for CLT with a step change in RH from 50% to 70% and 70% to 90%, respectively. For a step change in RH from 90% to 70%, a desorption diffusivity of 0.041 $in^2.day^{-1}$ (304×10^{-12} $m^2.s^{-1}$) was suggested. The influences of CLT thickness on diffusion coefficients were minimal. The mean values of K_e = 1.03×10^6 psi (7.09×10^6 kPa), K_k = 2.57×10^6 psi (17.71×10^6 kPa) and μ_k = 14.06×10^{10} psi-min (96.87×10^{10} kPa-min) were recommended for 3 - 5 layer CLT panels subjected to a stress level less than 15% f_c' in 50% RH. Under step change in RH, the mechano-sorptive constant values of 0.122×10^6 psi (0.84×10^6 kPa) and 0.127×10^6 psi (0.88×10^6 kPa) were

suggested for the step change between 50% to 70% and 70% to 90%, respectively. A variance less than 2% in axial strain in 3 layer and 5 layer CLT specimens subjected to RH changed between 50% and 70% is observed in a numerical example analysis.

3.6. Appendix

3.6.1. Fit data for diffusion moisture coefficient

3.6.1.1. Specimens in group 1 (3 layers, 3.9×24×24 in.)

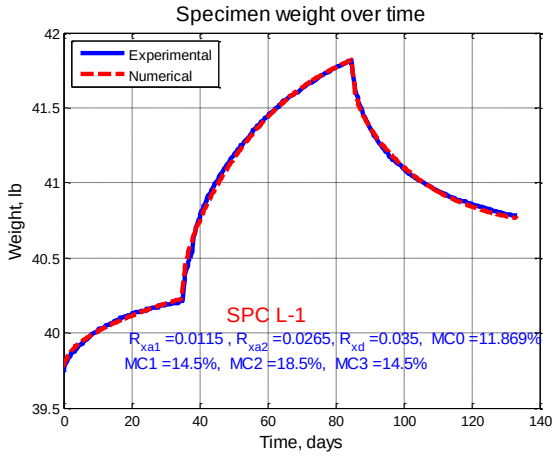

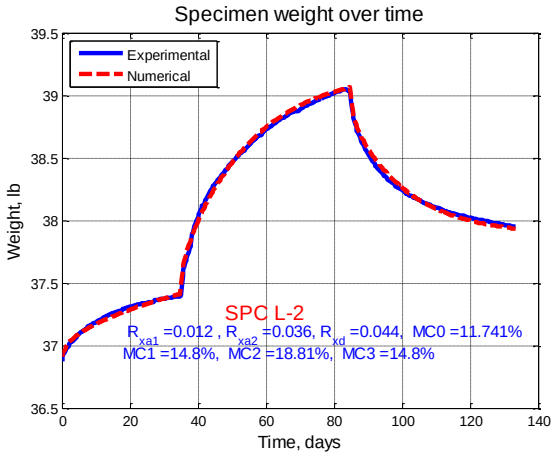

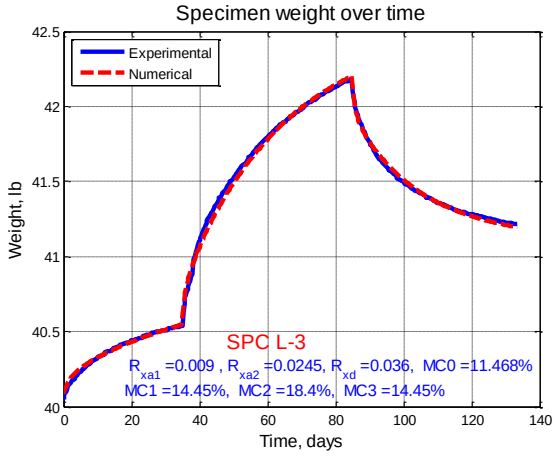

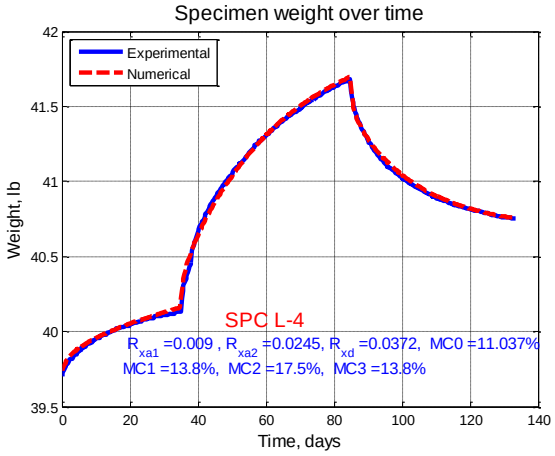

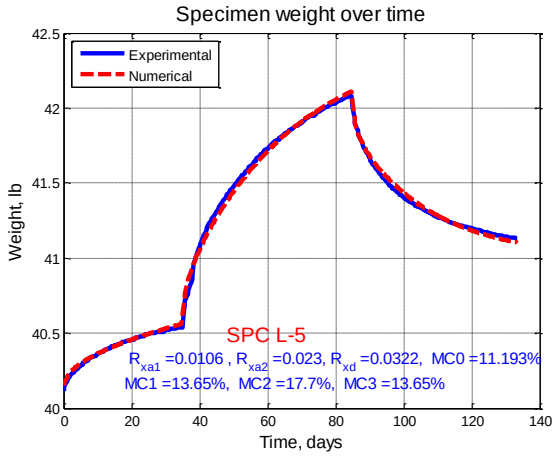

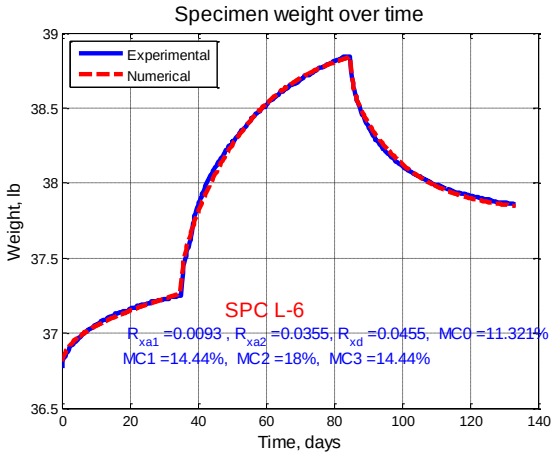

3.6.1.2. Specimens in group 2 (3 layers, 3.9×12×24 in.)

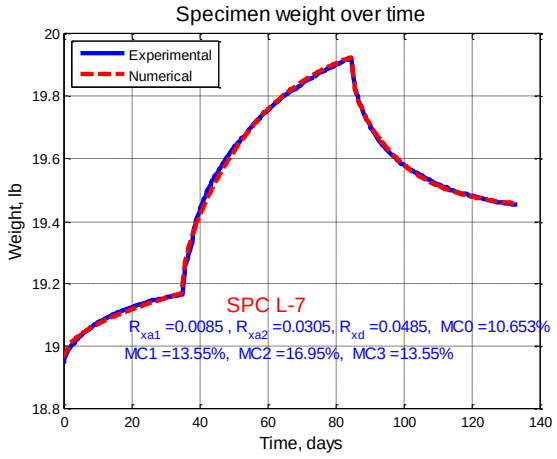

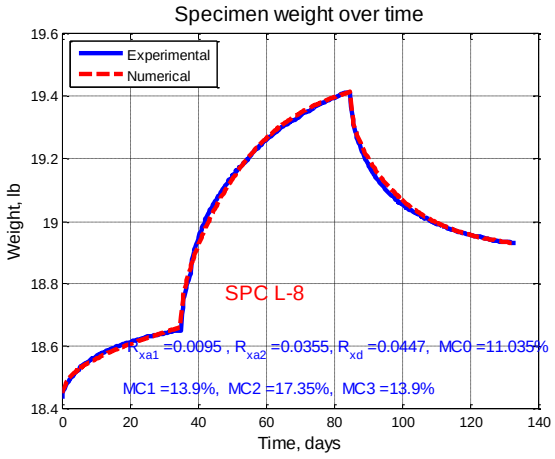

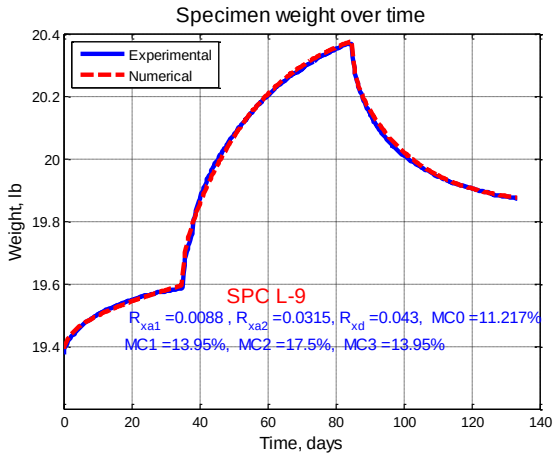

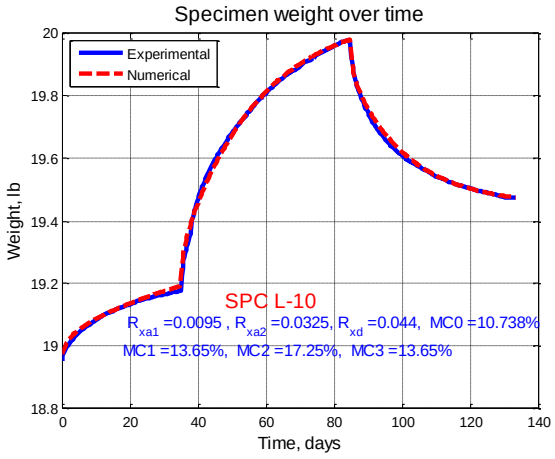

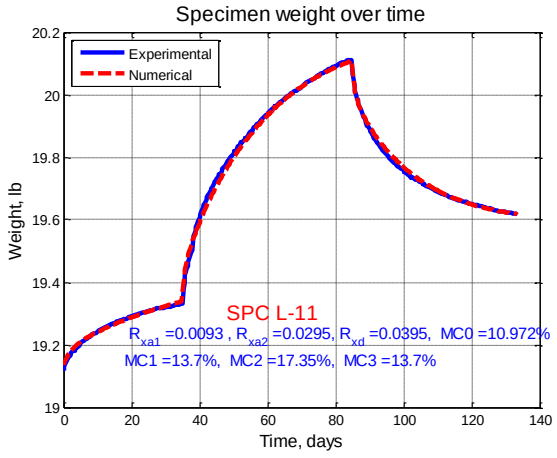

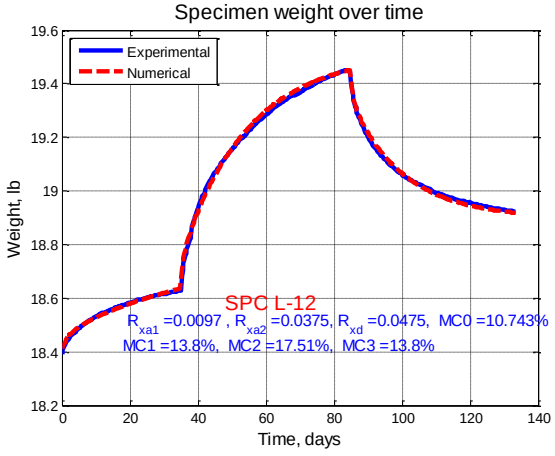

3.6.1.3. Specimens in group 3 (5 layers, 6.67×12×12 in.)

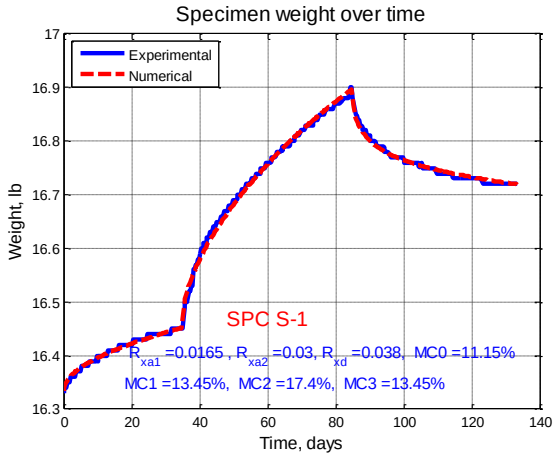

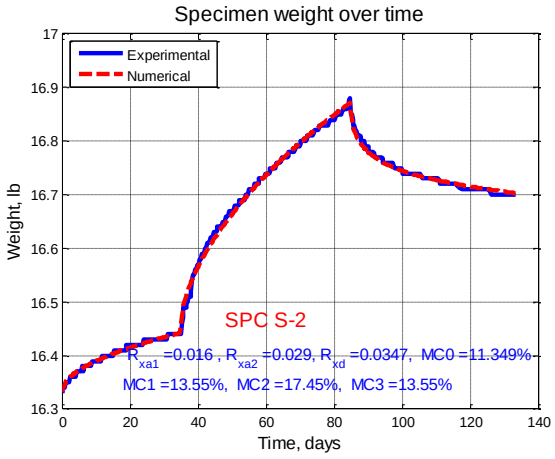

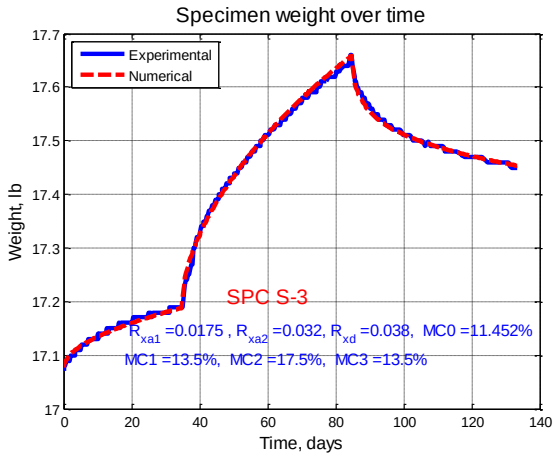

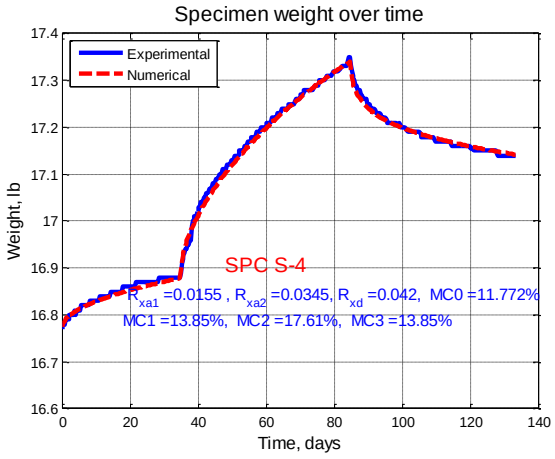

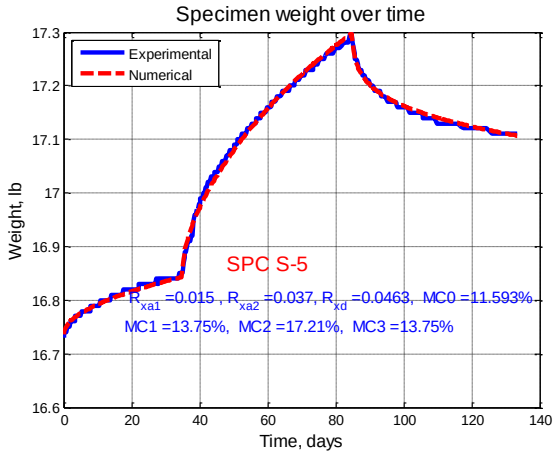

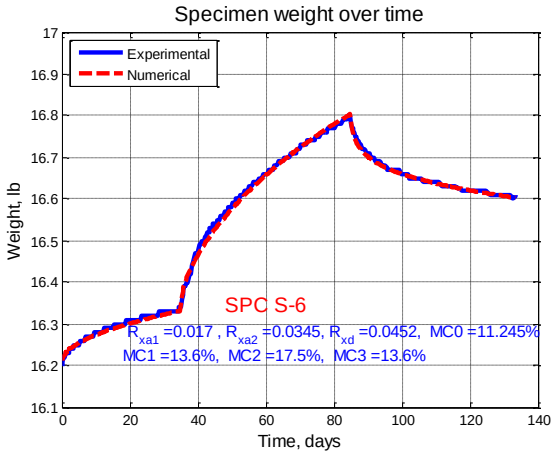

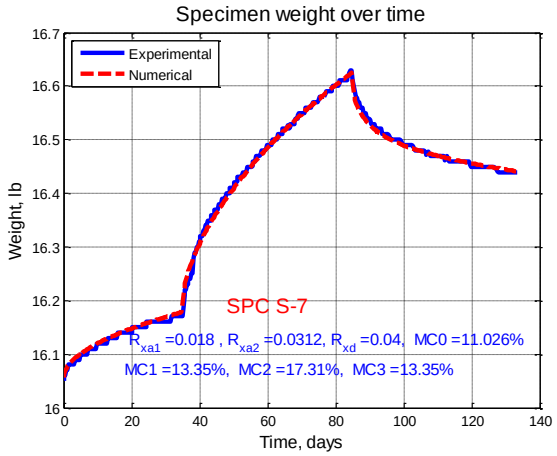
Specimen weight over time
Experimental
Numerical
SPC S-7
R_{xa1} =0.018 , R_{xa2} =0.0312, R_{xd} =0.04, MC0 =11.026%
MC1 =13.35%, MC2 =17.31%, MC3 =13.35%
Weight, lb
Time, days

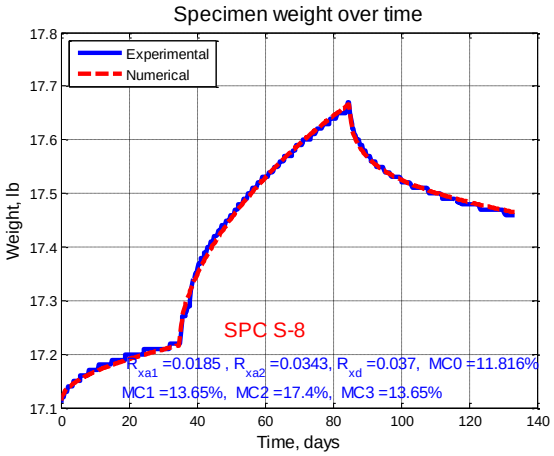
Specimen weight over time
Experimental
Numerical
SPC S-8
R_{xa1} =0.0185 , R_{xa2} =0.0343, R_{xd} =0.037, MC0 =11.816%
MC1 =13.65%, MC2 =17.4%, MC3 =13.65%
Weight, lb
Time, days

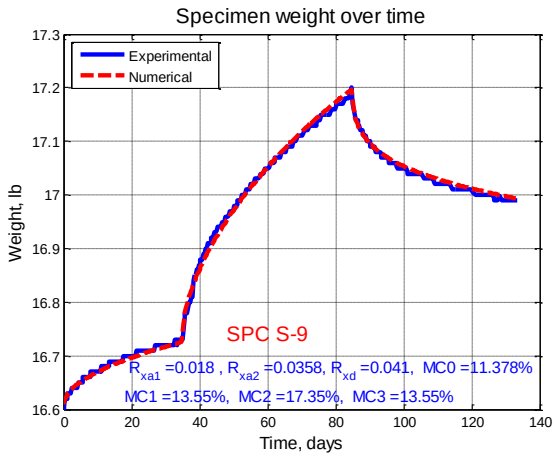
Specimen weight over time
Experimental
Numerical
SPC S-9
R_{xa1} =0.018 , R_{xa2} =0.0358, R_{xd} =0.041, MC0 =11.378%
MC1 =13.55%, MC2 =17.35%, MC3 =13.55%
Weight, lb
Time, days

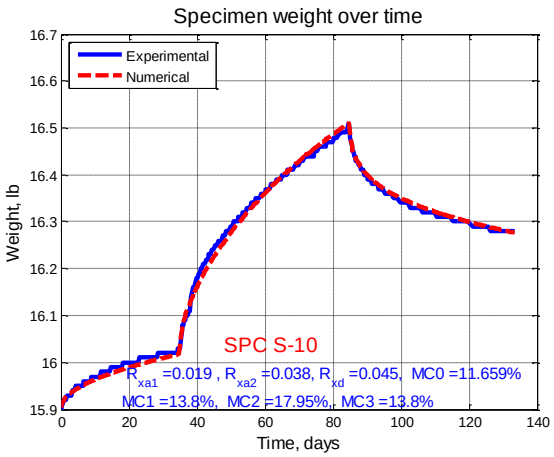
Specimen weight over time
Experimental
Numerical
SPC S-10
R_{xa1} =0.019 , R_{xa2} =0.038, R_{xd} =0.045, MC0 =11.659%
MC1 =13.8%, MC2 =17.95%, MC3 =13.8%
Weight, lb
Time, days

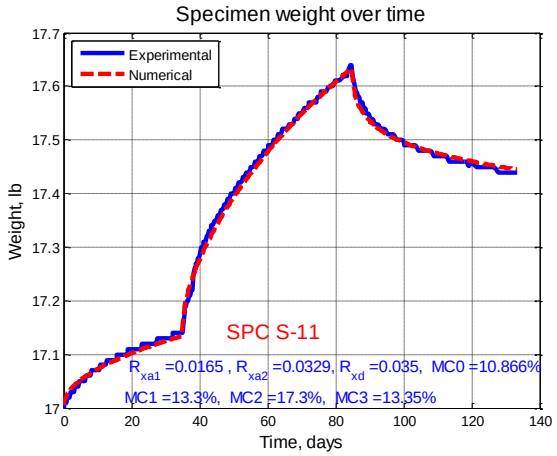
Specimen weight over time
Experimental
Numerical
SPC S-11
R_{xa1} =0.0165 , R_{xa2} =0.0329, R_{xd} =0.035, MC0 =10.866%
MC1 =13.3%, MC2 =17.3%, MC3 =13.35%
Weight, lb
Time, days

3.6.2. Visco-elastic creep model constants

3.6.2.1. Fit data for visco-elastic creep model constants

Groups	SPC	Location	K_e (10^6 psi)	K_k (10^6 psi)	μ_μ (10^{10} psi-min)
(1) 3 layers 0.05 f_c' L	C3L-5	2 - front	1.29	1.45	6
		2 - back	0.72	1.15	9
		2 - bottom	2.28	4.6	15
		3 - front	0.6	0.6	5.5
(2) 3 layers 0.10 f_c'	C3-10-A	front	1.03	2.1	6
		back	0.95	2.9	11
		2	1.09	3.4	9
	C3-10-B	front	1.24	4.7	18
		back	1.9	3.8	9
		1	0.75	4	8
	C3-10-C	front	0.9	2.4	13
		1	1.16	5.3	18
	C3-10-D	1	0.53	1.7	4
		2	1.05	3	10
(3) 5 layers 0.05 f_c' L	C5L-5	1 - front	1.12	1	20.5
		2 - front	1.01	1.3	22
		2 - back	0.8	1.5	21
		2 - top	0.89	1.6	22
		2 - bottom	0.74	1.7	20
		3 - front	0.96	0.4	16
(4) 5 layers 0.10 f_c'	C5-10-A	front	0.92	2	13
		back	1.08	2.5	16
		1	0.55	0.98	4
		2	0.9	3.2	14

	C5-10-B	front	1.71	2.6	19
		1	0.66	1.7	5
		2	1.66	3.6	21
		3	0.8	2.6	7
	C5-10-C	back	0.92	1.3	9
		1	0.81	1.8	9
		2	1.15	1.8	9
		3	0.74	1.1	6
	C5-10-D	front	1.06	0.8	6
		back	0.91	0.7	4
		1	0.7	1.3	6
		2	1.26	1	6
		3	0.85	1.6	9
(5) 5 layers 0.15 f_c'	C5-15-A	front	1.15	2.1	20
		2	1.1	5	16
		3	1.19	3.8	16
		4	0.89	2.4	16
	C5-15-B	front	1.12	2.7	35
		2	0.8	4.9	16
		4	1.18	10	25
	C5-15-C	front	0.92	1.5	23
		back	0.98	1.5	18
		2	1.06	3.9	25
		3	1.02	2.7	15
	C5-15-D	2	1.1	2.5	16
		3	1.3	3.6	27
		4	0.99	1.7	9
		5	0.99	4.5	17

3.6.2.2. Specimens in group 1, SPC C3L-5, (3 layers, 3.9×24×96 in., 5% f_c'

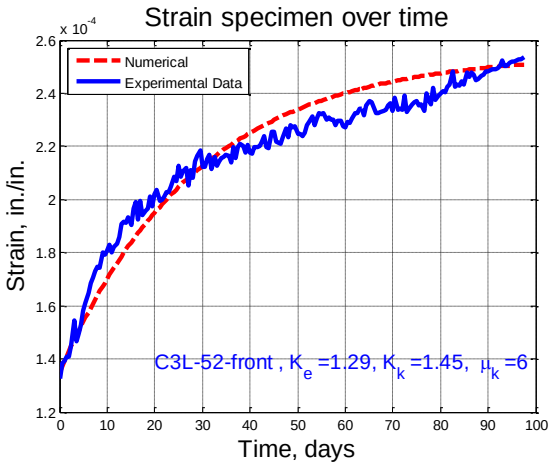

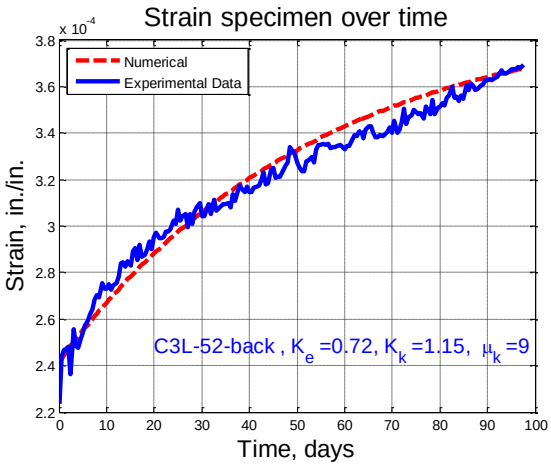

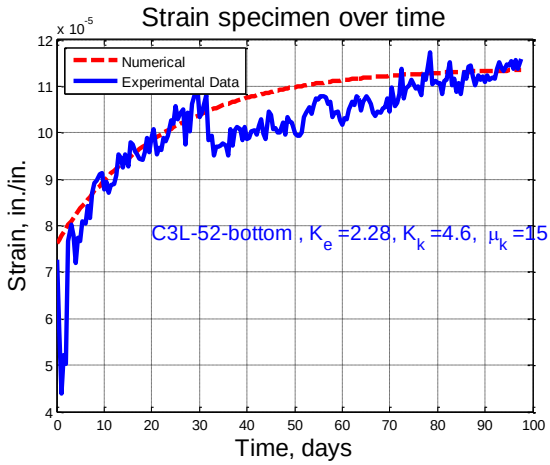

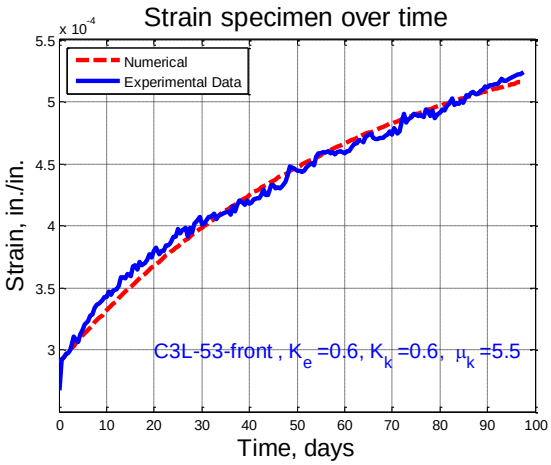

3.6.2.3. Specimens in group 2, SPC C3-10, (3 layers, 3.9×24×24 in.), 10 % f_c'

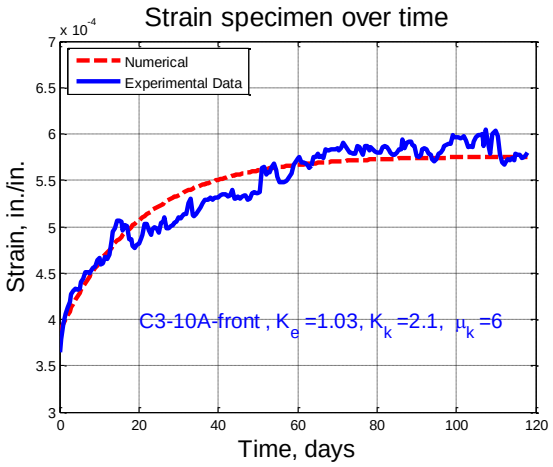

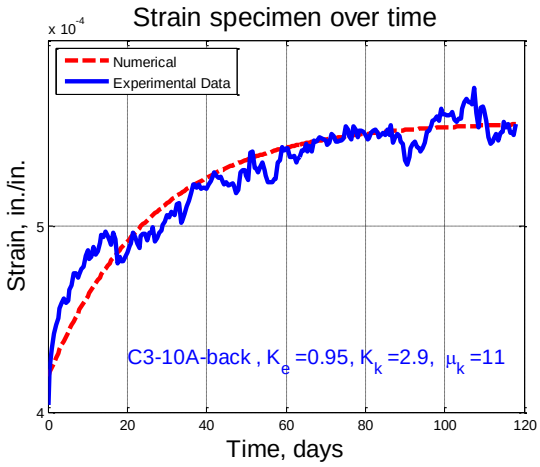

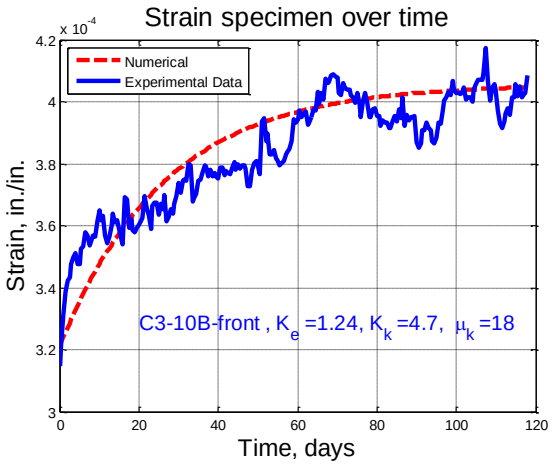

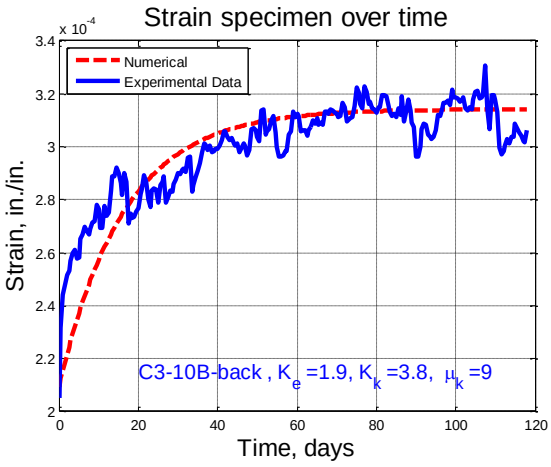

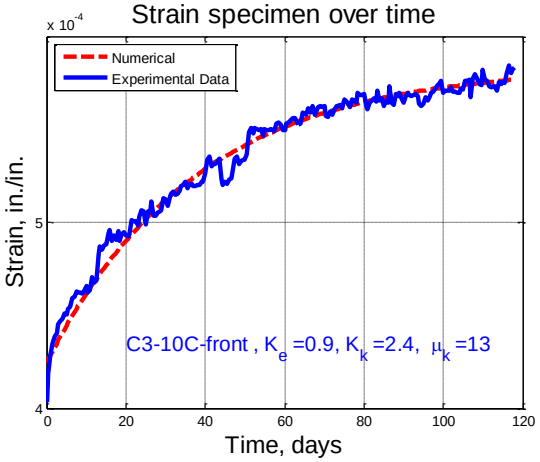

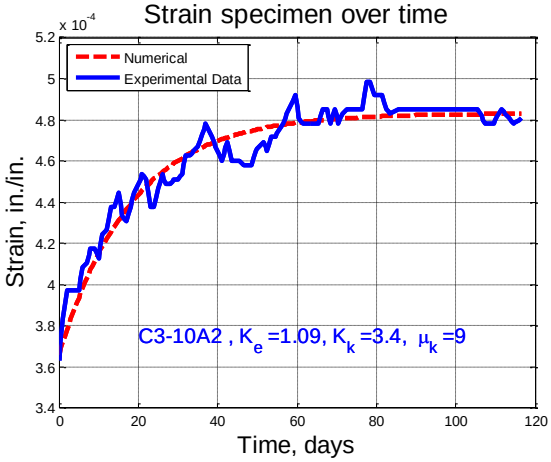

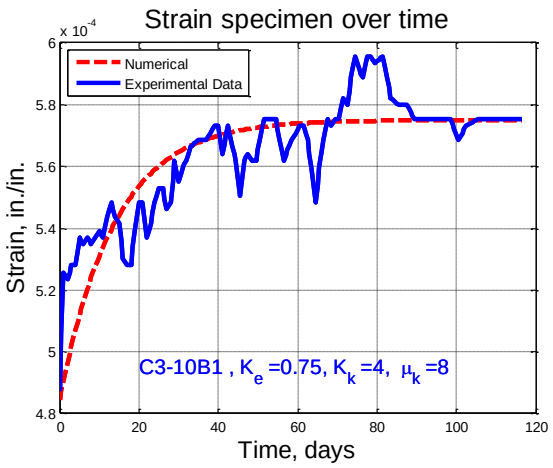
Strain specimen over time
x 10^-4
Numerical
Experimental Data
Strain, in./in.
Time, days
C3-10B1 , K_e =0.75, K_k =4, μ_k =8

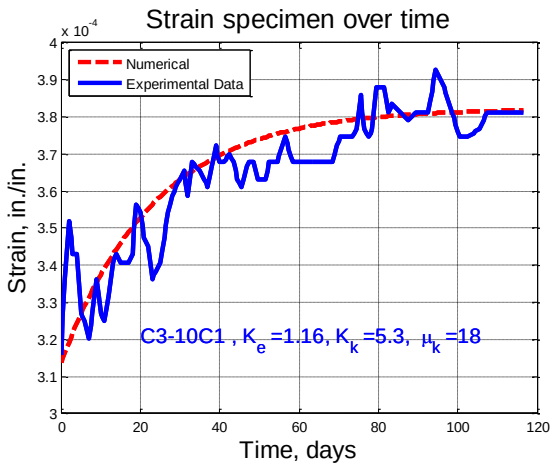
Strain specimen over time
x 10^-4
Numerical
Experimental Data
Strain, in./in.
Time, days
C3-10C1 , K_e =1.16, K_k =5.3, μ_k =18

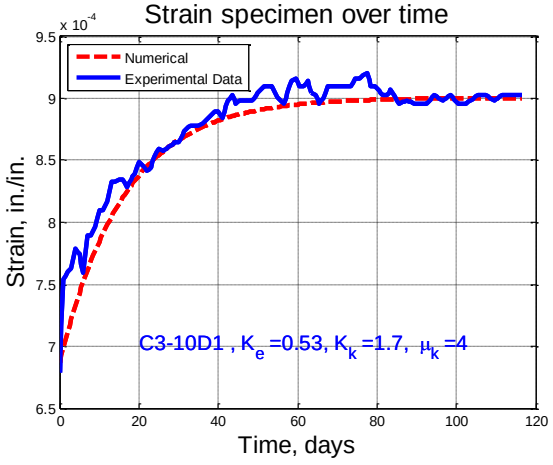
Strain specimen over time
x 10^-4
Numerical
Experimental Data
Strain, in./in.
Time, days
C3-10D1 , K_e =0.53, K_k =1.7, μ_k =4

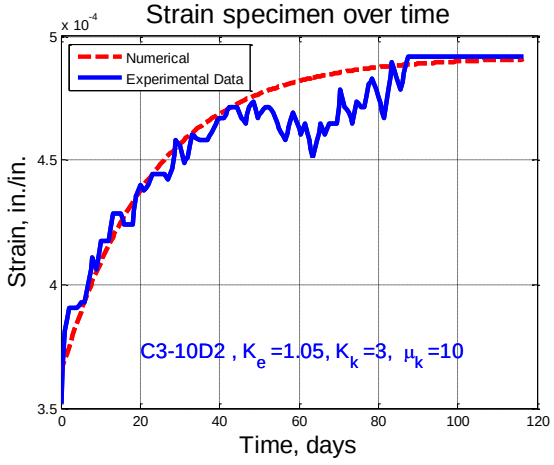
Strain specimen over time
x 10^-4
Numerical
Experimental Data
Strain, in./in.
Time, days
C3-10D2 , K_e =1.05, K_k =3, μ_k =10

3.6.2.4. Specimens in group 3, SPC C5L-5, (5 layers, 6.75×24×96 in.), 5% f_c'

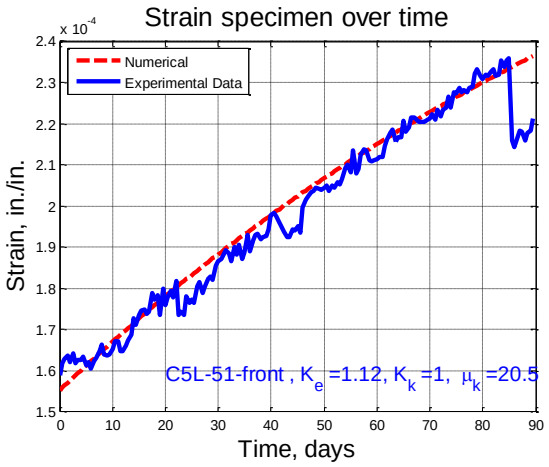

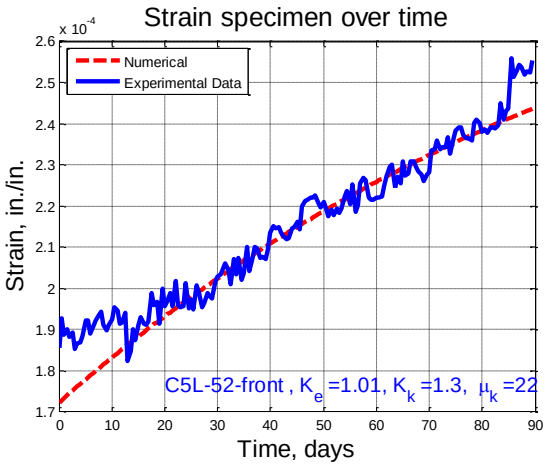

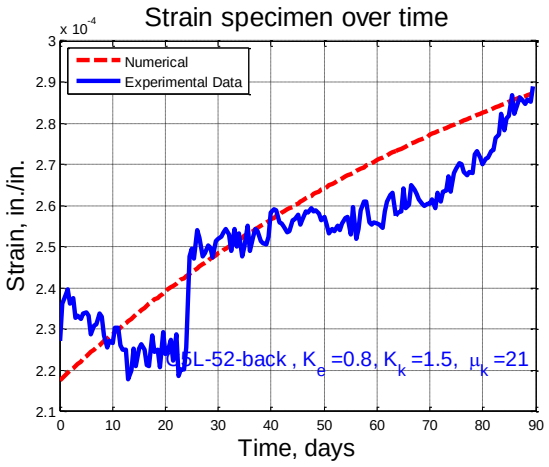

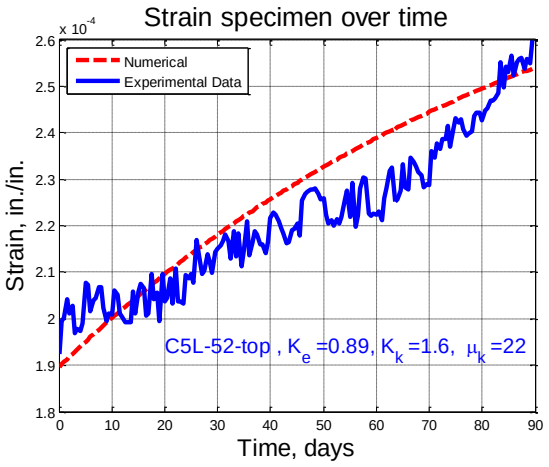

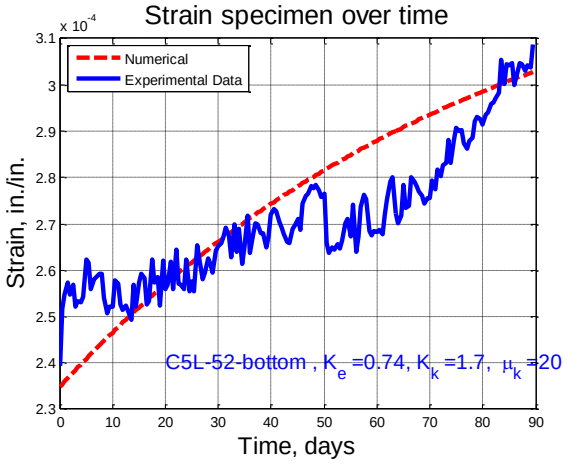

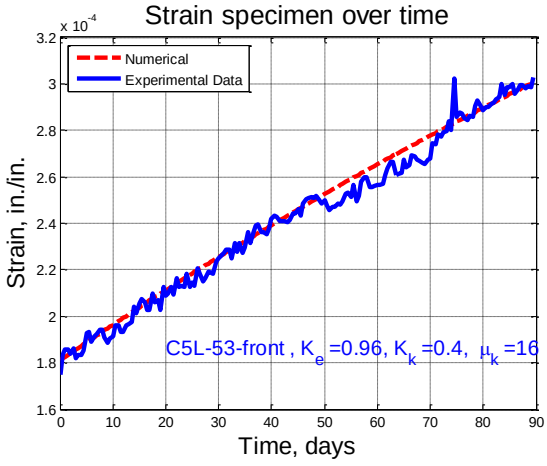

3.6.2.5. Specimens in group 4, SPC C5-10, (5 layers, 6.75×24×24 in.), 10% f_c'

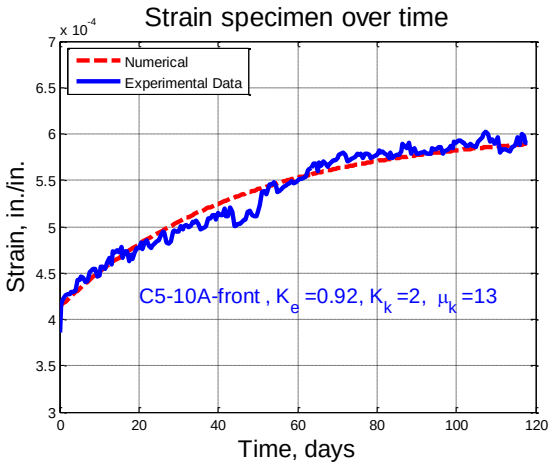

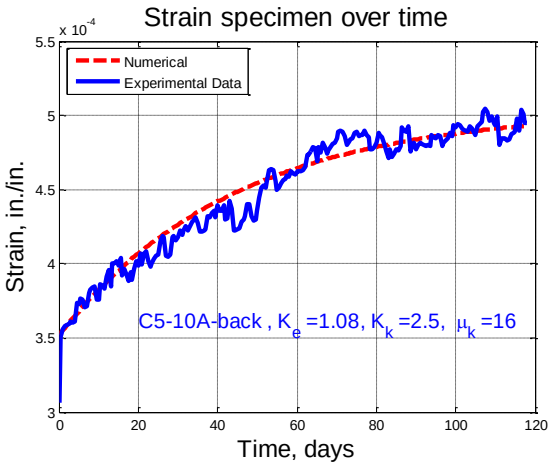

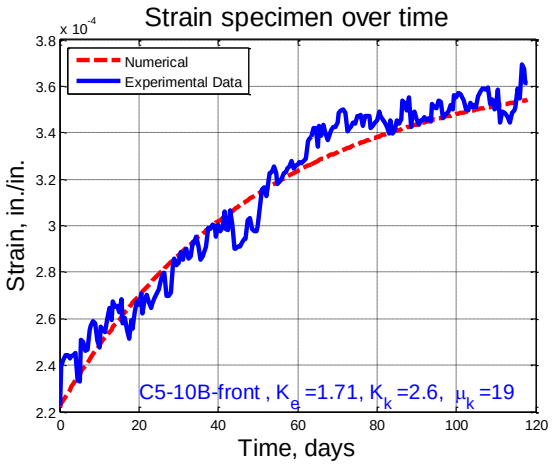

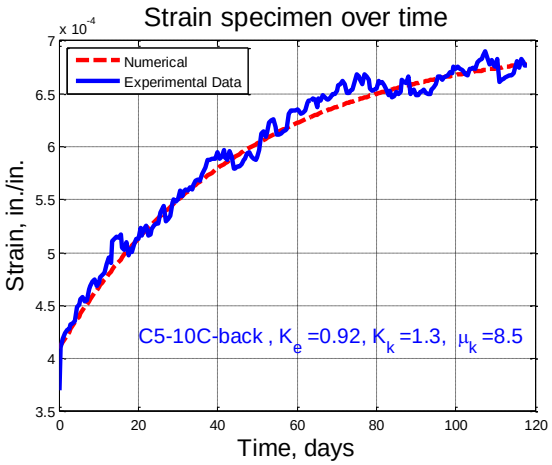

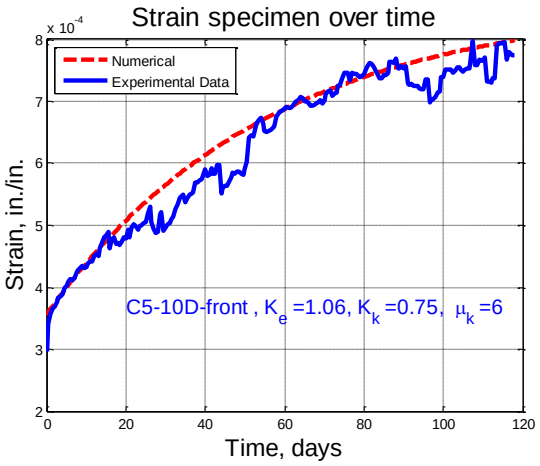

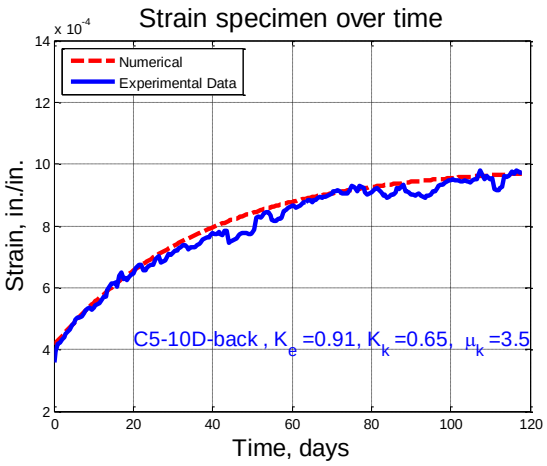

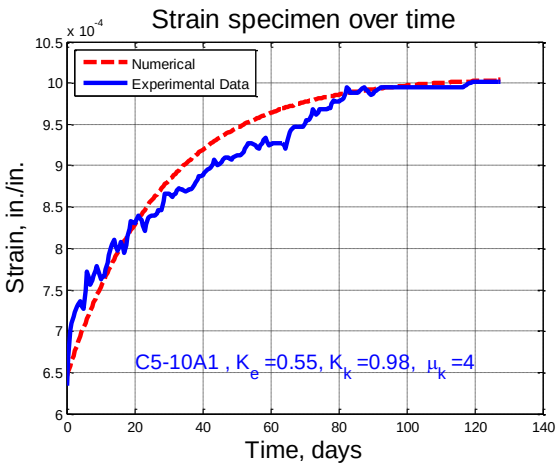
Strain specimen over time
x 10^-4
Numerical
Experimental Data
C5-10A1 , K_e =0.55, K_k =0.98, μ_k =4
Strain, in./in.
Time, days

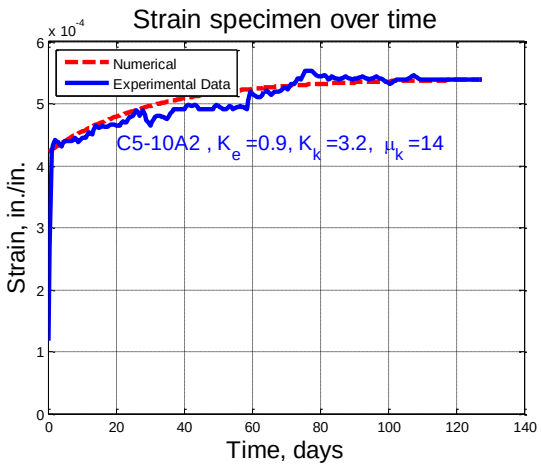
Strain specimen over time
x 10^-4
Numerical
Experimental Data
C5-10A2 , K_e =0.9, K_k =3.2, μ_k =14
Strain, in./in.
Time, days

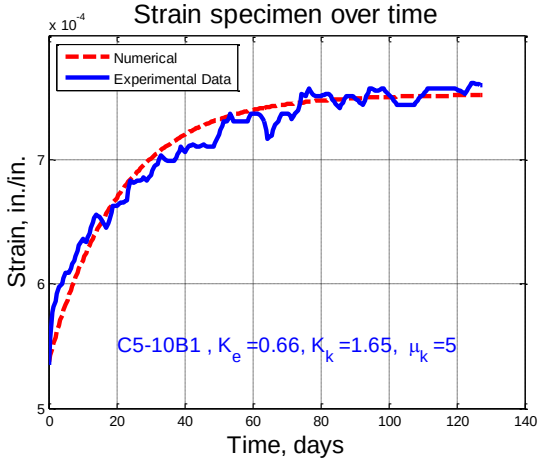
Strain specimen over time
x 10^-4
Numerical
Experimental Data
C5-10B1 , K_e =0.66, K_k =1.65, μ_k =5
Strain, in./in.
Time, days

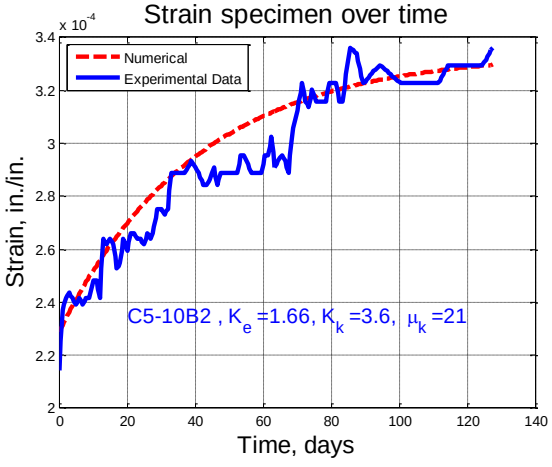
Strain specimen over time
x 10^-4
Numerical
Experimental Data
C5-10B2 , K_e =1.66, K_k =3.6, μ_k =21
Strain, in./in.
Time, days

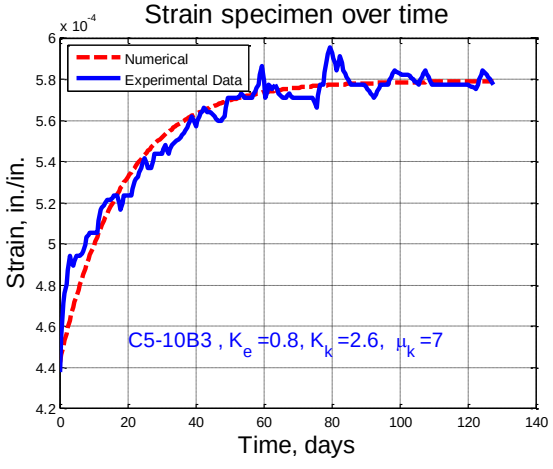
Strain specimen over time
x 10^-4
Numerical
Experimental Data
C5-10B3 , K_e =0.8, K_k =2.6, μ_k =7
Strain, in./in.
Time, days

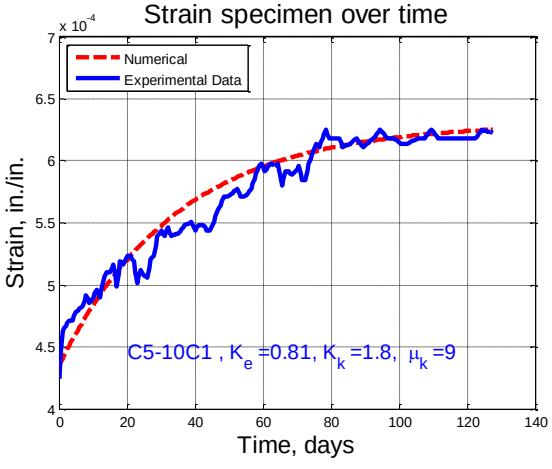
Strain specimen over time
x 10^-4
Numerical
Experimental Data
C5-10C1 , K_e =0.81, K_k =1.8, μ_k =9
Strain, in./in.
Time, days

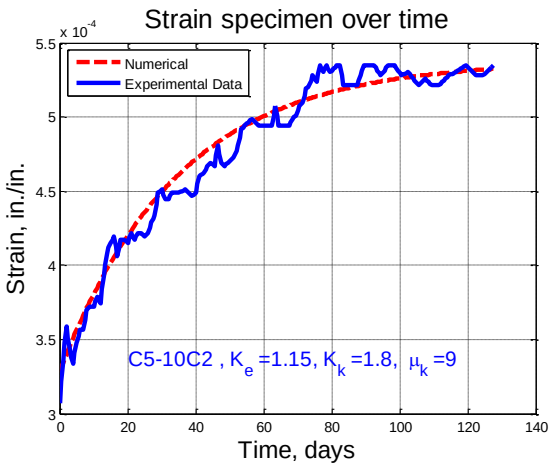
Strain specimen over time
x 10^-4
Numerical
Experimental Data
Strain, in./in.
Time, days
C5-10C2 , K_e =1.15, K_k =1.8, μ_k =9

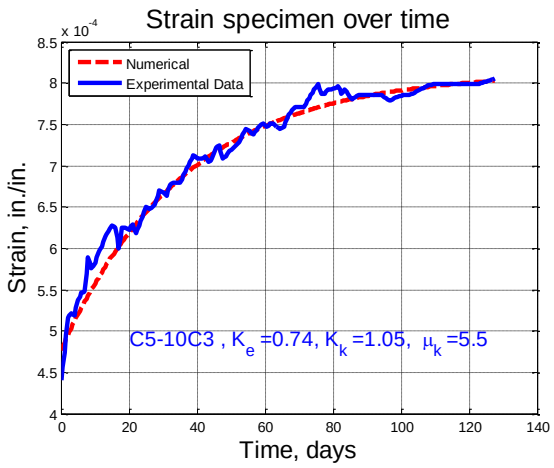
Strain specimen over time
x 10^-4
Numerical
Experimental Data
Strain, in./in.
Time, days
C5-10C3 , K_e =0.74, K_k =1.05, μ_k =5.5

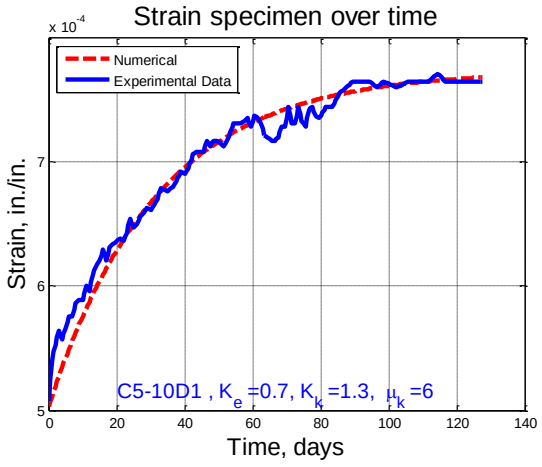
Strain specimen over time
x 10^-4
Numerical
Experimental Data
Strain, in./in.
Time, days
C5-10D1 , K_e =0.7, K_k =1.3, μ_k =6

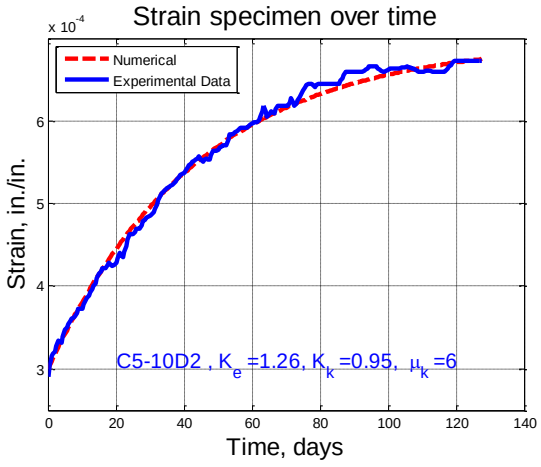
Strain specimen over time
x 10^-4
Numerical
Experimental Data
Strain, in./in.
Time, days
C5-10D2 , K_e =1.26, K_k =0.95, μ_k =6

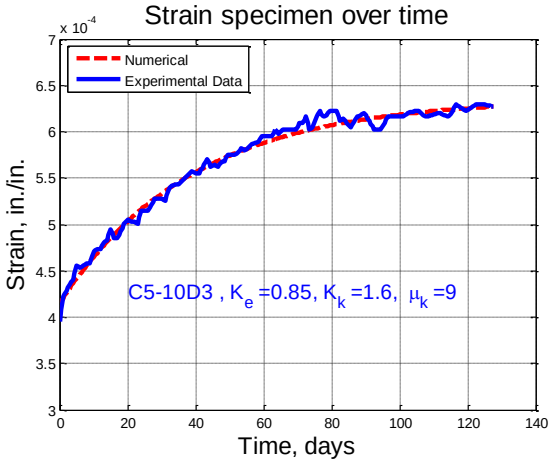
Strain specimen over time
x 10^-4
Numerical
Experimental Data
Strain, in./in.
Time, days
C5-10D3 , K_e =0.85, K_k =1.6, μ_k =9

3.6.2.6. Specimens in group 5, SPC C5-15, (5 layers, 6.75×24×24 in.), 15% f_c'

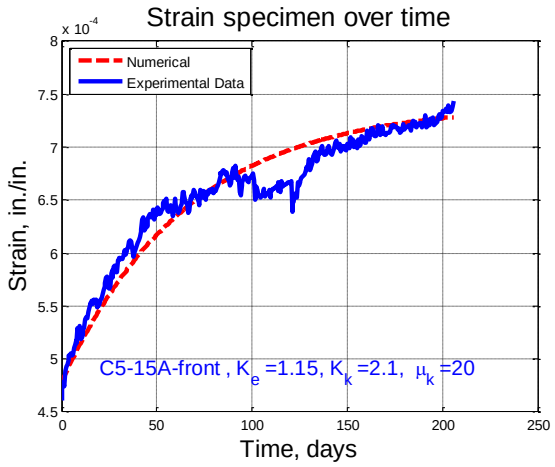

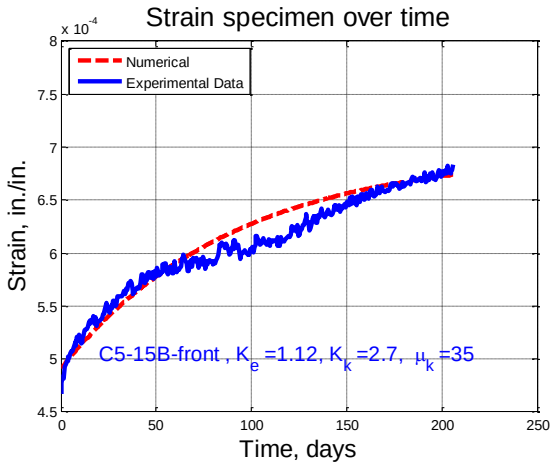

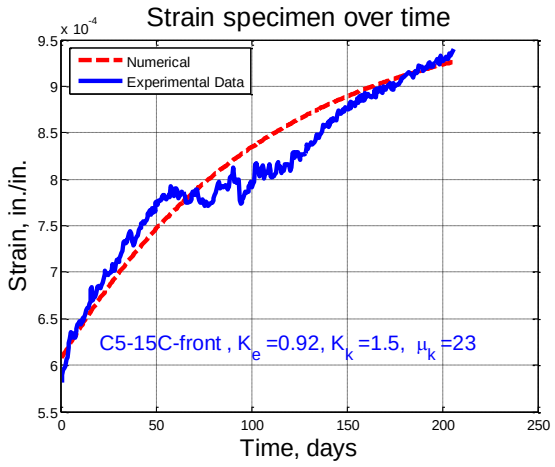

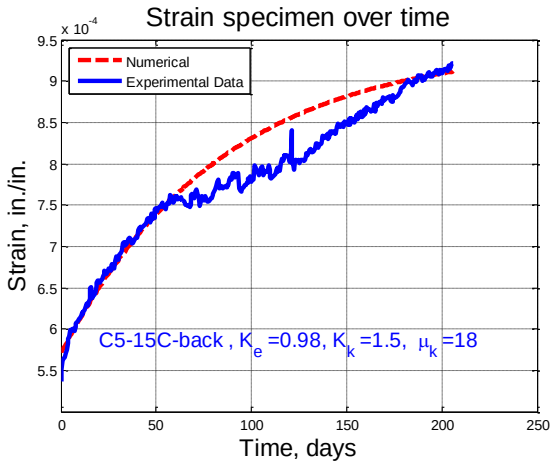

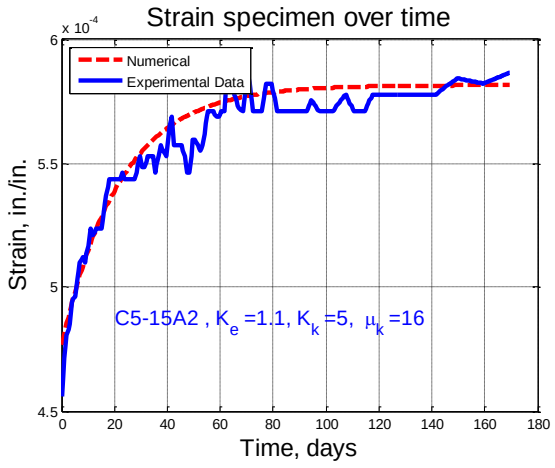

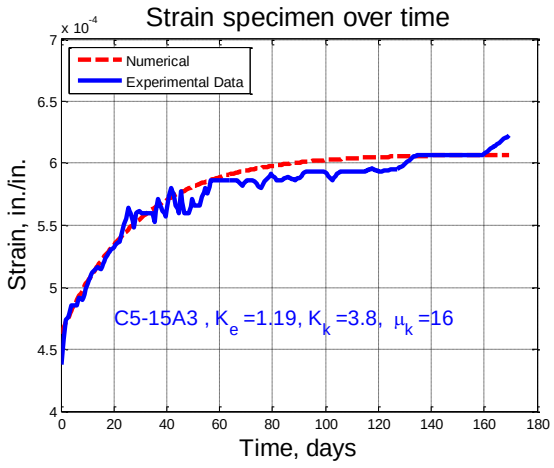

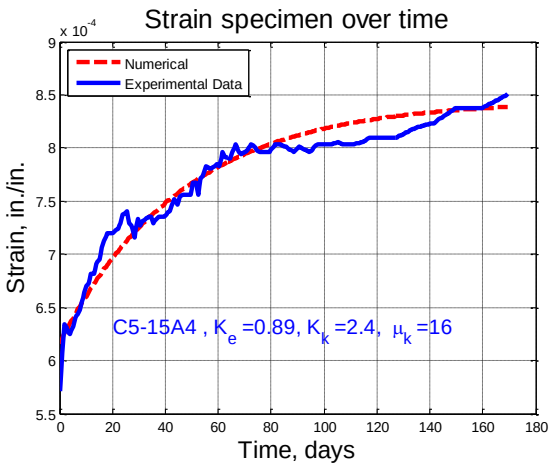
Strain specimen over time
x 10^-4
Numerical
Experimental Data
C5-15A4 , Ke =0.89, Kk =2.4, μk =16
Strain, in./in.
Time, days

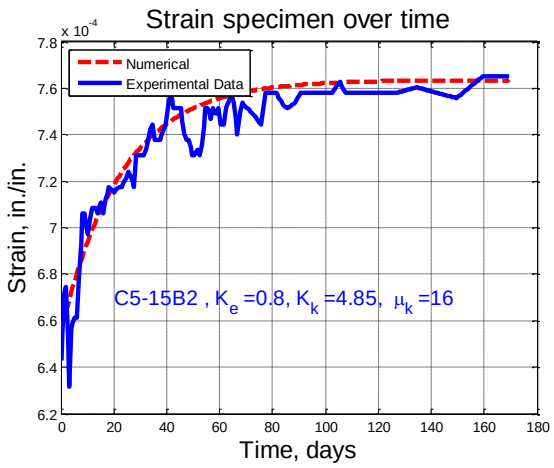
Strain specimen over time
x 10^-4
Numerical
Experimental Data
C5-15B2 , Ke =0.8, Kk =4.85, μk =16
Strain, in./in.
Time, days

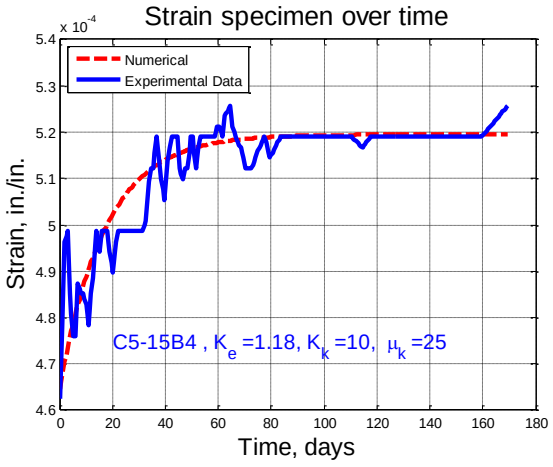
Strain specimen over time
x 10^-4
Numerical
Experimental Data
C5-15B4 , Ke =1.18, Kk =10, μk =25
Strain, in./in.
Time, days

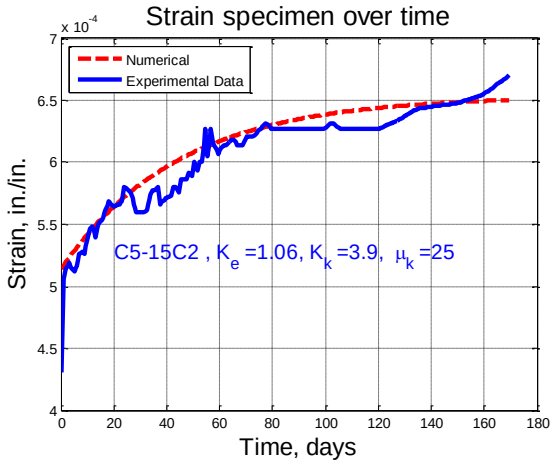
Strain specimen over time
x 10^-4
Numerical
Experimental Data
C5-15C2 , Ke =1.06, Kk =3.9, μk =25
Strain, in./in.
Time, days

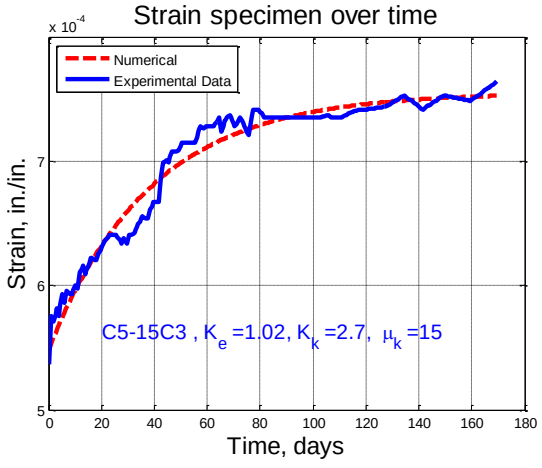
Strain specimen over time
x 10^-4
Numerical
Experimental Data
C5-15C3 , Ke =1.02, Kk =2.7, μk =15
Strain, in./in.
Time, days

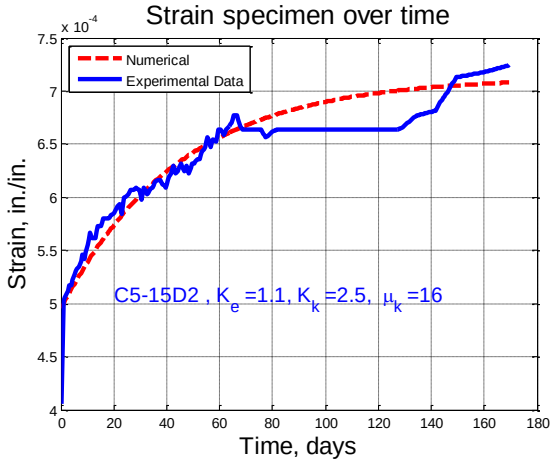
Strain specimen over time
x 10^-4
Numerical
Experimental Data
C5-15D2 , Ke =1.1, Kk =2.5, μk =16
Strain, in./in.
Time, days

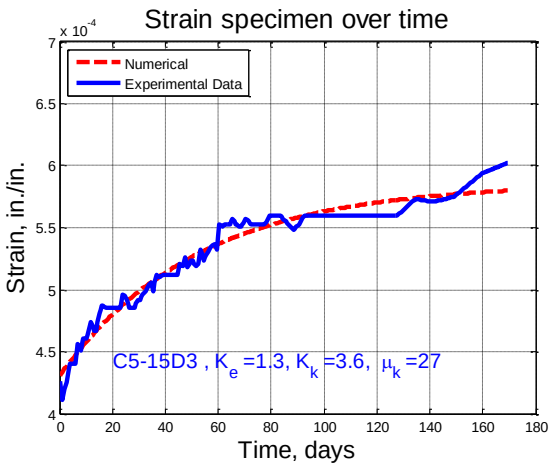
Strain specimen over time
x 10^-4
Numerical
Experimental Data
Strain, in./in.
Time, days
C5-15D3 , K_e =1.3, K_k =3.6, μ_k =27

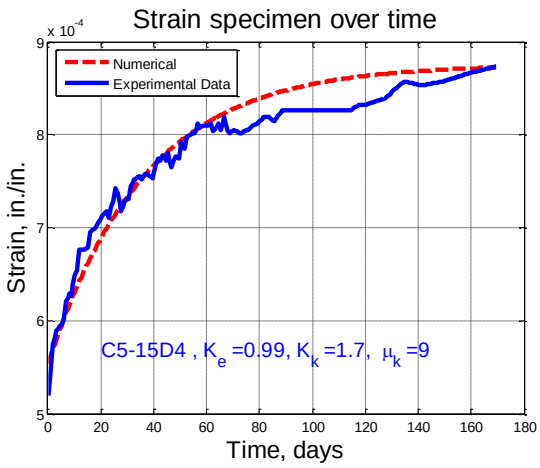
Strain specimen over time
x 10^-4
Numerical
Experimental Data
Strain, in./in.
Time, days
C5-15D4 , K_e =0.99, K_k =1.7, μ_k =9

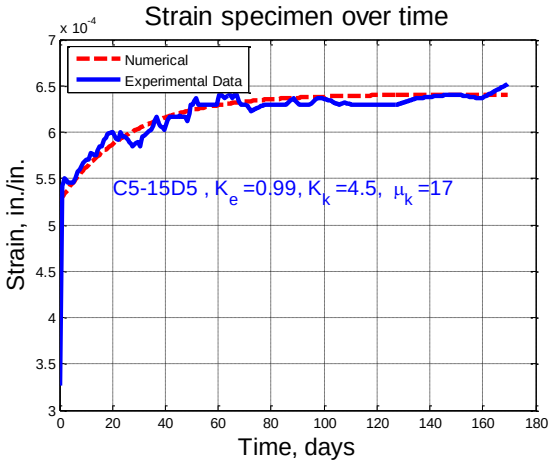
Strain specimen over time
x 10^-4
Numerical
Experimental Data
Strain, in./in.
Time, days
C5-15D5 , K_e =0.99, K_k =4.5, μ_k =17

3.7. References

Andi Asiz, Ian Smith, (2011). “Connection System of Massive Timber Elements Used in Horizontal Slabs of Hybrid Tall Buildings”. ASCE Journal of Structural Engineering; ASCE, ISSN 0733- 9445/2011/11-1390–1393.

ANSI/APA (American National Standards Institution/American Plywood Association) CLT (Cross-Laminated Timber) Standard Committee. (2012). “American national standard—Standard for performance rated cross-laminated timber.” ANSI/APA PRG 320-2012, APA–Engineered Wood Association, Tacoma, WA.

APA. (2017). “Product Report”. The Engineered Wood Association

ASTM D4442-15 "Standard Test Methods for Direct Moisture Content Measurement of Wood and Wood Based Materials”

ASTM D6815-09 Standard Specification for Evaluation of Duration of Load and Creep Effects of Wood and Wood-Based Products, ASTM International, West Conshohocken, PA, 2015.

Clouser, W. S. (1959). "Creep in small wood beams under constant bending load." Report No. 2150, U.S. Dept. of Agric. Forestry Service, Forest Products Lab., Madison, Wis.

E. Karacabeyli and B. Douglas, eds. (2013). “CLT handbook: cross laminated timber—US edition”, FPInnovations, Pointe-Claire, QC, Canada.

Erick G. Thompson. (2005). “Introduction to the Finite Element Method: Theory, Programming, and Applications”.

Fick, A. (1855). Annln Phys. 170, 59.

Fridley, K. J., Tang, R. C., and Soltis, L. A. (1992a). "Hygrothermal effects on mechanical properties of lumber." J. Struct. Engrg. ASCE, 118(2), 567-581.

Fridley, K. J., Tang, R. C., and Soltis, L. A. (1992b). "Creep behavior model for structural lumber." J. Struct. Engrg. ASCE, 118(8), 2261- 2277.

Gagnon, S., and Pirvu, C., eds. (2011). CLT handbook: Cross-laminated timber, FPInnovations Program, Pointe-Claire, QC, Canada.

Gerhards, C. C. (1980). “Effect of moisture content and temperature on the mechanical properties of wood: an analysis of immediate effects”. Forest Products J., 35(4), 18-26.

Gerhards, C. C. (1985). "Time-dependent bending deflections of Douglas fir 2 by 4's. Forest Products J., 35(4), 18-26

Ho, T.X., Dao, T.N., Aaleti, S., van de Lindt, J.W., Rammer, D.R. (2016). “Hybrid System of Unbonded Post-tensioned CLT Panels and Light-Frame Wood Shear Walls”, ASCE Journal of Structural Engineering; ISSN 0733-9445, 04016171.

Hoyle, R. I., Griffith, M. C, and Hani, R. Y. (1985). "Primary creep of Douglasfir beams of commercial size and quality." Wood Fiber Sci., 17(3), 300-314.

https://en.wikipedia.org/wiki/Creep_(deformation)

ICC (International Code Council). (2009). “International building code.” Washington, DC.

Liu Tong. (1987). “Moisture transport in wood and wood-based panels. A prestudy of sorption methods”. Rapport I8712078, TrateknikCentrum Stockholm, Sweden.

M. Mohammad, Sylvain Gagnon, Eng., Bradford K. Douglas, P.E., Lisa Podesto P.E., (2012). “Introduction to Cross Laminated Timber.” Wood Design Focus, 22(2).

Nakai, T., P. Grossman. (1983). “Deflection of wood under intermittent loading”. Wood. Sci. Technol. 17:55-67.

Nordstrom Jan-Erik P., Sandberg Dick, (1994).” The Rheology of Wood -Considerations of the Mechano-Sorptive Creep”. Royal Institute of Technology Department of Manufacturing Systems Division of Wood Technology and Processing Stockholm, Sweden.

Pirvu and Karacabeyli (2014). “Time-dependent behavior of CLT”. World Conference on Timber Engineering 2014, Quebec, Canada.

S. Gowda, M. Kortesmaa, and A. Ranta-Maunus., (1996). “Long term creep tests on timber beams in heated and non-heated environments”. VTT Publication 278. Espoo, Finland.

Sarisley E. F., Accorsi M. L., (1990). “Prestress level in stress-laminated timber bridges”. J Struct Eng 116:3003–3019.

Schaffer, (1982). “Influence of heat on the longitudinal creep of dry Douglas-Fir”. Pages 20-52 in R. W. Meyer and R. M. Kellog, eds. Structural uses of wood in adverse environments. Society of Wood Science and Technology. Van Nostrand Reinhold Company, New York.

Senft, J. F., and Suddarth, S. K. (1971). "An analysis of creep-inducing stress in sitka spruce." Wood Fib, 2(4), 321-327.

Tugce Akbas, Richard Sause, James M. Ricles, Ryan Ganey4; Jeffrey Berman, Sarah Loftus; J. Daniel Dolan, Shiling Pei, Ph.D., John W. van de Lindt, Hans-Erik Blomgren. (2017). “Analytical and Experimental Lateral-Load Response of Self-Centering Posttensioned CLT Walls”. ASCE Journal of Structural Engineering; ISSN 0733-9445.

United States Department of Agriculture, Forest Service, Forest Products Laboratory. (2010). "Wood handbook: wood as an engineering material". Madison, WI: U.S. Dept. of Agriculture, Forest Service, Forest Products Laboratory.

Vahab Bolvardi, Shiling Pei, John W. van de Lindt, James D. Dolan, (2016). "Direct Displacement Design of Tall CLT Building with Deformable Diaphragms". World Conference on Timber Engineering 2016, Vienna, Austria.

Wacker J. P., (2009). "Performance of stress-laminated timber highway bridges in cold climates". Cold Regions Engineering 2009.

Yazdani, N., Johnson, E., and Duwadi, S., "Creep Effect on Structural Composite Lumber (SCL) in Bridge Applications", ASCE Journal of Bridge Engineering, Vol. 9, No. 1, pp. 87-94, January 2004.

CHAPTER 4

LOSS OF TENDON FORCE DUE TO LONG-TERM CREEP IN UNBONDED POST-TENSIONED CLT PANELS

Abstract

Post-tensioned (PT) Cross-Laminated Timber (CLT) panels are innovative wood structures that can be used as load resisting components in tall wood buildings with self-centering capability that helps building improve its stability during a seismic event. The self-centering capability of PT CLT panels primarily relies on the ability to maintain post-tensioned forces in the tendon. CLT is a hygroscopic material, variations of ambient environment relative humidity (RH) may directly affect modulus of elasticity (MOE) of CLT. This leads to changes in strains of both CLT panels and tendons which may cause a loss of tendon forces in post-tensioned CLT panels. Controlling post-tensioning force losses is vital since the losses may result in lower self-centering capability in CLT panels and reduce the stability of tall building structures during seismic events. This chapter presented a numerical approach to estimate the loss of tendon forces in CLT panels under changing surrounding environment RH. A simplified equation to calculate the tendon force loss over time was also proposed. Numerical solutions from different CLT configurations and stress levels were used to compare with the results obtained from using the simplified equation. Under RH step between 50% and 70%, the minimal differences of tendon forces at different time periods (63 days, 179 days, and 271 days) were found. The total loss of tendon forces during 271 days varied from 0.6% to 6.5% in the entire tested specimens. The proposed simplified equation gave a good agreement with results from numerical model and the difference was less than 2%.

4.1. Introduction

Wood and wood-based materials have been applied in construction of residential structures for a long time in the United States. This material has many remarkable properties such as good thermal insulation and high strength to weight ratio (Mohammad et al., 2012). Despite of many good properties over other construction materials, the potential applications of wood material are still underused. Because of its own nature, customary wood structures are incapable to use in large span structures or tall buildings. Researchers attempt to improve wood structures performances, one of the most widespread methods is to apply post-tensioning forces on wood members.

Posttensioning is a technique of applying force on a member initially using high strength steel strands and bars. Depending on how the tensioning force transfers to the members, post-tensioned structures are divided into bonded and unbonded structures. While the tensioning forces in bonded structures are transferred through the end anchorages and the frictions between tendons and the structure material, the tensioning forces in the unbonded structures are only transported through the end anchorage systems. Numerous different materials with unbonded and bonded techniques have been applied to improve load resistant capacities for wood members. Based on the type of reinforcement materials it can be separated into two groups: (i) metal reinforcement, (ii) glass-fiber and other reinforcement (Bulleit, 1984). Some studies focused on reinforced laminated timber using unbonded metal reinforcement to improve the capacity of bending structures (Krueger, 1973; McConnell et al., 2014). Other applications of the posttensioning mostly focused on the bonded glass-fiber-reinforced-plastics (GFRP) (Saucier et al., 1975; Plevris and Triantafillou, 1992). Several studies were related to creep behaviors of the laminated members enhanced with the GFRP (Plevris et al., 1995; Gilfillan et al., 2003; Li et al.,

2016). In the recent decades, laminated wood industries have expanded their products and applications on fabricating tall wood buildings in North America and other regions, leading to the increase in the numbers of study on the wood laminated structures using unbonded post-tensioning. Multi-story buildings with post-tensioning laminated veneer lumber (LVL) members have been studied in New Zealand (Palermo et al., 2005; Buchanan et al., 2008; Smith et al., 2009). More recently, Dunbar et al., (2014) performed a uni and bi-directional quasi-static cyclic testing for the single panel and multi-panel post-tensioned CLT (Cross-Laminated Timber) walls. Several recent works in the United States focused on investigating analytical and experimental of the post-tensioned rocking walls (Ho et al., 2016; Tugce et al., 2017). When long-term post-tensioned forces are applied on wood panels in those applications, wood panels experience creep behaviors that may change the initial post-tensioned design loads.

Creep is a time-dependent deformation in structures; this phenomenon has been studied by many researchers over the years. Some of these studies focused on effects of loadings to creep of wood lumbers (Schaffer, 1982; Nakai and Grossman, 1983). Since wood is a hygroscopic material, the influences of the relative environmental factors to the creep behavior are significant. These effects were mentioned in several studies (Gerhards, 1980; Fridley et al., 1992). A number of recent researchers focused on creep behaviors of laminated timbers under changing the ambient environment (Gowda et al., 1996; Yazdani et al., 2004; Davies and Fragiacomo, 2011; Karacabeyli, 2014). Others have studied the creep of stressed laminated timbers under natural setting (Edward, 1990; Wacker, 2009). This study is an extension of the author's previous study on creep behavior of axially loaded CLT under the variation of ambient relative humidity (RH) (Nguyen et al., 2017).

Although post-tensioned wood structures have been researched for years, only a handful work focused on studying the applications of post-tensioned CLT panels for tall wood buildings. In the new tall wood building design concept, lateral force resisting components are made up by multi-CLT post-tensioned panels. Effects of creep on the post-tensioned CLT panels are more severe when exposed to a relatively high RH environment. Under the effects of creep, post-tensioned forces in the CLT panels significantly reduce with time. This process may decrease the self-centering capability of post-tensioned CLT members which may lead to large residual drift and damage in buildings after a seismic event. In order to be able to control and maintain the effectiveness of post-tensioned tendon in a structure over time, the loss of tendon force need to be addressed. In this study, a numerical model was developed to predict the loss of post-tensioning forces in CLT panels over time due to creeps under the variations of the relative moisture content in the surrounding environment. The experimental creep data from previous study were used in the numerical analysis. A simplified equation to predict the loss of tendon force in post-tensioned CLT panels over time was also proposed for design.

4.2. Model to predict creep behavior

Creep deformations in a material may cause additional deformations in CLT panels which could lead to the stress loss in pre-stressed tendons. The creep deformation is a function of time and often increases significantly at the early days after loading and slows down over time. Factors such as types of loading, surrounding temperature, and RH can affect to creep behavior of a material. For wood material, changing ambient RH would result in a variation of moisture content (MC), and affect directly to creep deformations of wood structures. Since creep behavior presents in the wood structures over long period, it often takes years to conduct long-term creep

tests. For that reason, most creep models were often developed using short-term data to predict the long-term creep behavior.

4.2.1. Five-element creep model

Fridley et al., (1992b) proposed a five-element model using short-term data from a series of creep tests on the Douglas-fir 2×4 structure lumbers. In this model, the long-term creep strain is predicted by equation:

$$\varepsilon(t) = \frac{\sigma}{K_e} + \left(\frac{\sigma}{K_k}\right)\left[1 - e^{-\frac{K_k.t}{\mu_k}}\right] + \frac{\sigma.t}{\mu_v} + \frac{\sigma}{\mu'_{ms}}|\Delta\omega|[1 - e^{-B_\omega.t_\omega}] \qquad (4.1)$$

where: $\varepsilon(t)$ is a total strain at time t; σ is a constant applied stress; K_e is a Hookean spring constant; K_k and μ_k are the Hookean spring and Newtonian dashpot of the Kelvin element; μ_v is a viscosity of the Newtonian dashpot; μ'_{ms} is a constant with units of force per unit area. B_ω is a constant associated with the time required to achieve moisture equilibrium; B_ω is dependent on the size of the sample. $|\Delta w| = \omega_e - \omega_i$, where ω_e is the eventual equilibrium MC in the new environment and ω_i is the initial MC in the original environment. Two hygrothermal variables, ω and θ have been introduced in that study

$$\omega = \frac{M - M_0}{M_0} \quad and \quad \theta = \frac{T - T_0}{T_0} \qquad (4.2, 4.3)$$

where: ω is a relative moisture content; M is an actual moisture content; M_o is a reference moisture content; θ is a relative temperature; T is an actual temperature; T_o is a reference temperature. The quadratic functions of ω and θ have been assumed for predicting the hygrothermal effects on wood properties K_e, K_k, μ_k, μ_v.

4.2.2. Modified five-element creep model

The Fridley's creep model was developed for predicting the creep behaviors of wood lumbers at structure level. It is inconvenient for applying this model for CLT material since many different CLT panel sizes are used in structures. In a study by Nguyen et al., (2017), a four-element creep model was introduced for CLT at material level. The four-element creep model is modified from the Fridley's creep model by removing viscous term $\sigma t/\mu_v$ and replacing a dependent specimen size mechano-sorptive term with a size-independent modulus element. The mathematical form is written by equation

$$\varepsilon(t) = \frac{\sigma}{K_e} + \left(\frac{\sigma}{K_k}\right)\left[1 - e^{-\frac{K_k.t}{\mu_k}}\right] + \frac{\sigma}{\mu_\omega}.\Delta MC \qquad (4.4)$$

where: μ_ω is the mechano-sorptive modulus; ΔMC is the moisture content difference between original environment to new environment, $\Delta MC = MC_a - MC_i$; MC_i is the original moisture content; MC_a is the moisture content of specimen at time *t*.

The mechano-sorptive modulus was calculated by equation

$$\mu_\omega = \frac{E_1.E_2.(MC_2 - MC_1)}{E_1 - E_2} \qquad (4.4a)$$

where: E_1 modulus of elasticity of CLT specimens at original environment; E_2 is the CLT modulus of elasticity at new environment.

The four-element creep model was employed in this study to develop a FEM subroutine for estimation of creep deformations in CLT panels and tendon force versus time.

4.3. Development cable force FEM model

Performance of a self-centering post-tensioned CLT system is governed by a cable force. This FEM model focused on the prediction of the changes in cable force due to the variations in the ambient RH and creep behavior in CLT panels.

4.3.1. Cable effective length

The stiffness of a post-tensioned CLT system depends on the stiffness of the cable and stiffness of the CLT panel. Under application of a post-tensioned force, the cable is elongated. The elongation is governed by the magnitude of the post-tensioned force and the cable stiffness. The stiffness of a cable can be calculated as:

$$K_c = \frac{E_c . A_c}{L_{co}} \tag{4.5}$$

where: K_c is the cable stiffness; A_c is the cable cross section; E_c is the cable modulus of elasticity; L_{co} is the rested cable length.

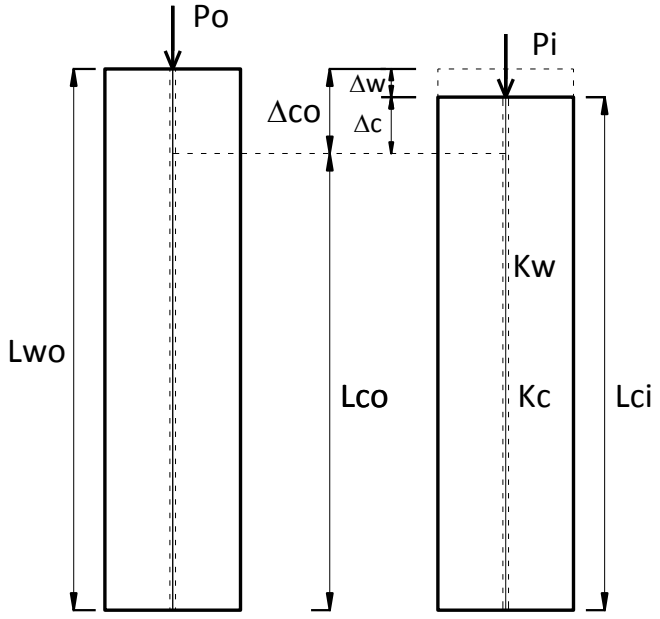

Fig. 4-1 Post-tensioned CLT panel system

To obtain the cable stiffness in a post-tensioned CLT system, the rested cable length needs to be evaluated. Fig. 4-1 illustrates the relationship between the lengths of cable before and after being post-tensioned. The displacement of the CLT panel Δ_w under the post-tensioned force P_0 can be estimated by equation

$$\Delta_w = \frac{P_0 + D + L}{K_w} \tag{4.6}$$

where: P_0 is the post-tensioned force; D is the dead load; L is the live load; K_w is the CLT panel stiffness.

At an equilibrium state, under the effects of post-tensioned force P_0 the cable elongation is estimated as

$$\Delta_c = \frac{P_0}{K_c} = \frac{P_0 . L_{co}}{E_c . A_c} \tag{4.7}$$

In which, Δ_c is the cable elongation

From Fig. 4-1, the two relationships can be written

$$L_{ci} = L_{co} + \Delta_c \tag{4.8}$$

$$L_{ci} = L_{wo} - \Delta_w \tag{4.9}$$

Combining the Eqs. (4.6) to Eqs. (4.9) the effective cable length L_{co} can be evaluated

$$L_{co} = \frac{L_{wo} - \Delta_w}{1 + \frac{P_0}{E_c . A_c}} = \frac{L_{ci}}{1 + \varepsilon_c} \tag{4.10}$$

where: ε_c is the cable strain after post-tension

$$\varepsilon_c = \frac{P_0}{E_c . A_c} \tag{4.10a}$$

4.3.2. Estimation of cable force versus time

When a post-tensioned CLT system reaches an equilibrium condition, any changes in the CLT panel stiffness would apparently result in a change of the cable deformation, and affects the post-tensioned force. Under environment change and creep behavior, CLT panel stiffness change due to the change of its total modulus of elasticity. The forces and displacements in cable and the CLT panel will redistribute to reach a new equilibrium state. The search for the new equilibrium state requires non-linear analysis in which the cable force and the CLT panel displacement are mutually dependent. An iteration subroutine was developed to calculate the new cable force and the CLT panel displacement, flowchart in Fig. 4-2 shows the procedure to search for the new equilibrium state when the stiffness of CLT panel change (as wood elastic modulus changes).

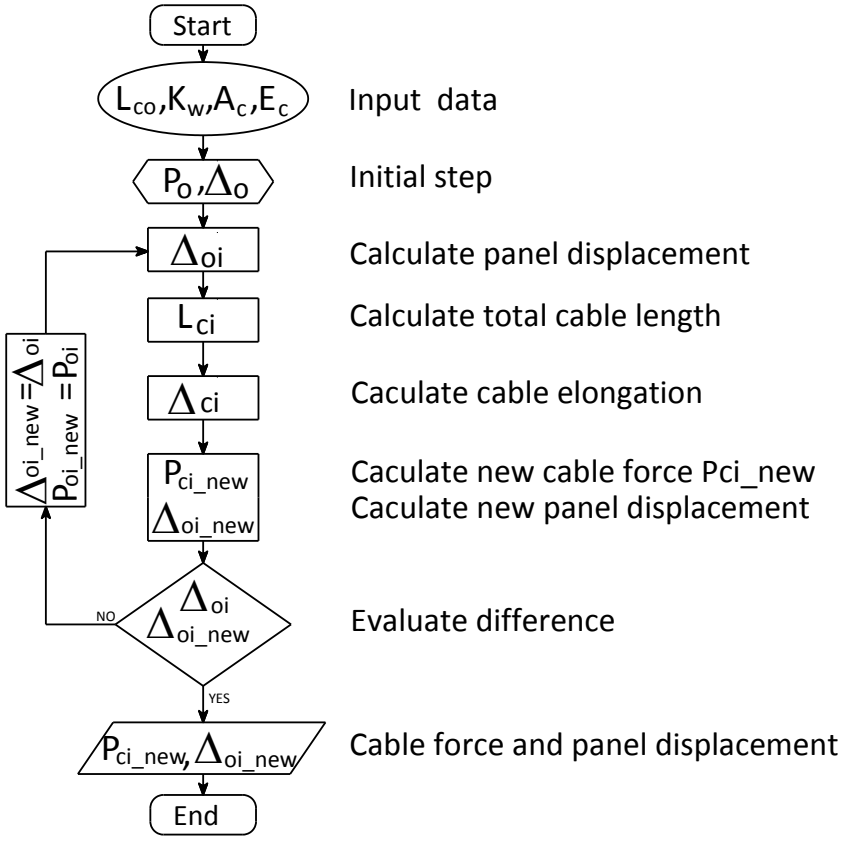

Fig. 4-2 Subroutine to search for the new equilibrium condition solution

4.3.3. Experimental data from previous study

In a previous study by the authors (Nguyen et al., 2017), the creep model constants for CLT were obtained by fitting parameters in the numerical model with data collected from the tests of specimens for various groups and listed in in Table 4-1 and Table 4-2.

Table 4-1 Constants of creep model from fitting experimental test data

Groups	SPC	Location	K_e (10^6 psi)	K_k (10^6 psi)	μ_μ (10^{10} psi-min)
3 layers 0.10 f_c'	C3-10-A	front	1.03	2.1	6
		back	0.95	2.9	11
		2	1.09	3.4	9
	C3-10-B	front	1.24	4.7	18
		back	1.9	3.8	9
		1	0.75	4	8
	C3-10-C	front	0.9	2.4	13
		1	1.16	5.3	18
	C3-10-D	1	0.53	1.7	4
		2	1.05	3	10
		3 - front	0.96	0.4	16
5 layers 0.10 f_c'	C5-10-A	front	0.92	2	13
		back	1.08	2.5	16
		1	0.55	0.98	4
		2	0.9	3.2	14
	C5-10-B	front	1.71	2.6	19
		1	0.66	1.7	5
		2	1.66	3.6	21
		3	0.8	2.6	7

	C5-10-C	back	0.92	1.3	9
		1	0.81	1.8	9
		2	1.15	1.8	9
		3	0.74	1.1	6
	C5-10-D	front	1.06	0.8	6
		back	0.91	0.7	4
		1	0.7	1.3	6
		2	1.26	1	6
		3	0.85	1.6	9
5 layers 0.15 f_c'	C5-15-A	front	1.15	2.1	20
		2	1.1	5	16
		3	1.19	3.8	16
		4	0.89	2.4	16
	C5-15-B	front	1.12	2.7	35
		2	0.8	4.9	16
		4	1.18	10	25
	C5-15-C	front	0.92	1.5	23
		back	0.98	1.5	18
		2	1.06	3.9	25
		3	1.02	2.7	15
	C5-15-D	2	1.1	2.5	16
		3	1.3	3.6	27
		4	0.99	1.7	9
		5	0.99	4.5	17

Table 4-2 Viscoelastic parameters and mechano-sorptive modulus of different CLT specimen groups and RH steps

Groups	SPC	Viscoelastic parameters			Mechano-sorptive μ_ω (10^6) psi	
		K_e (10^6) psi	K_k (10^6) psi	μ_k (10^{10}) psi-min	RH 50%-70 %	RH 70%-90 %
C3-10-	A	1.06	1.30	6.36	0.122	0.127
	B	1.56	5.49	12.70		
	C	0.99	2.53	8.91		
	D	1.14	3.55	15.04		
C5-10-	A	1.32	5.99	11.65		
	B	0.99	5.21	16.10		
	C	1.50	7.27	21.91		
	D	0.95	1.32	9.71		
C5-15-	A	1.42	1.33	19.18		
	B	1.25	2.77	16.40		
	C	1.06	2.39	11.72		
	D	0.97	1.12	6.34		

4.3.4. Numerical cable force from FEM model

The viscoelastic parameters and mechano-sorptive modulus in Table 4-1 and Table 4-2 were used in the numerical model to predict the change of post-tensioned tendon force in the three groups of CLT specimens. The ambient environment RH was kept constant at 50% for the first 60 days and then regularly switched between 50% and 70% at a period of 4 days. This moisture content profile was applied for all three groups. Details can be seen in Fig. 4-3a.

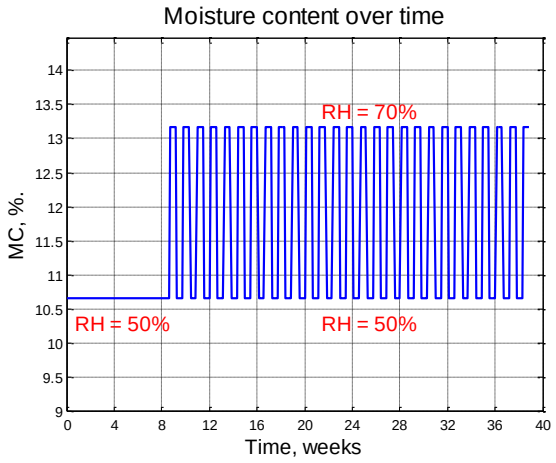

a) Moisture content profile

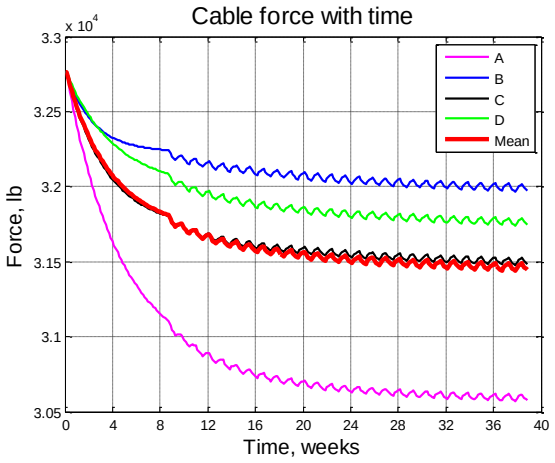

b) 3-layer 0.10 f_c'

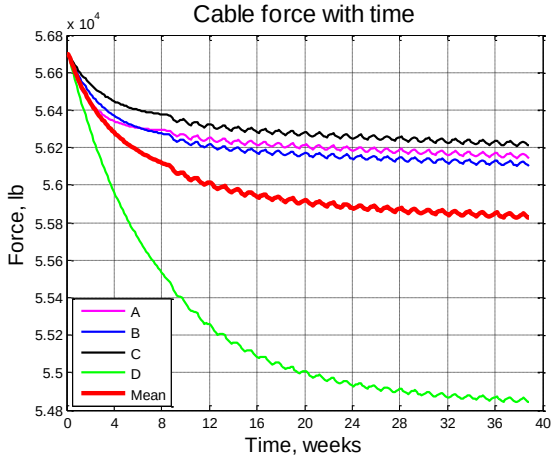

c) 5-layer 0.10 f_c'

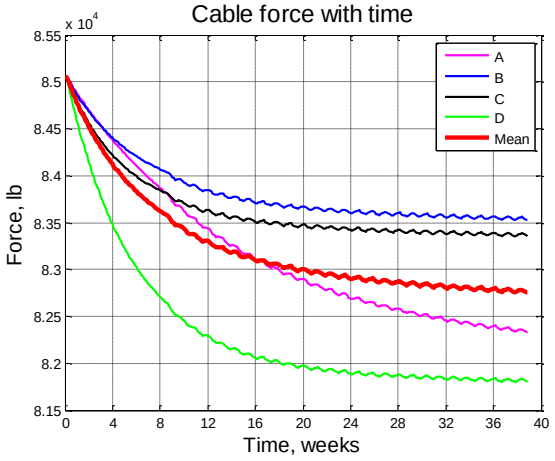

d) 5-layer 0.15 f_c'

Fig. 4-3 shows the variations of tendon forces in different CLT groups.

The mean tendon force values in each group were plotted as well. Numerical tests also performed on CLT specimens under the environment RH between 70% and 90%. The moisture content profile held similar pattern with the previous tests, but the ambient environment RH step was changed between 70% and 90% as in Fig. 4-4a.

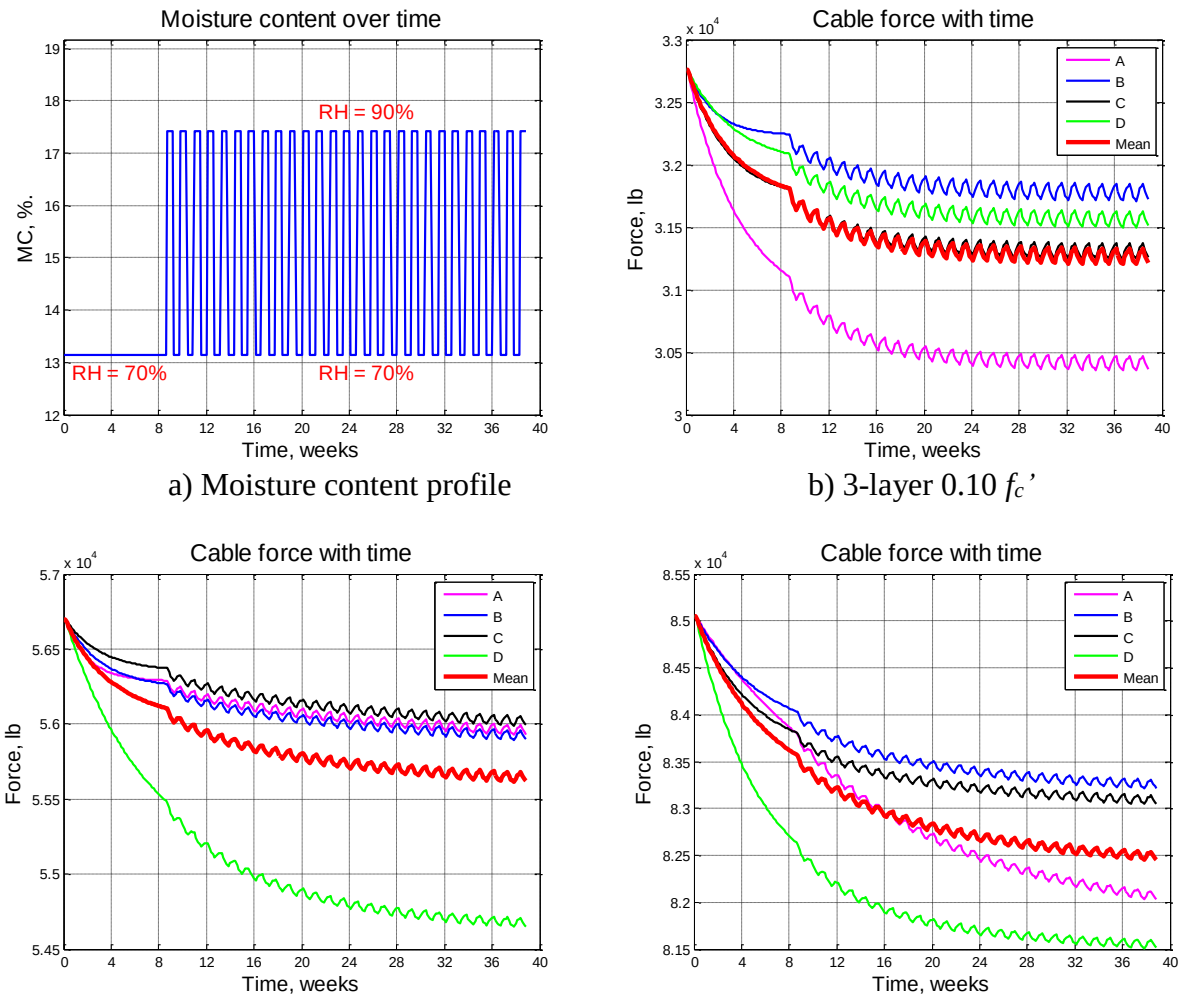

a) Moisture content profile

b) 3-layer 0.10 f_c'

c) 5-layer 0.10 f_c'

d) 5-layer 0.15 f_c'

Fig. 4-4 Moisture profile and cable force in CLT groups, RH from 70% to 90%

4.4. Development of cable force equation for design

To avoid the complexity of the numerical analysis during the design process, a simplified equation was developed to predict the change of post-tensioned cable force versus time due to creep deformation in CLT panels. The proposed equation was developed following the values of fitted parameters from test data. To be able to use the equation in the practical design, further study on reliability analysis of this equation is needed.

4.4.1. Proposed Simplified equation

The function for the post-tensioned force in cable, *P(t)*, of a post-tensioned CLT panel at a given time *t* can be expressed as follows:

$$P(t) = F[P_0, A_c, L_{c0}, A_w, L_{w0}, E_c, E_w(t)] \quad (4.11)$$

In which: $P(t)$ is the post-tensioned force history; F is a constitutional function; P_0 is the initial post-tensioned force in cable; A_c is the cable cross-section; L_{c0} is the rested cable length; A_w is the cross section of CLT panel ($A_w = b \times h$; b is the width of CLT panel; h is the thickness of CLT panel); L_{w0} is the initial length of the CLT panel; E_c is the cable modulus of elasticity; $E_w(t)$ is the CLT modulus of elasticity history versus time.

Under the effects of changing environmental conditions over time and creep behavior, the total MOE of CLT panel, $E_w(t)$, fluctuates over time, which leads to the change in cable force. By using the modified creep model, the total MOE in a CLT panel over time can be estimated, therefore, the loss in post-tensioned force can be determined. At the initial equilibrium, the displacements in the cable and CLT panel can be calculated:

$$\Delta_c = \frac{P_0 . L_{c0}}{E_c . A_c} = \frac{P_0}{K_c} \quad \text{and} \quad \Delta_w = \frac{P_0 . L_{w0}}{E_w . A_w} = \frac{P_0}{K_w} \quad (4.12, 4.13)$$

From Fig. 4-1, the relationship between the length of cable and CLT panel can be written:

$$L_{wo} - \Delta_w = L_{co} + \Delta_c \quad (4.14)$$

Combining Eqs. (4.12), Eqs. (4.13) and Eqs. (4.14), one can have:

$$L_{w0} - L_{c0} = P_0 \left(\frac{1}{K_c} + \frac{1}{K_w}\right) \quad (4.15)$$

At time *t* when the CLT panel has stiffness K_{wt}, this relationship becomes:

$$L_{w0} - L_{c0} = P(t) . \left(\frac{1}{K_c} + \frac{1}{K_{wt}}\right) \quad (4.15a)$$

where: $K_{wt} = E_{w(t)}.A_w/L_w$ is the CLT panel stiffness at time *t*.

Let $\alpha = E_{wt}/E_w$ is the ratio between the total elastic modulus of the CLT at time *t* and at the beginning. The total elastic modulus of CLT at time *t* can be calculated from the revised creep model as:

$$E_{wt} = \frac{\sigma}{\epsilon(t)} = \frac{1}{\frac{1}{E_w} + \left(\frac{1}{K_k}\right)\left[1 - e^{-\frac{K_k.t}{\mu_k}}\right] + \frac{1}{\mu_\omega}.\Delta MC} \qquad (4.15b)$$

In the Eqs. (4.15b), ΔMC is the projection of moisture content change in the specimen between the reference RH and at the new environmental RH.

From Eqs. (4.15) and Eqs. (4.15a), the relationship between the post-tensioned force at time *t* and the initial post-tensioned force can be estimated:

$$P(t) = \alpha.P_0.\left(\frac{K_c + K_w}{K_c + K_{wt}}\right) \qquad (4.16)$$

Let $\beta = K_w/K_c$ is the ratio between the stiffness of the CLT panel and cable stiffness. Eqs. (4.16) can be rewritten as:

$$P(t) = P_0.\alpha.\left(\frac{1+\beta}{1+\alpha.\beta}\right) \qquad (4.17a)$$

The loss of tendon force at time *t* is:

$$\Delta P(t) = P_0 - P(t) = P_0.\frac{1-\alpha}{1+\alpha.\beta} \qquad (4.17b)$$

The simplified equation (4.17a) can be used to estimate the tendon forces in post-tensioned CLT panels at a certain time based on the initial post-tensioned forces in tendon, CLT geometries, and tendon properties. By using the simplified equation (4.17b), the loss of a post-tensioned force in a post-tensioned CLT panel at a certain time can be calculated.

4.4.2. Examples to compare simplified equation with numerical model results

A series of numerical analysis of different CLT configurations and stress levels under two ambient environment RH steps were conducted. For each CLT specimen, the cable force was calculated at three specific times –at 63 days, at 179 days, and at 271 days.

Table 4-3 shows the tendon force values in post-tensioned CLT panels of different groups obtained from FEM model and simplified equation (4.17b) for RH step between 50% and 70%. Under RH 70% to 90%, the tendon force values were plotted in Fig. 4-5.

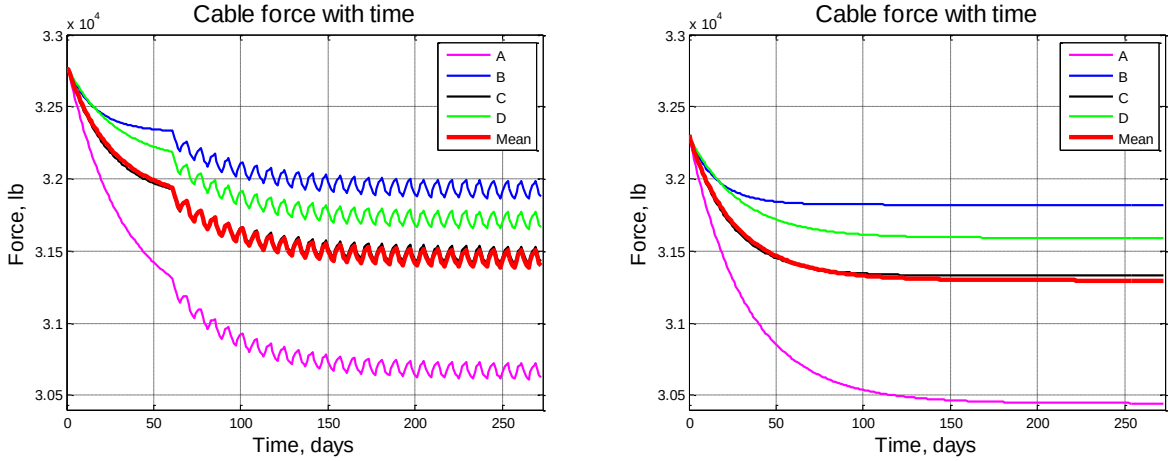

a) Numerical model b) Simplified equation

Fig. 4-5 Cable force from numerical model and simplified equation, group 1, RH 70% - 90%

Table 4-3 Cable force from numerical model and estimated values from equation, RH step between 50% and 70%

Groups	Initial Force (kip)	SPC	Cable force versus time P_t (lb.), RH 50% to 70%					
			Numerical			Simplified equation		
			63 days	179 days	271 days	63 days	179 days	271 days
(1) C3-10-3 layers 0.10 f_c'	32.72	A	31413.51	31052.61	31016.70	30882.73	30604.14	30595.38
		B	32355.10	32213.73	32184.21	31999.22	31989.33	31989.32
		C	31980.60	31790.36	31760.81	31562.55	31487.11	31486.47
		D	32216.55	32016.09	31985.52	31839.28	31755.40	31753.82
(2) C5-10-5 layers 0.10 f_c'	56.70	A	56323.49	56239.68	56213.97	55951.59	55947.05	55947.05
		B	56292.59	56189.48	56164.01	55918.06	55889.91	55889.79
		C	56399.91	56303.27	56277.28	56042.35	56023.19	56023.12
		D	55547.18	55039.76	54974.31	55006.14	54494.59	54445.92
(3) C5-15-5 layers 0.15 f_c'	85.05	A	83894.74	82869.76	82586.81	83190.71	82099.76	81804.65
		B	84108.04	83738.18	83686.05	83461.29	83162.64	83145.82
		C	83886.63	83551.64	83507.06	83197.34	82940.34	82932.15
		D	82756.84	82085.16	82021.06	81825.76	81168.50	81136.00

4.5. Data analysis

The loss of cable force in percentage at three specific locations was calculated as follows:

$$Loss\ cable\ force\ (\%) = \frac{P_{initial} - P_t}{P_{initial}} \times 100 \qquad (4.18)$$

The comparison of the cable force losses between numerical model and simplified equations is listed in Table 4-4 and 4-5.

Table 4-4 Loss of cable force from numerical model and estimated values from equation, RH step between 50% and 70%

Groups	Initial Forces (kip)	SPC	Loss cable force (%)					
			Numerical			Simplified equation		
			63 days	179 days	271 days	63 days	179 days	271 days
(1) C3-10-3 layers 0.10 f_c'	32.72	A	4.11	5.21	5.32	5.73	6.58	6.61
		B	1.24	1.67	1.76	2.32	2.35	2.35
		C	2.38	2.96	3.05	3.66	3.89	3.89
		D	1.66	2.27	2.36	2.81	3.07	3.07
(2) C5-10-5 layers 0.10 f_c'	56.70	A	0.66	0.81	0.86	1.32	1.33	1.33
		B	0.72	0.90	0.95	1.38	1.43	1.43
		C	0.53	0.70	0.75	1.16	1.19	1.19
		D	2.03	2.93	3.04	2.99	3.89	3.98
(3) C5-15-5 layers 0.15 f_c'	85.05	A	1.36	2.56	2.90	2.19	3.47	3.82
		B	1.11	1.54	1.60	1.87	2.22	2.24
		C	1.37	1.76	1.81	2.18	2.48	2.49
		D	2.70	3.49	3.56	3.79	4.56	4.60

Table 4-5 Loss of cable force from numerical model and estimated values from equation, RH step between 70% and 90%

Groups	Initial Forces (kip)	SPC	Loss cable force (%)					
			Numerical			Simplified equation		
			63 days	179 days	271 days	63 days	179 days	271 days
(1) C3-10-3 layers 0.10 f_c'	32.72	A	4.61	6.32	6.37	6.20	7.04	7.07
		B	1.45	2.52	2.52	2.84	2.87	2.87
		C	2.71	3.89	3.91	4.14	4.37	4.37
		D	1.92	3.16	3.17	3.31	3.56	3.57
(2) C5-10-5 layers 0.10 f_c'	56.70	A	0.69	1.10	1.19	1.63	1.64	1.64
		B	0.75	1.18	1.27	1.68	1.73	1.73
		C	0.56	0.98	1.08	1.47	1.51	1.51
		D	2.06	3.20	3.36	3.28	4.18	4.26
(3) C5-15-5 layers 0.15 f_c'	85.05	A	1.39	2.84	3.21	2.49	3.77	4.11
		B	1.14	1.82	1.93	2.17	2.52	2.54
		C	1.40	2.04	2.14	2.48	2.78	2.79
		D	2.73	3.75	3.87	4.08	4.85	4.89

To evaluate performances of the simplified equation, estimated cable forces from the simplified equation were compared to the cable force values from numerical calculations. The difference in percentage was calculated as follows:

$$Difference\ (\%) = \frac{Pt_{Simplified\ Equ.} - Pt_{Numerical}}{Pt_{Numerical}} \times 100 \qquad (4.19)$$

Table 4-6 Cable force difference from numerical model and estimated values from simplified equation under various RH

Groups	SPC	Difference (%)					
		RH 50% -70%			RH 70% - 90%		
		63 days	179 days	271 days	63 days	179 days	271 days
(1) C3-10-3 layers 0.10 f_c'	A	1.69	1.44	1.36	1.67	0.76	0.74
	B	1.10	0.70	0.61	1.40	0.36	0.35
	C	1.31	0.95	0.86	1.47	0.49	0.48
	D	1.17	0.81	0.72	1.41	0.42	0.41
(2) C5-10-5 layers 0.10 f_c'	A	0.66	0.52	0.47	0.94	0.55	0.46
	B	0.67	0.53	0.49	0.94	0.56	0.47
	C	0.63	0.50	0.45	0.92	0.53	0.43
	D	0.97	0.99	0.96	1.24	1.01	0.94
(3) C5-15-5 layers 0.15 f_c'	A	0.84	0.93	0.95	1.12	0.95	0.93
	B	0.77	0.69	0.65	1.05	0.71	0.63
	C	0.82	0.73	0.69	1.10	0.76	0.67
	D	1.13	1.12	1.08	1.39	1.14	1.06

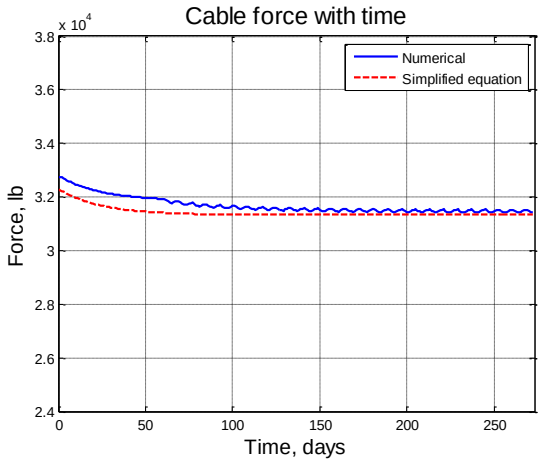

Fig. 4-6 Cable force difference in 3-layer specimen, RH 50% -70%

4.6. Discussion on the results

As can be seen in Table 4-4 and Table 4-5, the maximum cable force loss over 271 days is found in specimen A, group 1 (C3-10-A). This number is 5.32% under RH step from 50% to 70% and 6.37% for RH step from 70% to 90%. Comparing to the cable force losses obtained from simplified equation, the similar pattern is found, but slightly larger, which is 6.61% under RH step of 50% - 70% and 7.07% for RH step of 70% - 90%. As expected in wood, a natural material, the loss of cable force is found varying from specimen to specimen. For example in group 1, C3-10-, at the day of 271, the cable force loss in specimen A is 5.32% compared to 1.76% in specimen B. It can be explained that the loss of cable force in a CLT specimen largely depends on its creep deformation. Because of a large discrepancy in the viscoelastic parameters between specimen A and specimen B (as seen in Table 4-2), the difference in creep deformation between these two specimens was large which leads to a big variance in the loss of cable force as expected.

The differences of cable force loss between numerical model and simplified equation decrease over time as seen in Fig. 4-6 and Table 4-6. It can be explained that the moisture content in specimens at the beginning was different between approaches. For the numerical model, the moisture content in the specimens gradually changed from the initial condition to the new moisture content in the new environmental condition. In simplified equation approach, the moisture content change (in Eqs. 4.15b) was set constant and equal to the half of moisture content fluctuation between the two environmental conditions (which is the converging moisture content in CLT in the numerical model). For this reason, the simplified equation predicts better

in long-term cable force losses as the moisture content of CLT panels in numerical model converge closer to the mean value of the fluctuating moisture content.

The specimens' thickness also affects the accuracy of simplified equation. When the panels are thin, it takes shorter time for the moisture content in CLT panels converges to the projection moisture content in a fluctuating environment. It can be seen from Table 4-6, at 271 days the difference of predicted cable force between numerical model and simplified equation ranges from 0.35% to 0.74% in group (1) (3 layer, 0.10 f_c'), from 0.43% to 0.94% in group (2) (5 layer, 0.10 f_c'), and from 0.63% to 1.06% in group (3) (5 layer, 0.15 f_c').

4.7. Conclusion and recommendation

In this chapter, the losses of cable force in post-tensioned CLT panels were calculated based on FEM model using the data from moisture content and creep experiments. A simplified equation was proposed to calculate the loss of cable force in post-tensioned CLT panels for the design process. Numerical data from various post-tensioning CLT configurations and ambient environmental conditions were used to evaluate the accuracy of the simplified equation.

Analysis of the results from both methods showed that the simplified equation work well for prediction of long-term cable force losses. For thin CLT panels (3 layers or less), the simplified equation predicts well the loss of cable force after nine months of posttensioning force is applied on a CLT panel. The loss of post-tensioned cable force was found between 2.53% and 6.37% in 3-layer CLT panels post-tensioned at 10% of compression strength, between 1.08% and 3.36% in 5-layer CLT panels post-tensioned at 10% of compression strength, and from 1.93% to 3.87% in 5-layer CLT panels with post-tensioned force at 15% of compression strength. All of the losses were calculated at 271 days after post-tensioned.

Since wood is a natural material, the variation of cable force under the change of environmental conditions is large due to the creep behavior and the change of moisture content in CLT panels. For this reason, further validating experiments of the numerical model are recommended. The data from experiments and numerical model can be used to conduct a reliability analysis of the simplified equations before these can be used in the practical design to predict the cable force losses in post-tensioned CLT panels.

4.8. References

Buchanan, A. H., Deam, B., Fragiacomo, M., Pampanin, S., and Palermo, A. (2008). “Multi-storey prestressed timber buildings in New Zealand.” Struct. Eng. Int., 18(2), 166–173.

Bulleit, W. M. (1984). "Reinforcement of wood materials: A review." Wood and Fiber Sci., 16(3), 391-397.

Davies, M., and Fragiacomo, M. (2011). “Long-term behavior of prestressed LVL members. I: Experimental tests.” J. Struct. Eng., 137(12), 1553–1561.

Dunbar, A., Moroder, D., Pampanin, S., and Buchanan, A. (2014). “Timber core-walls for lateral load resistance of multi-storey timber buildings.” Proc., 13th World Conf. on Timber Engineering, Laval Univ. and FPInnovations, Quebec.

Fridley, K. J., Tang, R. C., and Soltis, L. A. (1992a). "Hygrothermal effects on mechanical properties of lumber." J. Struct. Engrg. ASCE, 118(2), 567-581.

Gerhards, C. C. (1980). “Effect of moisture content and temperature on the mechanical properties of wood: an analysis of immediate effects”. Forest Products J., 35(4), 18-26.

Gilfillan, J.R., Gilbert, S.G. & Patrick, G.R.H. “The use of FRP composites in enhancing the structural behaviour of timber beams.” Journal of Reinforced Plastics and Composites, 22(15):1373-1388. 2003

Ho, T.X., Dao, T.N., Aaleti, S., van de Lindt, J.W., Rammer, D.R. (2016). “Hybrid System of Unbonded Post-tensioned CLT Panels and Light-Frame Wood Shear Walls”, ASCE Journal of Structural Engineering; ISSN 0733-9445, 04016171.

Krueger, G. P. (1973). "Ultimate strength design of reinforced timber: State of the art." Wood Sci., (2), 175-186.

L. Li, Y. Xiao, (2015). “Creep Behavior of Glubam and CFRP-Enhanced Glubam Beams”, ASCE Journal of Composites for Construction; ISSN 1090-0268.

M. Mohammad, Sylvain Gagnon, Eng., Bradford K. Douglas, P.E., Lisa Podesto P.E., (2012). “Introduction to Cross Laminated Timber.” Wood Design Focus, 22(2).

McConnell, E., McPolin, D., & Taylor, S. (2014). “Post-tensioning of glulam timber with steel tendons”. Construction and Building Materials, 73, 426-433.

Nakai, T., P. Grossman. (1983). “Deflection of wood under intermittent loading”. Wood. Sci. Technol. 17:55-67.

Palermo, A., Pampanin, S., Buchanan, A., and Newcombe, M. (2005). “Seismic design of multi-storey buildings using laminated veneer lumber (LVL).” 2005 NZSEE Conf., New Zealand Society for Earthquake Engineering, Wellington, New Zealand, 8.

Pirvu and Karacabeyli (2014). “Time-dependent behavior of CLT”. World Conference on Timber Engineering 2014, Quebec, Canada.

Plevris, N., and Triantafillou, T. (1992). "FRP-reinforced wood as structural material.” Material, in Civ. Engrg., ASCE, 4(3).

Plevris, N., and Triantafillou, T. (1995). "Creep behavior of FRP-Reinforced wood member.” J. Struct. Engrg. ASCE, 121(2); ISSN 0733-9445.

S. Gowda, M. Kortesmaa, and A. Ranta-Maunus., (1996). “Long term creep tests on timber beams in heated and non-heated environments”. VTT Publication 278. Espoo, Finland.

Sarisley E. F., Accorsi M. L., (1990). “Prestress level in stress-laminated timber bridges”. J Struct Eng 116:3003–3019.

Saucier, J. R., and Holman, J. A. (1975). "Structural particleboard reinforced with glass fiber-Progress in its development." Forest Products J., 25(9), 69-72.

Schaffer, (1982). “Influence of heat on the longitudinal creep of dry Douglas-Fir”. Pages 20-52 in R. W. Meyer and R. M. Kellog, eds. Structural uses of wood in adverse environments. Society of Wood Science and Technology. Van Nostrand Reinhold Company, New York.

Smith, T., Fragiacomo, M., Pampanin, S., and Buchanan, A. (2009). “Construction time and cost estimates for post-tensioned multi-storey timber buildings.” Proc. of ICE, Construction Materials, Special Issue on Timber Structures, 162(4), 141–149.

Tu T. Nguyen., (2017). “Numerical Model for Creep Behavior of Axially Loaded CLT Panels”.

Tugce Akbas, Richard Sause, James M. Ricles, Ryan Ganey4; Jeffrey Berman, Sarah Loftus6; J. Daniel Dolan, Shiling Pei, Ph.D., John W. van de Lindt, Hans-Erik Blomgren. (2017). “Analytical and Experimental Lateral-Load Response of Self-Centering Posttensioned CLT Walls”. ASCE Journal of Structural Engineering; ISSN 0733-9445.

Wacker J. P., (2009). “Performance of stress-laminated timber highway bridges in cold climates”. Cold Regions Engineering 2009.

Yazdani, N., Johnson, E., and Duwadi, S., “Creep Effect on Structural Composite Lumber (SCL) in Bridge Applications”, ASCE Journal of Bridge Engineering, Vol. 9, No. 1, pp. 87-94, January 2004.

CHAPTER 5

SUMMARY, CONCLUSIONS AND FUTURE WORKS

5.1. Summary

Numerical and experimental approaches have been carried out in this study to examine the feasibility of the new hybrid structural systems, CLT-LiFS, in constructing the tall wood building in the seismic areas.

In numerical studies, a few numerical models have been proposed, including: 1) real-time delay algorithm to improve hybrid test for hybrid structural system; 2) moisture content diffusion for modeling the moisture content migrating in CLT panels; 3) four-element creep model for calculating the deformation of CLT panels due to the effects of creep and environmental conditions; 4) loss cable force model for estimating the loss of tendon force in post-tensioned CLT panels over time due to the effects of creep and the variation of environmental relative humidity; 5) design equation to estimate the cable force loss over time due to creep behavior and changing environmental conditions.

In experimental studies, the behaviors of CLT-LiFS under the cyclic loading and multiple earthquake motions have been carried out.

The detailed outcome of this dissertation study can be summarized as follows:

1. Real-time hybrid simulation with reducing the undesirable effects of time delay has been implemented for the new hybrid structural systems under cyclic loadings and multiple earthquake motions. Based on this experimental work, the following findings are obtained:

a) Online time delay has been successfully estimated and compensated for the performances of the hybrid simulation.

b) At the DBE level, the value of 1.90% and 0.9% were found for NPE and RMS, respectively.

c) The CLT-LiFS system performed well under MCE intensity with the maximum drift less than 1%.

d) The stiffness of CLT-LiFS primarily provided by CLT and a residual deformation around 0.2 in. was found after the test.

2. Moisture content diffusion in CLT panels has been modeled and the moisture content diffusion coefficients for CLT material have been proposed. The findings from this study are summarized as:

a) An absorption coefficient of 0.013 $in^2.day^{-1}$ was recommended for CLT with a step change in RH from 50% to 70%.

b) An absorption coefficient of 0.032 $in^2.day^{-1}$ and a desorption diffusivity of 0.041 $in^2.day^{-1}$ were suggested for CLT with a step change in RH between 70% and 90%.

c) The minimal effects of the CLT thickness were found on diffusion coefficients.

3. A four-element creep model with a mechano-sorptive constant to account for the effects of changing environmental conditions on creep behaviors of CLT material has been proposed. Numerical analysis was also implemented to examine the effects of changing RH from ambient environmental conditions to axial strain in CLT. The following outcome is obtained:

a) For the CLT panels less than 5 layers subjected to a stress level less than 15% f_c' in 50% RH, the mean values of $K_e = 1.03\times10^6$ psi, $K_k = 2.57\times10^6$ psi, and $\mu_k = 14.06\times10^{10}$ psi-min were recommended.

b) The mechano-sorptive constant values of 0.122×10^6 psi and 0.127×10^6 psi were suggested for the change of RH from 50% to 70% and from 70% to 90%, respectively.

c) For the CLT specimens under 5 layers subjected to RH changed between 50% and 70%, a variance less than 2% in the axial strain was found in a numerical analysis.

4. A loss cable force model has been proposed and a simplified equation to estimate the loss of cable force over time for design process has been also suggested. The findings from this study are including:

a) The long-term cable losses were well predicted by the simplified equation.

b) Simplified equation performed better in predicting the cable force loss for the three-layer CLT panels for 9 months period since the moisture content changes faster in three-layer CLT panels. For long-term prediction, simplified equation should work well for both three- and five- layer CLT panels.

c) Numerical data at 271 day after post-tensioned showed that the loss of post-tensioned cable force was between 2.53% and 6.37% in three-layer CLT panels loaded at 10% of compression strength, between 1.08% and 3.36% in 5-layer CLT panels loaded at 10% of compression strength, and from 1.93% to 3.87% in 5-layer CLT panels with load at 15% of compression strength.

5.2. Conclusions

This doctoral dissertation partially addressed the challenges of applying the CLT-LiFS to construct the mid-rise to tall wood buildings in the highly earthquake-prone areas. Real-time hybrid testing method was used to study the behaviors of the CLT-LiFS under earthquake

motions. Real-time delay algorithm has been developed to limit the undesirable effects of time delay to the performances of the real-time hybrid simulation.

The migration of moisture content in CLT panels due to the changes in the relative humidity from the ambient environmental conditions has successfully modeled. This model was then successfully applied to a numerical creep model to predict the creep behavior in CLT panels.

A four-element creep model has been proposed for calculating the creep deformation of CLT materials versus time. The effects of varying environmental conditions were considered through the mechano-sorptive constants. The model works with CLT panels at an arbitrary thickness and dimensions. The results showed that the effects of moisture content change in CLT on panel deformations due to creep cannot be neglected.

The loss of cable force estimated by FEM model and simplified equation were proposed and compared in this dissertation. The results showed that the loss of tendon force in post-tensioned CLT panels is significant and cannot be ignored, it ranges from 1% to 7% of the post-tensioned force.

5.3. Future works

A few problems exist in the present studies which need to be addressed in the future study

1) Investigate the CLT-LiFS in a 3-D boundary condition: The performances of a 3-story CLT-LiFS building has been limitedly carried out under mono-axial loading in this study. However, the behaviors of this structure under bi-axial loading need to address to have a better understanding.

2) Implement the creep test in a longer duration for the full-scale 5-layer CLT panels: Three months creep results for 8ft. long, 5-layer CLT under stress level of 5% f_c' showed the large variation in fitted parameters. Because the creep behavior in the full-scale 5-layer CLT panels was not well established and has not reached its creep deformation limit, the longer-term creep tests are recommended for this type of CLT panels.

3) Perform creep tests for CLT panels under periodic environmental condition change: The effects of changing RH from ambient environmental condition to axial strain in the creep model proposed in this study has only been validated by the numerical data. Therefore, experimental creep data under periodic environmental condition is recommended to validate FEM model.

4) Reliability analysis to calibrate the coefficients in the loss of cable force design equation: Since the simplified equation proposed in this study was based on the specific value of the numerical data. To apply this equation to practical design for predicting the cable force losses in post-tensioned CLT panels, the partial safety factors need to calibrate based on both numerical and experimental results, and the target reliability index should be adopted by the current code.

REFERENCES

Ahmadizadeh M, Mosqueda G, Reinhorn AM. (2011). “Compensation of actuator delay and dynamics for real-time hybrid structural simulation”. Earthquake Engineering & Structural Dynamics, 37(1):21–42.

Andi Asiz, Ian Smith, (2011). “Connection System of Massive Timber Elements Used in Horizontal Slabs of Hybrid Tall Buildings”. ASCE Journal of Structural Engineering; ASCE, ISSN 0733- 9445/2011/11-1390–1393.

ANSI/APA (American National Standards Institution/American Plywood Association) CLT (Cross-Laminated Timber) Standard Committee. (2012). “American national standard—Standard for performance rated cross-laminated timber.” ANSI/APA PRG 320-2012, APA–Engineered Wood Association, Tacoma, WA.

APA. (2017). “Product Report”. The Engineered Wood Association

ASCE/SEI (2010). “Minimum Design Loads for Buildings and Other Structures”. Reston, VA: American Society of Civil Engineers (ASCE).

ASTM D4442-15 "Standard Test Methods for Direct Moisture Content Measurement of Wood and Wood Based Materials”

ASTM D6815-09 Standard Specification for Evaluation of Duration of Load and Creep Effects of Wood and Wood-Based Products, ASTM International, West Conshohocken, PA, 2015.

ATC (2009). “Quantification of Building Seismic Performance Factors”, ATC-63, Project Report, Applied Technology Council, Redwood City, CA.

Atherton, G. H. (1983). ‘‘Ultimate strength of structural particleboard diaphragms.’’ Forest Products. J., 33(5), 22–26.

B. Yeh, D. Kretchmann, B. J. Wang. (2013). “Cross-laminated timber Manufactoring.” Chapter 2, CLT Hanbook: Crosslaminated timber - US edition. FPInnovations, Pointe-Claire, QC, Canada.

Buchanan, A. H., Deam, B., Fragiacomo, M., Pampanin, S., and Palermo, A. (2008). “Multi-storey prestressed timber buildings in New Zealand.” Struct. Eng. Int., 18(2), 166–173.

Bulleit, W. M. (1984). "Reinforcement of wood materials: A review." Wood and Fiber Sci., 16(3), 391-397.

Ceccotti A., Follesa M., Lauriola M.P., Sandhaas C. (2006b). Sofie Project – Test Results on the Lateral Resistance of Cross-Laminated Wooden Panels. First European Conference on Earthquake Engineering and Seismicity, Geneva, Switzerland.

Clouser, W. S. (1959). "Creep in small wood beams under constant bending load." Report No. 2150, U.S. Dept. of Agric. Forestry Service, Forest Products Lab., Madison, Wis.

Dao, T. N., and van de Lindt, J. W. (2014). "Numerical Seismic Performance of an Innovative CFS Mid-Rise Building Designed using DDD". ASCE Journal of Performance of Constructed Facilities, Vol 28 (5), 04014018.

Darby, A. P., Williams, M. S., & Blakeborough, A. (1999). "Stability and delay compensation for real-time substructure testing." Journal of Engineering Mechanics, ASCE, 128(12): 1276-1284.

Davies, M., and Fragiacomo, M. (2011). "Long-term behavior of prestressed LVL members. I: Experimental tests." J. Struct. Eng., 137(12), 1553–1561.

Deam, B. L., Dean, J. A., and Buchanan, A. H. (1991). ''Full scale testing of 3-story plywood shearwalls.'' Proc., Pacific Conf. on Earthquake Engineering.

Dion, C., Bouaanani, N., Tremblay, R., Lamarche, C.P., and Leclerc, M. (2011). "Real-time dynamic substructuring testing of viscous seismic protective devices for bridge structures", Eng. Struct., 33(12), 3351-3363.

Dunbar, A., Moroder, D., Pampanin, S., and Buchanan, A. (2014). "Timber core-walls for lateral load resistance of multi-storey timber buildings." Proc., 13th World Conf. on Timber Engineering, Laval Univ. and FPInnovations, Quebec.

E. Karacabeyli and B. Douglas, eds. (2013). "CLT handbook: cross laminated timber—US edition", FPInnovations, Pointe-Claire, QC, Canada.

Erick G. Thompson. (2005). "Introduction to the Finite Element Method: Theory, Programming, and Applications".

Falk, R. H., and Itani, R. Y. (1987). ''Dynamic characteristics of wood and gypsum diaphragms.'' J. Struct. Eng., 113(6), 1357–1370.

Fick, A. (1855). Annln Phys. 170, 59.

Folz, B. and Filiatrault, A. (2004). “Seismic Analysis of Woodframe Structures. I: Model Formulation,” Journal of Structural Engineering, 130(9), 1353-1360.

Fridley, K. J., Tang, R. C., and Soltis, L. A. (1992a). "Hygrothermal effects on mechanical properties of lumber." J. Struct. Engrg. ASCE, 118(2), 567-581.

Fridley, K. J., Tang, R. C., and Soltis, L. A. (1992b). "Creep behavior model for structural lumber." J. Struct. Engrg. ASCE, 118(8), 2261- 2277.

Gagnon, S., and Pirvu, C., eds. (2011). CLT handbook: Cross-laminated timber, FPInnovations Program, Pointe-Claire, QC, Canada.

Gerhards, C. C. (1980). “Effect of moisture content and temperature on the mechanical properties of wood: an analysis of immediate effects”. Forest Products J., 35(4), 18-26.

Gilfillan, J.R., Gilbert, S.G. & Patrick, G.R.H. “The use of FRP composites in enhancing the structural behaviour of timber beams.” Journal of Reinforced Plastics and Composites, 22(15):1373-1388. 2003

Ho, T.X., Dao, T.N., Aaleti, S., van de Lindt, J.W., Rammer, D.R. (2016). “Hybrid System of Unbonded Post-tensioned CLT Panels and Light-Frame Wood Shear Walls”, ASCE Journal of Structural Engineering; ISSN 0733-9445, 04016171.

Hoyle, R. I., Griffith, M. C, and Hani, R. Y. (1985). "Primary creep of Douglasfir beams of commercial size and quality." Wood Fiber Sci., 17(3), 300-314.

https://en.wikipedia.org/wiki/Creep_(deformation)

ICC (International Code Council). (2009). “International building code.” Washington, DC.

Iqbal, A., Pampanin, S., Fragiacomo, M., Palermo, A. and Buchanan, A. (2012). “Seismic Response of post-tensioned LVL walls coupled with plywood sheets”. Auckland, New Zealand: World Conference in Timber Engineering, Jul 2012.

Iztok Sustersic, Massimo Fragiacomo, and Bruno Dujic. (2015). “Seismic Analysis of Cross-Laminated Multistory Timber Buildings Using Code-Prescribed Methods: Influence of Panel Size, Connection Ductility, and Schematization”. 10.1061/ (ASCE) ST.1943-541X.0001344. American Society of Civil Engineers.

Jayesh K. Shinde and Michael D. Symans. (2010). “Seismic Performance of Light-Framed Wood Structures with Toggle-Braced Fluid Dampers”, 2010 Structures Congress © 2010 ASCE.

Karacabeyli, E., and Ceccotti, A. (1998). ‘‘Nailed wood-frame shear walls for seismic loads: Test results and design considerations.’’ Proc., Structural Engineering Worldwide, Paper No. T207-6, Elsevier Science, New York.

Krawinkler, H., Parisi, F., Ibarra, L., Ayoub, A., Medina, R., (2001). “Development of a testing protocol for woodframe structures,” CUREE Publication, No. W-02, Richmond, Calif.

Krueger, G. P. (1973). "Ultimate strength design of reinforced timber: State of the art." Wood Sci., (2), 175-186.

L. Li, Y. Xiao, (2015). “Creep Behavior of Glubam and CFRP-Enhanced Glubam Beams”, ASCE Journal of Composites for Construction; ISSN 1090-0268.

Lamarche, C.P., Tremblay, R., Léger, P., Leclerc, M. and Bursi, O.S. (2010). “Comparison between real-time dynamic substructuring and shake table testing techniques for nonlinear seismic applications”, Earth. Eng. & Struct. Dyn. 39(12): 1299–1320.

Liu Tong. (1987). “Moisture transport in wood and wood-based panels. A prestudy of sorption methods”. Rapport I8712078, TrateknikCentrum Stockholm, Sweden.

Loo, W., Quenneville, P., and Chouw, N. (2015). "Rocking Timber Structure with Slip-Friction Connectors Conceptualized As a Plastically Deformable Hinge within a Multistory Shear Wall." J. Struct. Eng., 10.1061 / (ASCE) ST.1943-541X.0001387 , E4015010.

M. Mohammad, Sylvain Gagnon, Eng., Bradford K. Douglas, P.E., Lisa Podesto P.E., (2012). “Introduction to Cross Laminated Timber.” Wood Design Focus, 22(2).

Mahin, S. A., Shing, P. B., Thewalt, C. R., & Hanson, R. D. (1989) “Pseudodynamic test method. Current status and future directions.” Journal of Structural Engineering, ASCE, 115(8): 2113-2128.

McConnell, E., McPolin, D., & Taylor, S. (2014). “Post-tensioning of glulam timber with steel tendons”. Construction and Building Materials, 73, 426-433.

NAHB Research Center Inc. (2000). “Residential Structural Design Guide”. Chapter 3: Design Loads for Residential Buildings.

Nakai, T., P. Grossman. (1983). “Deflection of wood under intermittent loading”. Wood. Sci. Technol. 17:55-67.

Nakashima, Kato, M., H. & Takaoka, E., (1992). “Development of real-time pseudo dynamic testing”. Earthquake Engineering and Structural Dynamics, 21(1), 79-92.

Nelson, E. L., Wheat, D. L., and Fowler, D. W. (1985). ‘‘Structural behavior of wood shear wall assemblies.’’ J. Struct. Eng., 111(3), 654– 666.

Nordstrom Jan-Erik P., Sandberg Dick, (1994).” The Rheology of Wood -Considerations of the Mechano-Sorptive Creep”. Royal Institute of Technology Department of Manufacturing Systems Division of Wood Technology and Processing Stockholm, Sweden.

Palermo, A., Pampanin, S., Buchanan, A., and Newcombe, M. (2005). “Seismic design of multi-storey buildings using laminated veneer lumber (LVL).” 2005 NZSEE Conf., New Zealand Society for Earthquake Engineering, Wellington, New Zealand, 8.

Pardoen, G., Waltman, A., Kazanjy, R., Freund, E., and Hamilton, C., (2003). “Testing and Analysis of One-Story and Two-Story Shear Walls under Cyclic Loading CUREE,” CUREE Publication, No. W-25, Richmond, Calif.

Pei, S., van de Lindt, J. W., and Popovski, M. (2013b). “Approximate R-factor for cross-laminated timber walls in multistory buildings.” J. Archit. Eng., 10.1061/ (ASCE) AE.1943-5568.0000117, 245–255.

Pirvu and Karacabeyli (2014). “Time-dependent behavior of CLT”. World Conference on Timber Engineering 2014, Quebec, Canada.

Plevris, N., and Triantafillou, T. (1992). "FRP-reinforced wood as structural material.” Material, in Civ. Engrg., ASCE, 4(3).

Plevris, N., and Triantafillou, T. (1995). "Creep behavior of FRP-Reinforced wood member.” J. Struct. Engrg. ASCE, 121(2); ISSN 0733-9445.

Priestley M J N, Sritharan S, Conley J R, Pampanin S. (1999). “Preliminary Results and Conclusions from the PRESSS Five-story Precast Concrete Test-building”, PCI Journal, 44(6): 42-67.

Rethinkwood (2014). “Summary Report: Survey of international tall wood buildings”. Retrieved from http://www.rethinkwood.com/webform/get-summary-report.

Rinaldin, G., Fragiacomo, M., (2016), “Non-linear simulation of shaking-table tests on 3- and 7-storey X-Lam timber buildings”. Engineering Structures 113, 133-148.

S. Gowda, M. Kortesmaa, and A. Ranta-Maunus., (1996). “Long term creep tests on timber beams in heated and non-heated environments”. VTT Publication 278. Espoo, Finland.

Sarisley E. F., Accorsi M. L., (1990). “Prestress level in stress-laminated timber bridges”. J Struct Eng 116:3003–3019.

Saucier, J. R., and Holman, J. A. (1975). "Structural particleboard reinforced with glass fiber-Progress in its development." Forest Products J., 25(9), 69-72.

Schaffer, (1982). “Influence of heat on the longitudinal creep of dry Douglas-Fir”. Pages 20-52 in R. W. Meyer and R. M. Kellog, eds. Structural uses of wood in adverse environments. Society of Wood Science and Technology. Van Nostrand Reinhold Company, New York.

Senft, J. F., and Suddarth, S. K. (1971). "An analysis of creep-inducing stress in sitka spruce." Wood Fib, 2(4), 321-327.

Shao, X., van de Lindt, J.W., Bahmani, P., Pang, W., Ziaei, E., Symans, M., Tian, J. and Dao, T. (2014). "Real-Time Hybrid Simulation of a Multi-story Wood Shear Wall with First-Story Experimental Substructure Incorporating a Rate-Dependent Seismic Energy Dissipation Device." Smart Structures and Systems 14(6):1031-1054.

Shing, P. B., Nakashima, M., & Bursi, O. S. (1996). "Application of pseudodynamic test method to structural research." Earthquake Spectra, EERI, 12(1):29-54.

Smith, T., Fragiacomo, M., Pampanin, S., and Buchanan, A. (2009). "Construction time and cost estimates for post-tensioned multi-storey timber buildings." Proc. of ICE, Construction Materials, Special Issue on Timber Structures, 162(4), 141–149.

Smith, T., Ludwig, F., Pampanin, S., Fragiacomo, M., Buchanan, A.H., Deam, B.L. and Palermo, A. (2007). "Seismic Response of Hybrid-LVL Coupled Walls under Quasi-static and Pseudo-dynamic Testing". Palmerston North, New Zealand: New Zealand Society of Earthquake Engineering 2007 Conference (NZSEE 2007).

Sumidenwire (2014). "ASTM A416 – Low Relaxation 7 - Wire Strand". Retrieved from http://www.sumidenwire.com.

T. Horiuchi, M. Inoue, T. Kondo and Y. Namita (1999). "Real-time hybrid experimental system with actuator delay compensation and its application to a piping system with energy absorber". Earthquake Engng. Struct. Dyn. 28, 1121-1141.

Tu T. Nguyen., (2017). "Numerical Model for Creep Behavior of Axially Loaded CLT Panels".

Tugce Akbas, Richard Sause, James M. Ricles, Ryan Ganey4; Jeffrey Berman, Sarah Loftus; J. Daniel Dolan, Shiling Pei, Ph.D., John W. van de Lindt, Hans-Erik Blomgren. (2017). "Analytical and Experimental Lateral-Load Response of Self-Centering Posttensioned CLT Walls". ASCE Journal of Structural Engineering; ISSN 0733-9445.

United States Department of Agriculture, Forest Service, Forest Products Laboratory. (2010). "Wood handbook: wood as an engineering material". Madison, WI: U.S. Dept. of Agriculture, Forest Service, Forest Products Laboratory.

Vahab Bolvardi, Shiling Pei, John W. van de Lindt, James D. Dolan, (2016). "Direct Displacement Design of Tall CLT Building with Deformable Diaphragms". World Conference on Timber Engineering 2016, Vienna, Austria.

van de Lindt and T. N. Dao, (2009). "Performance-Based Wind Engineering for Wood-Frame Buildings," Journal of Structural Engineering-Asce, vol. 135, pp. 169-177.

van de Lindt, J. (2004). “Evolution of wood shear wall testing, modeling, and reliability analysis: Bibliography.” Pract. Period. Struct. Des. Constr., 10.1061/ (ASCE) 1084-0680(2004)9:1(44), 44–53.

Wacker J. P., (2009). “Performance of stress-laminated timber highway bridges in cold climates”. Cold Regions Engineering 2009.

Yazdani, N., Johnson, E., and Duwadi, S., “Creep Effect on Structural Composite Lumber (SCL) in Bridge Applications”, ASCE Journal of Bridge Engineering, Vol. 9, No. 1, pp. 87-94, January 2004.